

*In Situ* Designer Lipid Production: Integration of Novel  
Characteristics and Behaviors into Synthetic Cell Membranes

by

DANIELLE S. KONETSKI

B.S., University of Texas, 2012

A thesis submitted to the  
Faculty of the Graduate School of the  
University of Colorado in partial fulfillment  
of the requirement for the degree of  
Doctor of Philosophy  
Department of Chemical and Biological Engineering  
2018

This thesis entitled:

*In Situ* Designer Lipid Production: Integration of Novel Characteristics  
and Behaviors into Synthetic Cell Membranes

written by Danielle Stephanie Konetski

has been approved for the Department of Chemical and Biological Engineering

---

Christopher N. Bowman, Committee Chair

---

Andrew P. Goodwin, Committee Member

Date \_\_\_\_\_

The final copy of this thesis has been examined by the signatories, and we find that both the content and the form meet acceptable presentation standards of scholarly work in the above mentioned discipline.

Konetski, Danielle Stephanie (PhD, Chemical and Biological Engineering)

*In Situ* Designer Lipid Production: Integration of Novel Characteristics and Behaviors into Synthetic Cell Membranes

Thesis directed by Professor Christopher N. Bowman

This thesis investigated the coupling of lysolipids and functionalized tails for *in situ* formation of synthetic liposomes designed to enable specific characteristics or behaviors in applications ranging from drug delivery to the advancement of artificial cell development. Copper-catalyzed Azide-Alkyne Cycloaddition (CuAAC) mediated lipid coupling was improved *via* incorporation of a photoinitiation system. Here, photo-CuAAC enabled spatiotemporal control over liposome assembly, an over 400-fold increase in formation density, and control over the maximal cross-sectional area of the liposomes formed.

Thiol-Michael mediated lipid coupling was enabled using thiol-functionalized lysolipids and acrylate tails where phospholipids were produced over 48 hours with approximate 90% conversion. Coupling was achieved using the thiol-Michael addition reaction for designer lipid synthesis by forming lipids bearing terminal alkyne functionalities in the presence of a visible light-sensitive photoinitiator over 48 hours to reach approximately 90% conversion followed by irradiation to homopolymerize the lipid tails.

Dynamic lipid bilayers were formed using thiol-thioester exchange for *in situ* liposome formation between thiol-functionalized lysolipids and phenyl thioester-functionalized aliphatic tails. Two tails, a C7 phenyl thioester and a C11 phenyl thioester, reacted with thiol lysolipid to greater than 90% conversion over 48 hours and 12 hours,

respectively. These phospholipid products produced liposomes with differences in self-assembly behavior and enhanced permeability was found in the C11 thioester-containing phospholipid system. Following phospholipid formation with the C11 tail, addition of C7 phenyl thioester enabled exchange to convert between 30 and 40% of C11 thioester-containing phospholipids into C7 thioester-containing phospholipids over 96 hours.

Finally, photo-cleavable lipids synthesized using CuAAC-mediated coupling were mixed with natural lipids to enable photo-induced pinocytosis behavior in liposomes formed either *via* lipid film hydration or the pull-down technique. The lipid film hydration method liposomes displayed consistent pinocytosis in liposomes with pearled structures or aspect ratios greater than 2, indicating that they possessed a critical volume-to-surface area ratio. Morphological transitions and 31x greater liposome formation using an asymmetric formation technique with photocleavable lipid in the outer leaflet indicate a dependence upon asymmetric lipid distribution, decreasing the outer leaflet to inner leaflet ratio during irradiation, to cause engulfment. Pinocytosis in spherical, unilamellar systems using osmotic pressure followed by irradiation lead to an average of 44% of the imaged population undergoing pinocytosis, making this approach potentially applicable to protocell and artificial cell systems.

## **Dedication**

To Mike, who helped me more than he could possibly know

## **Acknowledgements**

To begin, I'd like to thank my advisor, Chris Bowman, who has been an amazing mentor to me not only in my research studies but in my development as a scientist and a member of the greater science community. Chris has an unending passion for the work that we do which helps to motivate and propel the lab forward, and he is instrumental in the development of our careers. When I first met with Chris during the project selection process, he mentioned that he endeavors to tailor his interaction with each student to best suit their productivity and growth and I have seen constant proof that he truly does exert endless energy to ensure that each student gets the mentorship they need. Without Chris, I would be nowhere close to where I am today.

My committee has been instrumental in the development of my thesis work. Daniel Schwartz has been key in the characterization of the photo-induced pinocytosis behavior and Andrew Goodwin gave essential advice and provided analysis using instrumentation in his lab to enable characterization for the photo-CuAAC project. Veronica Vaida and Michael Shirts also provided thoughtful insight into my thesis work during yearly committee meetings.

I'd like to thank my friends in the lab: Katelyn Long and Nick Bongiardina, who have been as supportive as they have been distracting while waiting for a multitude of time points or "hurry-up-and-wait" steps, and Heidi Culver who has been not only a supportive friend but a helpful colleague. Additionally, I'd like to thank my second lab family from the labs of Jennifer Cha and Andrew Goodwin who have treated me not only as a "plus one" but as part of this wonderful friend group.

I would like to thank my incoming graduate school classmates who were indispensable during my transition to engineering from a nutrition science background. Also, I'd like to thank my friends from my class and the department: Peter Otoupal, Sarah Dischinger, Milly Dong, Stanley Chu, Lucas Ellis, Glenn Hafenstine, Nick Blum and Eftalda Becka for making these five years so memorable.

Without the mentorship and assistance from my lab, this work would not have been possible. I'd like to thank each member of my lab, as well as the Stansbury lab, for being available for helpful conversation during my thesis work. Specifically, I'd like to thank Sudhi Mavila, Brady Worrell, Tao Gong, and Austin Baranek for teaching me all of the chemistry that I know. Also, I would like to thank my undergraduate student Su Sie Park for assisting me in a wide range of studies during her time with me.

Throughout my work I was lucky to have the support of core staff to enable the work presented herein. I'd like to thank Joseph Dragavon and Jian Tay for their assistance with microscopy image collection and analysis, respectively. I'd also like to thank Jeremy Balsbaugh and Thomas Lee for assistance with mass spectrometry and Garry Morgan for collecting Cryo-TEM images of my liposomes. Finally, I'd like to extend a huge thank you to Dominique Devangel. Dom was not only exceedingly helpful with graduate school paperwork and organization, but he took my multitude of calls during my application to join CU Boulder with overwhelming kindness and made volunteer work developing graduate school recruiting weekends an absolute joy.

Last, but certainly not least, I'd like to thank my family. I would not be who I am today without my parents, David and Lisa, and my siblings, Jackson and Elke. Thank you for supporting me through all of my nerdiness starting back in grade school and continuing

through today. Also, in the last few years I have enjoyed the additional loving support of Terry and John Brasino, thank you.



## Table of Contents

### Chapter

1. Introduction.....	1
1.1. Liposome Structure and Early Characterization.....	1
1.2. Commercial and Research Applications of Liposomes.....	2
1.3. Artificial and Proto-cell Studies.....	3
1.4. Assembly of Liposomes.....	4
1.5. Overview of the Present Work.....	7
2. Objectives.....	9
3. Photoinduced Vesicle Formation via the Copper-Catalyzed Azide-Alkyne Cycloaddition Reaction.....	14
3.1. Introduction.....	14
3.2. Methods.....	16
3.3. Results and Discussion.....	19
3.4. Conclusion.....	30
3.5. Supplementary Figures.....	31
4. Formation of Lipid Vesicles <i>in situ</i> Utilizing the Thiol-Michael Reaction.....	34
4.1. Introduction.....	34
4.2. Methods.....	36
4.3. Results and Discussion.....	39
4.4. Conclusion.....	48

5. Production of Dynamic Lipid Bilayers Using the Reversible Thiol-Thioester Exchange	
Reaction.....	49
5.1. Introduction.....	49
5.2. Methods.....	50
5.3. Results and Discussion.....	55
5.4. Conclusion.....	62
5.5. Supplementary Figures.....	63
6. Photoinduced Pinocytosis for Artificial and Proto-cell Systems.....	64
6.1. Introduction.....	64
6.2. Methods.....	66
6.3. Results and Discussion.....	70
6.4. Conclusion.....	79
7. Conclusions and Future Directions.....	81
7.1. Development of Novel <i>In Situ</i> Liposomes Formation Methods.....	81
7.2. Introduction of Synthetic Functionalities Using the <i>In Situ</i> Method.....	84
7.3. Outlook and Future Directions.....	86
8. Bibliography.....	87

## List of Tables

**Table 6.1.** Liposome Formation Methods

## List of Figures

**Figure 3.1.** A schematic illustrating the use of a radical generating photo-initiator to reduce copper(II) to copper(I) in the presence of visible light. This now-catalytic copper (I) goes on to initiate the CuAAC formation of phospholipids resulting in the transition of micelles and stabilized oil droplets into bilayer membranes. These membranes then form small, spherical vesicles or large, irregular vesicles and tubules dependent upon exposure conditions all with the simultaneous benefit of a high, localized density.

**Figure 3.2.** Upon exposure to 20mW/cm<sup>2</sup> 400-500 nm light for either 30 (left) or 60 (right) minutes, a sample containing alkyne functionalized lysolipid (2.5 mM), dodecyl azide (2.5 mM), and CAP, a copper-ligand complex that functions as a visible light photoinitiator (1 wt%), showed nearly complete consumption of the alkyne lysolipid [2] and formation of triazole phospholipid [4] one hour after irradiation was completed. In addition, hypophosphonate salts [1] (for structure see Figure S3.5) and freed PMDETA [3] were observed following irradiation. No formation was seen when no light was exposed or when the CAP was absent.

**Figure 3.3.** Slides containing alkyne functionalized lysolipid (2.5 mM), dodecyl azide (2.5 mM), CAP (1 wt%), and fluorescent dye (2 uM) were irradiated with 400 nm light over an area of 500 um x 500 um at an intensity of 20 mW/cm<sup>2</sup> for 30 minutes. Following development overnight, these slides exhibited localized formation of vesicles, albeit with patterns limited by vesicle diffusion. The area between the inserted white lines indicates the approximate boundaries of the irradiated area while the expanded areas enable better visualization of giant vesicle formation. Due to the image stitching and uneven fluorescent excitation within each frame, boundaries between frames sometimes appeared darker than normal.

**Figure 3.4.** Initiation of vesicle formation from alkyne lysolipid (2.5 mM) and dodecyl azide (2.5 mM) using sodium ascorbate (2.5 mM) and copper sulfate (0.25 mM) (top) versus initiation using CAP (1 wt%) exposed to 400 nm light over an area of 200 um x 200 um at an intensity of 20 mW/cm<sup>2</sup> for 1 hour (bottom). Resulting vesicle densities from sodium ascorbate initiation (left) versus photo-initiation (right) indicate an over 400-fold increase when formation is initiated using light.

**Figure 3.5.** Sealed slides containing alkyne lysolipid (2.5mM), aliphatic azide (2.5mM), CAP (1wt%) and rhodamine-DHPE (2uM) were photopatterned with 400nm light over an area of 2mmx2mm at an intensity of 20mW/cm<sup>2</sup> for 10 minutes (left) or 50mW/cm<sup>2</sup> for 4 minutes (right). Representative images from each slide were taken to demonstrate formation of giant vesicles visible by fluorescence microscopy. An increase in vesicles of the largest dimensions is found in slides exposed at a lower intensity, while the density of the smaller vesicles appears to increase upon exposure to the higher intensity.

**Figure 3.6.** Vesicle initiation using a rapid, high dose (50 mW/cm<sup>2</sup> for 4 minutes) versus a slower dosing (20 mW/cm<sup>2</sup> for 10 minutes) when equal quantities of lipid precursors

([alkyne lysolipid]=[dodecyl azide]=2.5 mM) were used resulted in the formation of drastically different populations. Under the higher intensity exposure, vesicles have smaller cross-sectional areas with greater overall numbers while the slower dose results in larger vesicles that are fewer in number.

**Figure S3.1.** Mixtures containing alkyne functionalized lysolipid (2.5 mM), dodecyl azide (2.5 mM), and CAP (1 wt%), showed no formation of triazole phospholipid when left in the dark (left) and the same formulation for which CAP was removed and a 20mW/cm<sup>2</sup>, 400-500nm light exposure was applied for 60 minutes (right) also saw no formation of triazole phospholipid.

**Figure S3.2.** Samples containing alkyne functionalized lysolipid (2.5 mM), dodecyl azide (2.5 mM), CAP (1 wt%), and sulforhodamine (100uM) were either exposed to 20mW/cm<sup>2</sup> 400-500nm light for 30 minutes or were left in the dark. After 4 hours of development, both were diluted 1:10 on slides and imaged using fluorescent microscopy. Those exposed to light produced vesicles (left) while samples kept in the dark did not (right).

**Figure S3.3.** Cryo-TEM images of a standard formulation ([alkyne]=[azide]=2.5 mM and [CAP]= 1 wt%) exposed to 20mW/cm<sup>2</sup> 400-500nm light for 30 minutes. Scale bar denotes 200nm.

**Figure S3.4.** Vials containing alkyne functionalized lysolipid (2.5 mM), dodecyl azide (2.5 mM), and CAP (1 wt%) were exposed to 20mW/cm<sup>2</sup> 400-500nm light for 10 minutes. Formation of triazole phospholipid progressed over the first 2 hours following exposure, resulting in incomplete consumption of the alkyne lysolipid.

**Figure S3.5.** Hypophosphonate salts (left) produced from CAP photoinitiator (right) upon exposure to 400-500nm light.

**Scheme 4.1.** A lysolipid bearing a free thiol functionality (1) readily and rapidly undergoes thiol-Michael addition with an acrylate functionalized tail (2) in the presence of a water-soluble, nucleophile catalyst, 2-methylimidazole, to produce a thioether-containing phospholipid product (3). The precursors in this process assemble into micelles and stabilized oil droplets and transition to bilayer structures and liposomes *in situ* upon addition of the second aliphatic tail and the subsequent Michael addition reaction.

**Figure 4.1.** LC-MS coupled with an Evaporative Light Scattering Detector (ELSD) monitoring the progression of the thiol-Michael addition reaction. Reaction solutions of 5mM thiol lysolipid (SHPC) [1], 5mM aliphatic acrylate tail [2], and 2.5mM 2-methylimidazole catalyst were mixed and sampled at various time points to determine conversion (A). SHPC peak area, normalized to 0 hours, and product peak area, normalized to 48 hours, demonstrate almost 90% conversion over the course of 48 hours (B). When catalyst is absent, the reaction occurs to approximately 50% conversion over the course of 48 hours (C,D).

**Figure 4.2.** Microscopy images of liposomes assembled from thioether-containing phospholipid products [3]. 5mM reduced SHPC and aliphatic AT were reacted in the presence of 2.5mM 2-methylimidazole. For fluorescence microscopy imaging, 2uM rhodamine-DHPE was included in the reaction mixture. After 48 hours of reaction, fluorescence microscopy demonstrated liposome formation (left) with most liposomes assembled in a unilamellar fashion as demonstrated using cryo-TEM (right).

**Scheme 4.2.** A schematic illustrating the formation of a designer lipid bearing a terminal alkyne using the thiol-Michael formation method. A new terminal alkyne functionalized AT [4] couples to SHPC [1] in the presence of 2-methylimidazole resulting in liposomes with terminal alkynes buried in their hydrophobic core. These liposomes themselves enable subsequent modification of the membrane characteristics or behavior and as a whole demonstrate the ability to incorporate a wide array of new functionalities using this formation chemistry. As one example of characteristics enabled with this formulation, homopolymerization could be used to temporarily enhance permeability upon the generation of radicals.

**Figure 4.3.** Designer lipid with terminal alkyne functionality synthesized using thiol-Michael addition. LC-MS with ELSD tracks the formation reaction with SHPC peak values normalized to the peak area at 0 hours while product peak values were normalized to the peak area at 48 hours. SHPC [1] and an alkyne-terminated acrylate tail [4] were reacted in the presence of 2.5mM 2-methylimidazole and 5mM LAP photoinitiator resulting in nearly 90% conversion to phospholipid [5] over the course of 48 hours. Subsequently, alkyne-functionalized phospholipids were irradiated with 10mW/cm<sup>2</sup> 400-500nm light for 10 minutes, resulting in complete consumption of the phospholipid as the alkyne polymerizes (A). Fluorescence microscopy verified the assembly of functionalized lipids into giant liposomes (B).

**Scheme 5.1.** A schematic illustrating the formation of synthetic phospholipids using the thiol-thioester exchange reaction. Thiol-functionalized lysolipids [1] undergo reversible exchange with either C7 [2] or C11 [3] phenyl thioesters in the presence of a basic catalyst, triethylamine (TEA), to generate phospholipid products [4 and 5]. These lipid products are then capable of assembling into bilayers to form liposomes.

**Figure 5.1.** LC-MS-ELSD chromatography monitoring reactions containing 5mM reduced thiol lysolipid (SHPC) [1], 10mM TEA and 5mM thioester tail [2 or 3] (A, C). C7 thioester tails and SHPC, normalized to 0 hours, undergo approximately 90% conversion to phospholipid **4**, normalized to 48 hours, over the course of 48 hours (B) and C11 thioester tails with SHPC, normalized to 0 hours, undergo nearly complete exchange over 12 hours to produce phospholipid **5**, normalized to 24 hours (D).

**Figure 5.2.** Fluorescence microscopy and cryo-TEM images of phospholipid assemblies. C7 thioester tails (5mM) undergo exchange with reduced SHPC (5mM) in the presence of 10mM TEA over 48 hours to produce predominantly unilamellar liposomes, as evidenced by fluorescence microscopy (A) and cryo-TEM (B). When reacted at 30°C for 24 hours, C11 thioester tails (5mM) undergo exchange with reduced SHPC (5mM) in the presence of

10mM TEA to produce liposomes, visualized using fluorescence microscopy (C) but at room temperature assemble into tubular micelles, visualized using cryo-TEM (D).

**Figure 5.3.** Photobleaching assays of phospholipid **4** and phospholipid **5** liposomes. Both systems enable bleaching of internal HPTS upon irradiation. Mean internal fluorescence normalized to initial fluorescence values shows restoration of fluorescence over 20 seconds for phospholipid **5** systems and no restoration of fluorescence for phospholipid **4** systems.

**Figure 5.4.** Phospholipid **5** undergoes exchange with C7 phenyl thioester tails. Following formation of phospholipid **5** over the course of 24 hours, equimolar C7 thioester tails [3] were added. Exchange of the two tails progressed over the course of 96 hours to convert over 30% of phospholipid **5**, normalized to 0 hours, to phospholipid **4**, normalized to 96 hours (A). Fluorescence microscopy verified persistence of liposomes following addition of C7 phenyl thioester tails after 48 hours of continued development at 30°C (B).

**Figure S5.1.** LC-MS-ELSD chromatography monitoring control reactions containing 5mM reduced thiol lysolipid (SHPC) [1] and 5mM thioester tail [2 or 3] but no catalyst. No formation of thioester-containing phospholipid product is apparent 48 hours after mixing SHPC [1] with C7 phenyl thioester tail [2] (A) or 12 hours after mixing SHPC [1] with C11 phenyl thioester tail [3] (B).

**Figure 6.1.** Liposome formulations consisted of a mixture of DOPC, NBPC, and cholesterol at a molar ratio of 2:2:1, respectively. NBPC undergoes photo-induced cleavage upon irradiation to produce lysolipids, carbon dioxide, and aliphatic tails. DOPC ensures fluidity of the membrane at room temperature and cholesterol increases stability.

**Figure 6.2.** Liposomes formed using a precipitation method to produce asymmetric assembly of lipids between the inner and outer leaflet was used here to probe the leaflet selectivity of NBPC. Liposomes were formed with NBPC exclusively in the outer (B) or inner leaflet mixture (A), resulting in pronounced differences in the quantity of liposomes generated. Liposomes are indicated by a fluorescent interior marked by AlexaFluor 647 and membrane fluorescence assessed by rhodamine-DHPE.

**Figure 6.3.** Fluorescence microscopy images during irradiation of elongated liposomes demonstrate photo-induced pinocytosis. Liposomes were formed *via* lipid film hydration composed of 2:2:1 NBPC:DOPC:cholesterol with rhodamine-DHPE. Internal compartments encapsulate 500uM fluorescein in an external solution of 100uM sulforhodamine B and 350mM glucose. Irradiation with 365nm 10mW/cm<sup>2</sup> light results in photo-cleavage of NBPC in the membrane and a shape change transition from lobed structures and tubules to oblate ellipsoids and closed stomatocytes. Each strip contains representative images of time points progressing left to right illustrating shape change steps of each vesicle. Strip length does not correlate to irradiation time.

**Figure 6.4.** Microfluidic wells contain liposomes composed of 2:2:1:0.02 NBPC:DOPC:cholesterol:rhodamine-DHPE encapsulating 1mM AlexaFluor647 and 200mM

sucrose. External solvent (200mM glucose) is exchanged with 300mM glucose to apply osmotic pressure to deform the liposomes. Following deformation, irradiation with 405nm light results in pinocytosis in an average of 44% of the imaged liposomes as observed here where the post-exposure vesicles are shown to contain internalized structures.



## Chapter 1

### Introduction

#### Section 1.1. Liposome structure and early characterization

Liposomes, often referred to as spherulites in the early days of their characterization, are self-assembled lipid bilayers that encapsulate an aqueous core kept separate from the external media. Bilayer lipid structures composed of lecithin and cholesterol were first visualized using negative-staining for electron microscopy by Bangham and Horne in the early 1960s<sup>1</sup>, and this enclosed lipid bilayer system served as a competitive cell membrane model to the “black lipid membrane” (BLM)<sup>2</sup>. Since that discovery at the Babraham Institute, liposomes have been applied as models to study anesthetics, cell dynamics, and even lung surfactants<sup>3</sup> while also being used and studied for a wide range of other purposes, both fundamental and practical. Specifically, liposomes were rapidly applied as simplified systems to study membrane proteins<sup>4,5</sup>, bilayer properties<sup>6-12</sup>, mitochondrial behavior<sup>13</sup>, and the interaction of membranes with peptides<sup>14</sup>, proteins<sup>15-21</sup> and drugs<sup>22-24</sup>, all just within that initial decade following their discovery.

In the time since their initial development, liposomes have become such a beloved and integral part of research that upon retirement, Bangham wrote to fellow scientists requesting thoughts, poems, etc. and published the results as the Liposome Letters<sup>3,25</sup>. One such poem, written by the first principal investigator to publish upon the application of liposomes to drug delivery<sup>26</sup>, is presented here:

*Little fatty vesicles of bilayer fame  
Protean and elusive, fragile all the same,  
Aloof and enigmatic beneath your many skins,  
Unyielding to the vigour of thousands of spins,  
Descended from the pastures of Babraham we are told,  
You never cease to wrinkle, expand and then to fold  
Embracing sodium ions and such electrolytes.  
Twinkling guide stars to throngs of acolytes  
Desirous of your membranous semi-barriers.  
Precursors of bion, potential drug carriers.*  
**Gregory Gregoriadis** in *Liposome Letters*

## **Section 1.2. Commercial and Research Applications of Liposomes**

The unique amphiphilic bilayer of liposome structure enables the encapsulation of hydrophilic compounds within internal compartments and hydrophobic compounds within the core of the self-assembled bilayer. Encapsulation in this manner provides benefits such as sustained release, protection from degradation, or reduced off-target toxicity. These attributes have found particular utility in the fields of drug and cosmetics delivery. To date, at least eight formulations of drug-loaded liposomes have been approved by the FDA<sup>27</sup> and progress in the field has prompted a multitude of reviews<sup>27-43</sup>. Meanwhile, the presence of lipids in cosmetic formulations is great enough to compel a conference, the “Lipids & Cosmetics” conference held in 2018 in Bordeaux<sup>44</sup>.

While the native structure of liposomes enables drug encapsulation for delivery, research into increasing efficiency of liposome systems for drug delivery has introduced targeting behavior, increased stealth and stimuli-responsive release. Although drugs may benefit from the protection provided by the liposome shell, this approach can also result in slow delivery, which has the potential for decreasing the therapeutic effect. To improve delivery rates, acidic conditions present in tumors have been utilized to facilitate site-

specific uptake of liposomes<sup>45</sup> while rapid delivery of liposomal contents is also possible upon application of an external stimulus to induce permeability of the liposome barrier. Permeability has been induced using ultrasound in liposomes containing air<sup>46,47</sup>, near-IR with photosensitizers<sup>48,49</sup> or porphyrin-functionalized lipids<sup>50,51</sup>, UV-induced lipid cleavage<sup>52</sup>, photo-induced lipid isomerization using azobenzene<sup>53</sup> and spiropyran<sup>54</sup>, and photo-induced polymerization using double<sup>55</sup> or triple bonds<sup>56</sup> embedded in the hydrophobic chains and many others. Additionally, liposomes suffer from rapid clearance as a result of circulation, so hydrophilic polymers such as PEG have been used to decorate the outside of the liposomal bilayer to improve the “invisibility” of the liposome to the immune and other body systems. Finally, targeting of liposome carriers to disease sites has been oft explored although the benefits of this approach still remain under debate<sup>32</sup>.

Beyond commercial applications, liposomes have also been applied in research as microreactors to spatially segregate reactions<sup>57</sup>, to monitor conversion upon mixing of two small volumes<sup>58</sup>, and for sensing applications<sup>59</sup>. Membrane dynamics that are designed to mimic cell processes have been studied using liposomes as a much simpler environment as compared to that found in the crowded cell, enabling deconvolution of the importance or activity of various components. In addition, liposomes have been utilized to study sunlight fueled development of proton gradients<sup>60</sup>, membrane remodeling<sup>61</sup>, organelle generation<sup>62</sup>, morphological changes<sup>63-69</sup>, and much more.

### **Section 1.3. Artificial and Proto-cell Studies**

Perhaps most importantly, insofar as this thesis is concerned, liposomes have become a popular model for cell membranes as used for origin-of-life studies and bottom-

up artificial cells, and for their use in protocells. Origin-of-life studies focus upon compounds that may have been available to generate early compartments<sup>70</sup> or simplified systems to deduce how complexity might have evolved<sup>71-73</sup>. In contrast, protocells add components one at a time to result in compartments capable of synthesizing molecules or proteins of interest without restrictions on the complexity of the components added<sup>74</sup>. Similarly, bottom-up artificial cells build complexity into systems until a status of “living” can be applied. While definitions of “living” vary, common themes are the self-contained expression of a genetic code and the ability to replicate and evolve<sup>75-80</sup>. To this end, significant work has been reported on the necessary components for protocells and bottom-up artificial cells. For protein expression, cell-free expression systems have been reported<sup>81</sup> and used in liposome systems<sup>82-86</sup>. This encapsulation of protein machinery protects the proteins from degradation; however, the bilayer liposomal boundary can also hamper expression if reactants cannot readily cross into the compartment. To increase reactant access, methods such as protein channels and translocation machinery<sup>83,87-98</sup>, microinjection<sup>99,100</sup>, and increased membrane permeability using surfactants<sup>101,102</sup> have been reported. Additionally, these systems have been taken a step further to produce liposomes with internal compartments that recreate organelles with confined reactions<sup>58,103</sup>. Finally, evolution of synthetic systems requires the division of individual compartments to create new progeny, and so growth-dependent division behaviors have been explored<sup>104-107</sup>.

#### **Section 1.4. Assembly of Liposomes**

Early studies on the structure of liposomes at the Babraham Institute involved the shaking of lipids in water to produce a liposome dispersion<sup>3</sup>. The ease of liposome assembly demonstrated by this simple approach represented the utility liposomes could provide to a host of applications. It can therefore be of no great surprise that in the years since their identification a host of new formation methods have been developed to more tightly control the desired properties achieved by the assembly. The simplest and earliest method, developed in the years following the original liposome characterization, is the lipid film hydration method<sup>108,109</sup>. This method involves the gentle hydration of a dried lipid film in the aqueous media of choice. Formation using this method is dependent upon the diffusion of solvent and compounds across the bilayer to produce an internal compartment. For this reason, the ability to encapsulate hydrophilic compounds of interest (i.e. the encapsulation efficiency) is low and the resulting structures are often heterogeneous and multilamellar. Regardless, the sheer simplicity drives its continued use.

Following the lipid film hydration method came the electroformation method<sup>110</sup>. Here, lipid films were subjected to an oscillating electric current to generate more unilamellar structures. However, this approach also suffers from low encapsulation efficiency. In contrast, to produce liposomes encapsulating higher concentrations of the desired compounds, two methods are of note. The pull-down technique utilizes centrifugal force to pull water-in-oil droplets loaded with molecules of interest through an oil/water interface<sup>111-113</sup>. Liposomes produced in this manner have higher encapsulation efficiencies and are predominantly unilamellar but with limited control over size. On the other hand, double emulsion microfluidic devices have precise control over internal and external aqueous solutions to establish high encapsulation efficiencies as well as utilizing fine-tuned

control over flow rates to generate uniform liposome populations<sup>77,114–117</sup>. A significant drawback to microfluidic formation, however, is the substantial amount of technical experience required to master this technique.

Finally, the most recent formation technique is the direct *in situ* coupling of aliphatic tails to lysolipids (phospholipid-based molecules with the zwitterionic headgroup and a single aliphatic tail built off of a glycerol backbone). Upon coupling, assemblies of micelles and stabilized oil droplets transition to liposomes<sup>118</sup>. Original work on this formation chemistry revolved around the use of the copper-catalyzed azide-alkyne cycloaddition reaction (CuAAC) which couples an azide precursor to an alkyne in the presence of a reduced, Cu(I) catalyst to produce a triazole product. Early work on this assembly process utilized a reducing agent, sodium ascorbate, but copper could also be reduced using a radical-generating photo-initiation system<sup>119,120</sup> or the catalyst could be done away with entirely if a strained cyclo-octyne precursor was developed, a common technique for the bio-orthogonal labeling of substrates *in vitro*<sup>121</sup>.

The CuAAC reaction is broadly classified as a “click” reaction, a classification of reactions which could be further explored for alternative lipid coupling reactions. Originally designated by Sharpless *et al.* in 2001<sup>122</sup>, the term “click” refers to reactions which hold the properties of being orthogonal, fast, high yielding, stereospecific, and amenable to ambient conditions, among others. These characteristics make “click” reactions an excellent starting point from which to explore the production of liposomes which require the presence of water, are dilute systems, and are generally developed for conditions at or near those of physiological relevance. Two other reactions to which the “click” designation is generally applied are the radical-mediated thiol-ene reaction and the

thiol-Michael addition. Thiol-ene reactions involve the addition of a thiol to a double bond mediated by a thiyl radical intermediate<sup>123,124</sup>. The thiol-Michael reaction similarly involves thiols, but the reaction is catalyzed by a thiolate anion intermediate adding to an electron deficient double bond to produce a thioether product in the presence of a base or nucleophile catalyst<sup>125</sup>.

### **Section 1.5. Overview of the Present Work**

In the present thesis, I have striven to build-upon the current field of designer lipid (lipid-based compounds with novel functionalities integrated into their structure for enhanced functionality) synthesis. To achieve this aim, I have developed new chemistries for the *in situ* liposome formation system. Additionally, I have used the *in situ* method to make designer lipids with numerous functionalities of interest. *In situ* liposome formation has the capacity to simplify designer lipid synthesis by utilizing the second aliphatic tail as a carrier system for moieties not found in natural lipids but which might increase the functionality of the liposome or otherwise alter its behavior and responsiveness in a desirable manner. A large benefit found in the field of “click” reactions is the specificity of the reactive groups, making them orthogonal to many reactions and frequently amongst themselves. For this reason, I worked first with thiol-Michael addition to enable lipid formation using base or nucleophile catalyst systems, and to establish orthogonality to functional groups such as terminal alkynes for downstream modification. Additionally, I implemented the thiol-thioester exchange reaction for membrane formation to enable exchange of one added aliphatic tail for another. From this toolbox of *in situ* formation chemistries I looked to incorporate synthetic functionalities into the membrane to modify

characteristics or behaviors of the liposome. Two examples of such functionalities were the incorporation of moieties capable of homopolymerization and photo-cleavable structures. Utilizing the thiol-Michael reaction a tail terminated in an alkyne was coupled into the membrane. This functionality could photopolymerize upon irradiation to temporarily increase membrane permeability and deliver encapsulated compounds or could be used for future modification reactions such as thiol-yne or CuAAC. Photo-induced pinocytosis, enabled by a photo-cleavable o-nitrobenzyl moiety coupled into the lipid membrane mediated by the CuAAC reaction, laid groundwork for future artificial cell feeding applications. Upon irradiation, these lipids release the second aliphatic tail, driving engulfment of external fluid in liposomes bearing reduced volume-to-surface area ratios. This behavior would enable spatiotemporal control over artificial cell feeding when incorporation of resources is necessary while not losing previously encapsulated compounds. While powerful, these incorporated functionalities demonstrate only a subset of what is possible with this *in situ* formation reaction.



## Chapter 2

### Objectives

Liposome development for applications from molecular delivery to fundamental membrane studies requires the manipulation of components such as the bilayer formation technique to the structure of the lipids themselves. These manipulations strive to control the properties and characteristics of the membrane as its structure dictates the ability to load the material(s) of interest and the downstream fate of those loaded molecules. For this reason a new technique to manipulate the system of self-assembly using covalent attachment of an aliphatic tail to a lysolipid structure has been developed. Using this technique as a launching point, the objectives of this thesis aimed to expand the chemistries available to drive liposome formation and apply those systems to incorporate functionalities into the lipid molecules to alter behavior and induce characteristic changes in the bilayer membrane as a model for cell membrane recreation.

To advance the former area, phospholipid coupling reactions were designed, developed, and characterized. First, the CuAAC coupling reaction developed by collaborators at UCSD was expanded upon to incorporate spatiotemporal control using a photoinitiation system to reduce the copper catalyst that leads to the phospholipid formation. Second, the toolbox of chemistries for coupling of a lysolipid to a second aliphatic tail was expanded by introduction of a thiol-Michael coupling pair. Lastly, a reversible chemistry, the thiol-thioester exchange reaction, was developed for phospholipid formation.

To manipulate behaviors of the liposome or to modulate characteristics of the membrane, various coupling reactions were applied to the formation of phospholipids

bearing functionalities of interest. Using the thiol-Michael reaction for phospholipid formation enabled the formation of a lipid bilayer that was capable of subsequent photoinduced homopolymerization. Next, the thioester exchange reaction was used to enable remodeling of the bilayer through the exchange of one aliphatic tail for another. Finally, photo-cleavable lipids were synthesized using the CuAAC coupling reaction, which when applied in a mixed lipid system, enabled engulfment of external fluid during irradiation, i.e., pinocytosis.

**Specific Aim 1: Enable spatiotemporal control and enhance the control over liposome characteristics and structure by developing a photo-initiated CuAAC *in situ* formation reaction.**

For this aim, a radical generating photoinitiator bound to a copper complex was incorporated into the Copper-catalyzed Azide-Alkyne Cycloaddition (CuAAC) reaction-based phospholipid formation system. This photoinitiator generates radicals upon irradiation with visible light that subsequently reduce copper (II) to copper (I) to catalyze the CuAAC reaction and ultimately lead to phospholipid formation. Following characterization of the photoinitiation of the lipid coupling reaction, the effect of control over photon dose was analyzed. Spatiotemporal control over irradiation and the modulation of intensity of light applied was utilized to enhance control over liposome size, density and location.

**Specific Aim 2: Expand the toolbox of *in situ* formation reactions by developing thiol-Michael mediated lipid formation.**

To realize the second specific aim, a thiol-functionalized lysolipid and an acrylate-functionalized tail were designed and synthesized for the implementation of the thiol-Michael reaction as a lipid coupling reaction. Catalyst systems were tested for their ability to catalyze the reaction without enhancing the rate of hydrolytic breakdown of lipid structures and the phospholipid and subsequent liposome formation were characterized. To demonstrate the added utility of this new coupling reaction, a terminal alkyne functionality was incorporated into the final lipid structure using a synthesized tail with both acrylate and alkyne functionalities. Newly functionalized lipids were examined for their ability to form liposomes and to homopolymerize upon introduction of radical species.

**Specific Aim 3: Enable lipids to remodel *via* introduction of a reversible lipid coupling reaction.**

Building upon work in the previous aim, the tested thiol lysolipid was applied to facilitate the thiol-thioester exchange reaction using synthesized phenyl-thioester tails. For this work, two different tails were analyzed for their ability to form synthetic phospholipids capable of assembling into liposomal structures upon mixing with a base catalyst. Again, concentrations were surveyed to allow catalysis without lipid degradation. Following initial exchange of thiol lysolipid with phenyl-thioester tails, the capability to exchange one tail for another was assessed.

**Specific Aim 4: Replicate a native cell behavior, pinocytosis, using photo-induced cleavage of lipids in the membrane.**

For the final aim, the CuAAC-based formation of lipids was utilized to produce a synthetic lipid bearing a photo-cleavable moiety. These synthetic lipids were mixed with natural lipid molecules to form liposomes using multiple formation techniques. These systems were manipulated to produce extended liposome morphologies, operating away from the spherical volume to surface area ratio. Using light to alter the bilayer structure, the ability to photo-induce engulfment of external fluid, i.e., pinocytosis, was demonstrated and analyzed.

### **Summary of Work**

The work detailed in this thesis advances the field of synthetic lipid production for applications in a wide array of fields. This work increases the methods for lipid coupling *in situ* thereby increasing the range of orthogonal functionalities that are able to be incorporated into lipid tails and demonstrates several of those characteristics. For increased control over a preexisting formation chemistry, Chapter 3 incorporates a photoinitiation system into the CuAAC induced formation of synthetic phospholipids thereby enhancing control over liposome density, size, and location. Adding to the repertoire of formation chemistries, Chapter 4 develops a thiol-Michael addition reaction for lipid synthesis and applies it to the incorporation of a terminal alkyne functionality that is capable of subsequent downstream homopolymerization while Chapter 5 introduces reversibility into the lipid coupling reaction *via* a thiol-thioester mediated lysolipid-tail coupling. Finally, Chapter 6 applies a photo-cleavable lipid formed using the lipid coupling systems to the inducement of a novel photo-induced pinocytosis behavior. Together, this work will facilitate the creation of future synthetic liposome systems by speeding up the

“build” step in the design-build-test iteration and adds to the capabilities of synthetic liposomes for future artificial cell or liposomal delivery systems.

## Chapter 3

### Photoinduced Vesicle Formation via the Copper-Catalyzed Azide-Alkyne

#### Cycloaddition Reaction

##### Section 3.1. Introduction

Vesicles are the product of the self-assembly of amphiphilic phospholipid molecules to produce enclosed bilayer membranes. Interest in the use of vesicles in fields ranging from drug delivery<sup>37,126</sup> and cosmetics<sup>127</sup> to their use as cell membrane mimics<sup>58,76</sup> and in the study and evaluation of membrane dynamics<sup>128</sup> has increasingly grown in the years since their discovery in 1964<sup>1</sup>. For artificial cell and membrane dynamics studies, giant unilamellar vesicles (GUVs), which are characterized as having a diameter greater than 1  $\mu\text{m}$ , are of particular significance and as such, have solicited much attention toward developing simple, reproducible means of formation<sup>129</sup>. Popular vesicle formation methods include lipid film hydration<sup>108,109</sup> and electroformation<sup>110</sup>, which require little in the way of specialized equipment or expertise but suffer from restrictions over the charged nature of the lipids used<sup>130,131,129</sup>. Ethanol-injection<sup>132,133</sup> and the pull-down, or inverted emulsion<sup>111-113</sup>, technique similarly require minimal experience but may suffer from continued presence of the solvation medium<sup>129</sup>, and the use of microfluidics<sup>114,134</sup> yield highly regular formation with excellent encapsulation efficiency but require a more complicated set up and technical know-how<sup>129</sup>.

To remedy some of the pitfalls of the aforementioned methods, recent studies have been conducted to enhance the control over vesicle formation while maintaining relative simplicity in the techniques used. Novel approaches that achieve at least some level of

spatiotemporal control over the formation involve the use of focused IR heating<sup>135,136</sup> or ultraviolet (UV) exposure<sup>137</sup>. However, these techniques require exposure to UV light or increased temperature which could be potentially harmful to encapsulated materials, depending on the nature and purpose of the vesicle. Another technique involving the use of ultrasound<sup>138</sup> allows for the formation of vesicles with control over their size without UV exposure or heating but largely sacrifices the spatial control afforded by the other approaches. One paper did in fact adapt their previous method to form a vesicle under laser irradiation in the visible range but it required the incorporation of a bulky, photochromic molecule<sup>137</sup>.

Methods to allow for phospholipid generation *in situ* offer a new perspective on vesicle formation. Utilizing the efficiency of click reactions, a method involving the Copper-catalyzed Azide-Alkyne Cycloaddition reaction (CuAAC)<sup>139</sup> was developed to induce the transition of micelles to vesicles through the covalent attachment of a second aliphatic tail to a chemically modified lysolipid in the presence of a reducing agent<sup>118</sup>. This method enables the formation of vesicles *in situ*; however, it too still lacks spatiotemporal control, and little has yet been demonstrated in the way of controlling the vesicle structure or size. Light-induced reduction of copper has been readily documented in the literature through the use of a variety of complexes<sup>119,140-142</sup> and we have demonstrated previously the initiation of vesicle formation through the incorporation of a ruthenium tris-bipyridine photoinitiation system into the aforementioned CuAAC-based method<sup>143</sup>. Here, we demonstrate this formation using a more efficient, radical based reduction of the copper catalyst<sup>120</sup>, resulting in a greater ability to control the vesicle formation process and structure. The overall approach developed here is illustrated in Figure 3.1.

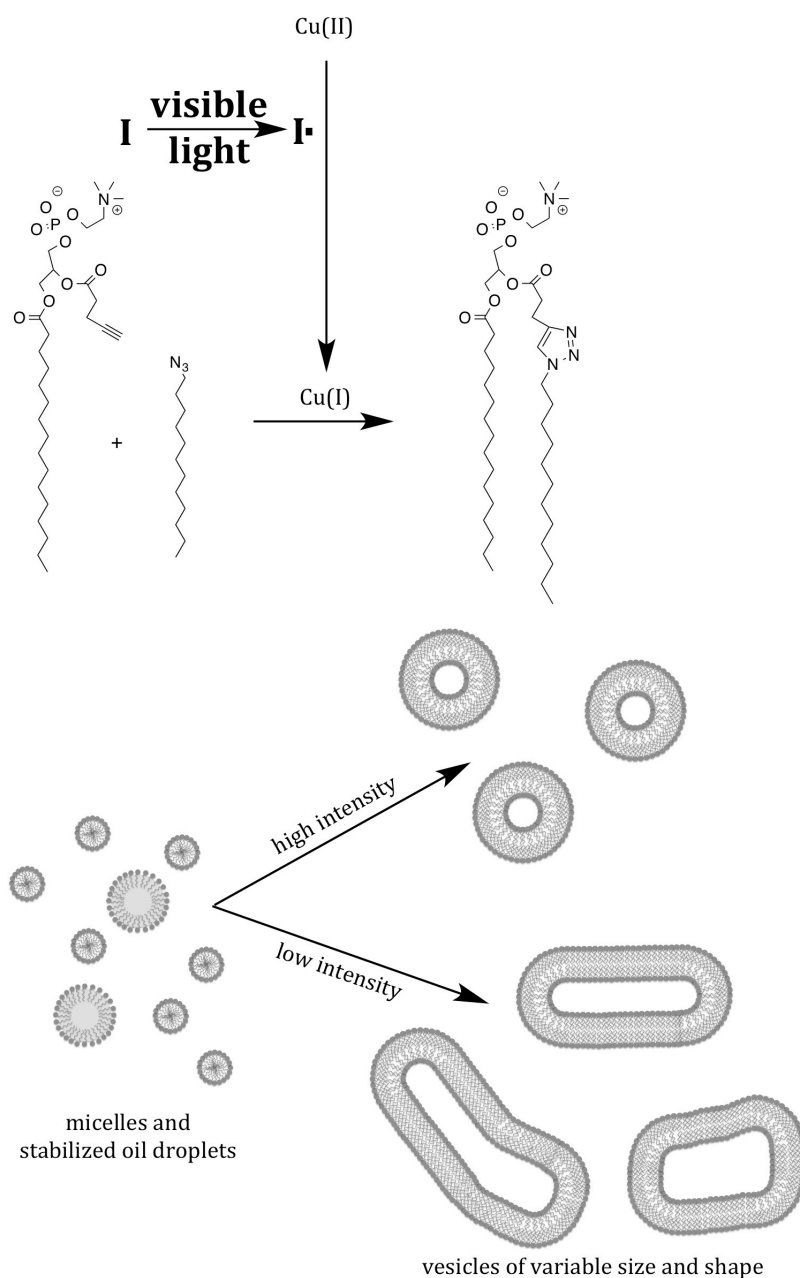


**Figure 3.1.** A schematic illustrating the use of a radical generating photo-initiator to reduce copper(II) to copper(I) in the presence of visible light. This now-catalytic copper (I) goes on to initiate the CuAAC formation of phospholipids resulting in the transition of micelles and stabilized oil droplets into bilayer membranes. These membranes then form small, spherical vesicles or large, irregular vesicles and tubules dependent upon exposure conditions all with the simultaneous benefit of a high, localized density.

### Section 3.2. Methods



**General.**  $^1\text{H}$  nuclear magnetic resonance (NMR) spectra for product verification were gathered on a Bruker Ascend 400 spectrometer and electrospray ionization mass spectrometry measurements were recorded by a Synapt G2 spectrometer. Preparative thin-layer chromatography (TLC) was carried out on glass-backed Silicycle TLC plates. The alkyne functionalized lysolipid<sup>118</sup> as well as the copper(II) acylphosphinate-PMDETA (CAP)<sup>120</sup> complex can be and were synthesized as previously reported. Briefly, dodecyl azide was synthesized by adding 12.7 mL 1-bromododecane in portions to 3.46 mg sodium azide dissolved in 40 mL DMSO. This solution was stirred overnight at room temperature and quenched using 20 mL of water. The crude product was extracted in ether, washed with water and brine, and dried over sodium sulfate before purification using column chromatography.  $^1\text{H}$ NMR (400 MHz,  $\text{CDCl}_3$ ):  $\delta$  3.25 (t,  $J$ = 6.8 Hz, 2H), 1.59 (quin,  $J$ = 7.2 Hz, 2H), 1.22-1.40 (m, 18H), 0.88 (t,  $J$ = 7.0 Hz, 3H). Other compounds were purchased from standard sources and were used as received.

**Preparation and Photoinitiation of Lipid Systems.** For initiation of vesicle formation in solution, a 100  $\mu\text{L}$  emulsion of dodecyl azide in water (2.5 mM) was prepared in the presence of alkyne lysolipid (2.5 mM) and CAP (1 wt%) in HPLC vials fitted with 350  $\mu\text{L}$  Supelco glass inserts. Photoinitiation was performed using an Acticure 4000 lamp with a 400-500 nm bandgap filter to expose the sample to various intensities and durations. The resulting solution was left at room temperature to allow complete assembly of vesicles.

Spatially refined liposome formation was carried out using a similar emulsion ([alkyne]=[azide]=2.5 mM, [rhodamine B 1,2-dihexadecanoyl-sn-glycero-3-phosphoethanolamine (rhodamine DHPE)]= 2  $\mu\text{M}$ , and [CAP]= 1 wt%). Microscope slides

containing the emulsion were prepared and sealed. Photoirradiation of finite areas was performed on a Nikon Ci-L upright microscope equipped with Mightex Polygon 400 multiwavelength dynamic spatial illuminator and Mightex BLS-series BioLED light source control module. Irradiated samples were left overnight to develop completely.

In all cases, solely visible light induced formation of vesicles was explored using wavelengths no shorter than 400nm so as to exclude UV irradiation from the samples.

**Microscope Imaging.** Fluorescent imaging was performed using a Nikon Te-2000 inverted widefield microscope equipped with EXFO Photonic Solutions X-Cite 120 LED lamp and Nikon Digital Sight DS-QiMc CCD camera and a Nikon A1R laser scanning confocal microscope controlled by Nikon Elements software version 4.20. In both cases, a 561nm laser was employed to excite the fluorescent dye. Images over the exposed location and surrounding area were acquired using Nikon Elements stitching software. For acquisition of TEM images, 4  $\mu\text{l}$  of sample solution was transferred onto a lacey holey-carbon grid, blotted for 1-2 seconds, and then plunge-frozen using an FEI-Vitrobot Mark IV at room temperature. The resulting vitrified sample was imaged on an FEI Tecnai F20 FEG-TEM, operating at 200kV and 25,000x magnification, using a Gatan US4000 CCD camera. The electron dose per image was limited to 20 electrons/ $\text{\AA}^2$ , with a defocus of  $-2\mu\text{m}$ , using the low-dose mode of Serial EM acquisition software.

**Vesicle Counting and Sizing.** Images acquired from fluorescence microscopy were imported into ImageJ. For density measurements, intensity thresholds were selected followed by application of the watershedding algorithm to produce vesicles with maximal

separation and minimal object loss. The resulting objects were counted with retained location coordinates. To determine vesicle sizes in solution, initiation of formation was conducted in HPLC vials as described above. Undisturbed samples were taken from each vial and diluted 1:300. Vesicles sizes were measured using a Malvern LM10 Nanoparticle Tracking Analysis (NTA) instrument equipped with a 532nm laser. For each sample, five 30-second videos were acquired and analyzed with the Malvern NTA software. To ensure consistency between samples, camera level (11) and detection threshold (3) were kept the same.

**LC-MS of Product Formation.** Vesicle formation was conducted in HPLC vials fitted with 350uL glass inserts as described above with 4uL samples taken over the course of the reaction. Samples were injected onto an analytical Agilent LC-MS with Sedex Evaporative Light Scattering Detector controlled by ChemStation software and fitted with Agilent Zorbax Eclipse Plus c8 column. A binary solvent system of 0.1% formic acid in both methanol and water was used at a flow rate of 1mL/minute.

**Encapsulation Experiments.** Vesicle formation was conducted in HPLC vials as described above in the presence of 100uM sulfo-rhodamine. Samples were allowed four hours to develop followed by a 1 to 10 dilution on microscope slides and imaging using fluorescent microscopy.

### **Section 3.3. Results and Discussion**

#### **A Novel Method for the Simple, Photo-Induced Formation of Vesicles *In Situ***

In an effort to produce a simple method for the production of vesicles with limited exposure to potentially damaging stimuli while maintaining spatiotemporal control, this project aimed to incorporate photoinitiation systems into the previously documented<sup>118</sup> CuAAC induced vesicle formation process. To this end, 2.5 mM lysolipid precursors containing an alkyne functionality in place of the hydroxyl group were combined with 2.5 mM aliphatic chains functionalized at one end with an azide. However, rather than producing the copper(I) catalyst via incorporation of a reducing agent and a Cu(II) source, a copper-ligand complex that functions as a visible light sensitive photoinitiator, copper(II)acylphosphinate-PMDETA (CAP), was substituted in place of sodium ascorbate and Cu(II) salts at a concentration of 1wt%. Following mixing in HPLC vials, 400-500nm light was exposed at an intensity of 20mW/cm<sup>2</sup> for either 30 or 60 minutes. Samples were taken at various time points and injected into an analytical LC-MS with an Evaporative Light Scattering Detector (ELSD), demonstrating nearly complete conversion to triazole phospholipid one hour after exposure (Figure 3.2). To ensure that this conversion was due to the photoinitiation of the system, samples were produced which lacked the CAP photoinitiator. Following exposure to 20mW/cm<sup>2</sup> light for 60 minutes, no formation of triazole phospholipid was evidenced. Additionally, formulations that contained all reaction components but were left in the dark saw no production of triazole phospholipid (Figure S3.1). This outcome represents one of the first cases of photoinitiated formation of phospholipids *in situ*, widening the possible approaches available for vesicle formation.

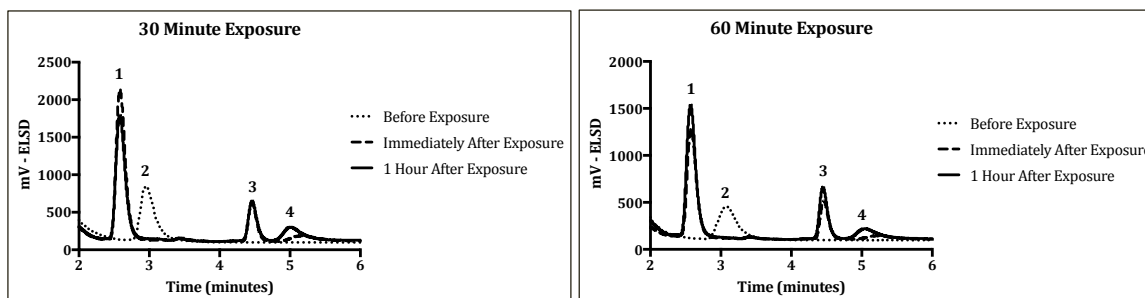


**Figure 3.2.** Upon exposure to  $20\text{mW}/\text{cm}^2$  400-500 nm light for either 30 (left) or 60 (right) minutes, a sample containing alkyne functionalized lysolipid (2.5 mM), dodecyl azide (2.5 mM), and CAP, a copper-ligand complex that functions as a visible light photoinitiator (1 wt%), showed nearly complete consumption of the alkyne lysolipid [2] and formation of triazole phospholipid [4] one hour after irradiation was completed. In addition, hypophosphonate salts [1] (for structure see Figure S3.5) and freed PMDETA [3] were observed following irradiation. No formation was seen when no light was exposed or when the CAP was absent.

To determine the level of control over where vesicle formation was occurring, the system was transferred to a new platform to allow for spatial control over the light exposure. Similar to the previous formulation, 2.5 mM alkyne lysolipid and 2.5 mM aliphatic azide were combined with 1wt% CAP and 2  $\mu\text{M}$  of a lipid bound fluorescent dye, rhodamine-DHPE. Using a digital light processing (DLP) system, patterned 400 nm light was projected onto the solution, which had been sealed to eliminate evaporation. Following exposure, these slides were left overnight to ensure complete development of the vesicles followed by imaging with fluorescence microscopy.

Observations suggested that large exposure areas of 2 mm x 2 mm could be initiated by shorter exposures ( $20\text{mW}/\text{cm}^2$  for 10 minutes) while smaller areas of 200  $\mu\text{m}$  x 200  $\mu\text{m}$  required longer ( $20\text{mW}/\text{cm}^2$  for 1 hour) exposures and intermediate areas of 500  $\mu\text{m}$  x 500  $\mu\text{m}$  required intermediate ( $20\text{mW}/\text{cm}^2$  for 30 minutes) exposures to facilitate vesicle formation. To elucidate fully the level of spatial control over formation, large images were generated using the stitching software available in Nikon Elements to scan a large area

over and around the localized irradiation. These images demonstrated localized formation of vesicles; however, due to their ability to diffuse away from their region of formation, the spatial resolution was limited (Figure 3.3).

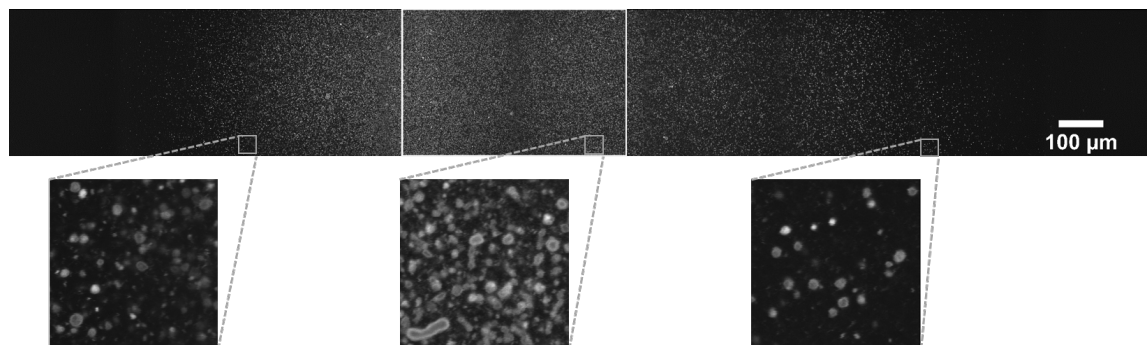


**Figure 3.3.** Slides containing alkyne functionalized lysolipid (2.5 mM), dodecyl azide (2.5 mM), CAP (1 wt%), and fluorescent dye (2  $\mu$ M) were irradiated with 400 nm light over an area of 500  $\mu$ m x 500  $\mu$ m at an intensity of 20 mW/cm<sup>2</sup> for 30 minutes. Following development overnight, these slides exhibited localized formation of vesicles, albeit with patterns limited by vesicle diffusion. The area between the inserted white lines indicates the approximate boundaries of the irradiated area while the expanded areas enable better visualization of giant vesicle formation. Due to the image stitching and uneven fluorescent excitation within each frame, boundaries between frames sometimes appeared darker than normal.

To determine if the spreading was due to diffusion of vesicles or the Cu(I) catalyst, initiation was conducted in the presence of a Cu(I) scavenger, 4-dimethylaminopyridine (DMAP) using the same protocol as before. However, rather than using the copper-liganded photo-initiator, 2.5 mM lithium phenyl-2,4,6-trimethylbenzoylphosphinate<sup>144</sup> and 2.5 mM copper sulfate were used to focus on the copper catalyst independently. After irradiation and development, spreading was still apparent although overall vesicle generation had been decreased leading us to believe that vesicle diffusion, not catalyst diffusion, was responsible for the appearance of vesicles outside the exposed area.

To verify that the structures produced by these formation methods were indeed vesicles, encapsulation experiments were conducted in the presence of 100uM sulforhodamine dye followed by dilution after the samples had been given sufficient time to develop. Fluorescence microscopy confirmed the formation of vesicles only upon exposure to 400-500nm light (Figure S3.2). Multilamellarity of the vesicle compartments was identified using cryo-TEM (Figure S3.3).

Overall, these results proved the ability to irradiate a solution of reaction components to induce the formation of vesicles. This solution, as it does not involve the spatially constrained requirements of techniques such as lipid film hydration or microfluidics, would allow for the flow of this reaction mixture into a wide range of environments. This flexibility opens up the possibility to form vesicles on command wherever the researcher requires, eliminating time consuming steps that could lead to the potential application of stressing forces. Because this reaction is dependent upon a reduced copper catalyst, it can be assumed that the elimination of oxygen from the system would only serve to enhance the efficiency of bilayer formation.

Additionally, through the use of a visible light photoinitiator, this system introduces the potential for spatiotemporal control over vesicle formation without the potentially damaging exposures that are involved in some previously documented techniques. A large sector of the interest in vesicles is generated by those studying membrane dynamics or those working on artificial cells, both of which involve the encapsulation of DNA or proteins, or the integration of proteins into the lipid bilayer. These molecules can be particularly sensitive, resulting in structural, functional, or mutagenic changes upon exposure to UV<sup>145</sup> or denaturation from excessive heating. Because studies are focused on

the activity of these encapsulated compounds, it is necessary to maintain their native structure. Therefore, if they are to be incorporated into the formation medium, it becomes necessary that not only the experimental conditions but also the formation conditions are mild. To this end, this formation procedure offers a distinct approach as compared to those which used UV exposure<sup>137</sup> or localized IR heating<sup>135,136</sup> to generate vesicles in a spatiotemporally controlled manner by instead introducing a stimulus that is less damaging to many encapsulated biologically active compounds. Additionally, the copper used to catalyze this reaction will not negatively impact the biological molecules intended to be studied; however, the toxicity of copper in living systems will require the determination of biocompatibility of this system and potentially the integration of more biologically inert ligands<sup>146,147,148</sup> if this system is to be translated into a living cell framework in the future.

Beyond the utility of a more mild stimulus, the use of visible light to generate the catalyst opens up the possibility for two-wavelength systems. By building upon previously documented studies on control over vesicle characteristics or behavior, using 400-500 nm light enables the subsequent processing of the vesicles by exposure to a second wavelength of light. For example, following formation, behaviors such as fusion or disruption<sup>52-54,56,149-152</sup> can be induced using UV or red wavelengths all from the original reaction solution.

### **Enhanced density and control over size *via* photo-initiation**

An unexpected benefit found upon photoinitiation of the CuAAC formation reaction was the development of a much higher vesicle density upon irradiation as opposed to the previously developed sodium ascorbate system. In order to quantify this difference in



density and vesicle characteristics, initiation of vesicle formation was conducted using a high exposure (20 mW/cm<sup>2</sup> for 1 hour) over an area of 200 um x 200 um in the presence of CAP (1 wt%) for one sample while 2.5 mM sodium ascorbate and 0.25 mM CuSO<sub>4</sub> were used to initiate an otherwise similarly prepared sample. Both samples contained the same alkyne lysolipid (2.5 mM), dodecyl azide (2.5 mM) and rhodamine-DHPE (2 uM). Scans were taken of both samples after overnight development and the resulting images were processed using ImageJ software to generate a vesicle count based on distance along the x-axis. Graphing these counts, it became apparent that, over a 100 um stretch, an approximate 400-fold increase in vesicle density was achieved by photoinitiating the reaction (Figure 3.4). Due to the crowding resulting from the high density at the center of formation, it was not always possible to separate each vesicle boundary from that of its neighbor resulting in a lower than normal count at the center, suggesting that this number could potentially be even higher.

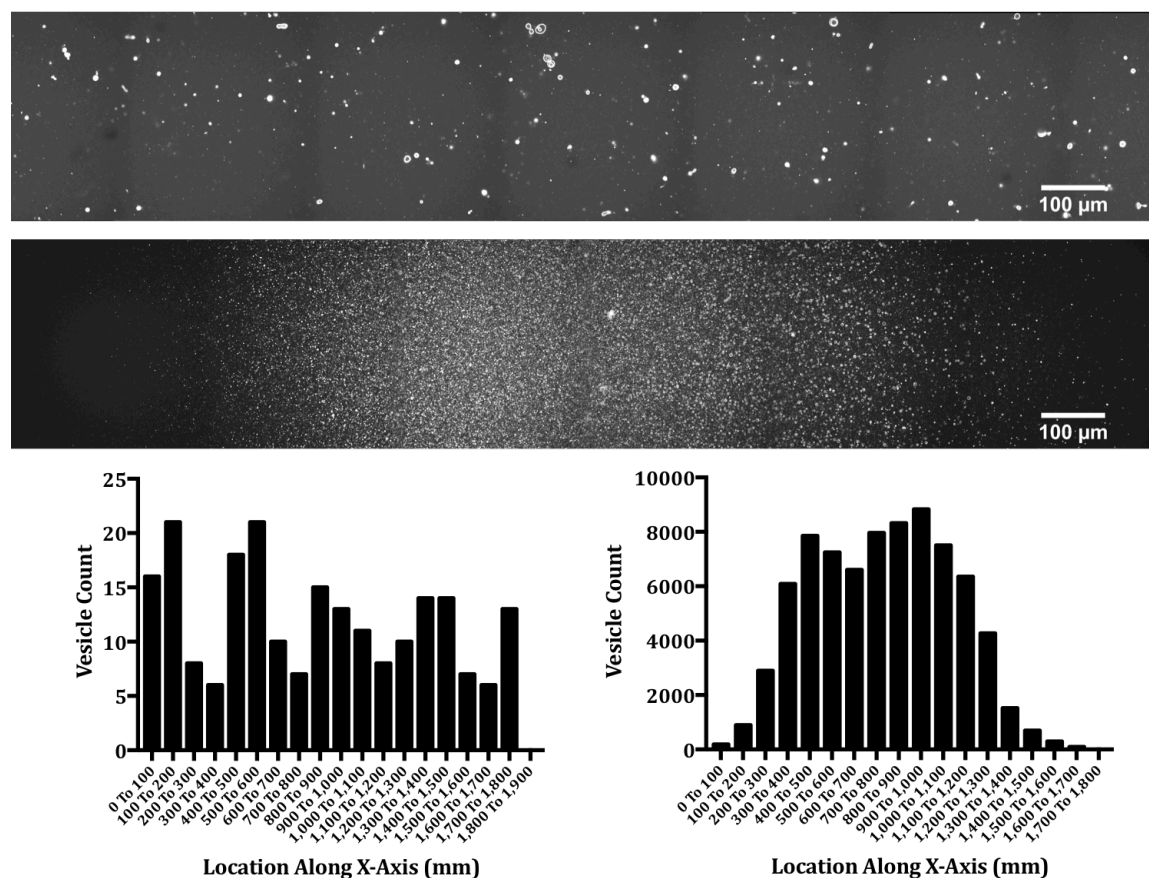


**Figure 3.4.** Initiation of vesicle formation from alkyne lysolipid (2.5 mM) and dodecyl azide (2.5 mM) using sodium ascorbate (2.5 mM) and copper sulfate (0.25 mM) (top) versus initiation using CAP (1 wt%) exposed to 400 nm light over an area of 200 μm x 200 μm at an intensity of 20 mW/cm<sup>2</sup> for 1 hour (bottom). Resulting vesicle densities from sodium ascorbate initiation (left) versus photo-initiation (right) indicate an over 400-fold increase when formation is initiated using light.

This enhanced density provides multiple benefits for the study of vesicles. In any study, it allows for more simple location and identification of the vesicles. More importantly, it makes it possible to observe many vesicles all at once, allowing for the collection of statistically significant data on the impact of various stimuli on phospholipid membranes.

Beyond the benefit of increased formation density, as different initiation conditions were tested, it became apparent that the maximum cross-sectional area of the vesicles present in each slide was responsive to the initiation conditions. To test the extent of this effect,

vesicle formulations containing alkyne functionalized lysolipid (2.5 mM) and aliphatic azide (2.5 mM) along with rhodamine-DHPE (2  $\mu$ M) and CAP (1 wt%) were sealed under coverslips with 76  $\mu$ m spacers to reduce compression and distortion of the formed vesicles. These slides were exposed to a 2 mm x 2 mm square of 400 nm light using the DLP system at either 20 mW/cm<sup>2</sup> for 10 minutes or 50 mW/cm<sup>2</sup> for 4 minutes for a more rapid exposure to the same dose of photons. Following development overnight, these slides were imaged using fluorescence microscopy. While both samples showed development of small vesicles away from the periphery of the exposed area (as they can diffuse more quickly) and giant vesicles within the exposed area, a slight increase in maximal vesicle diameter can be seen when a lower intensity was used (Figure 3.5).

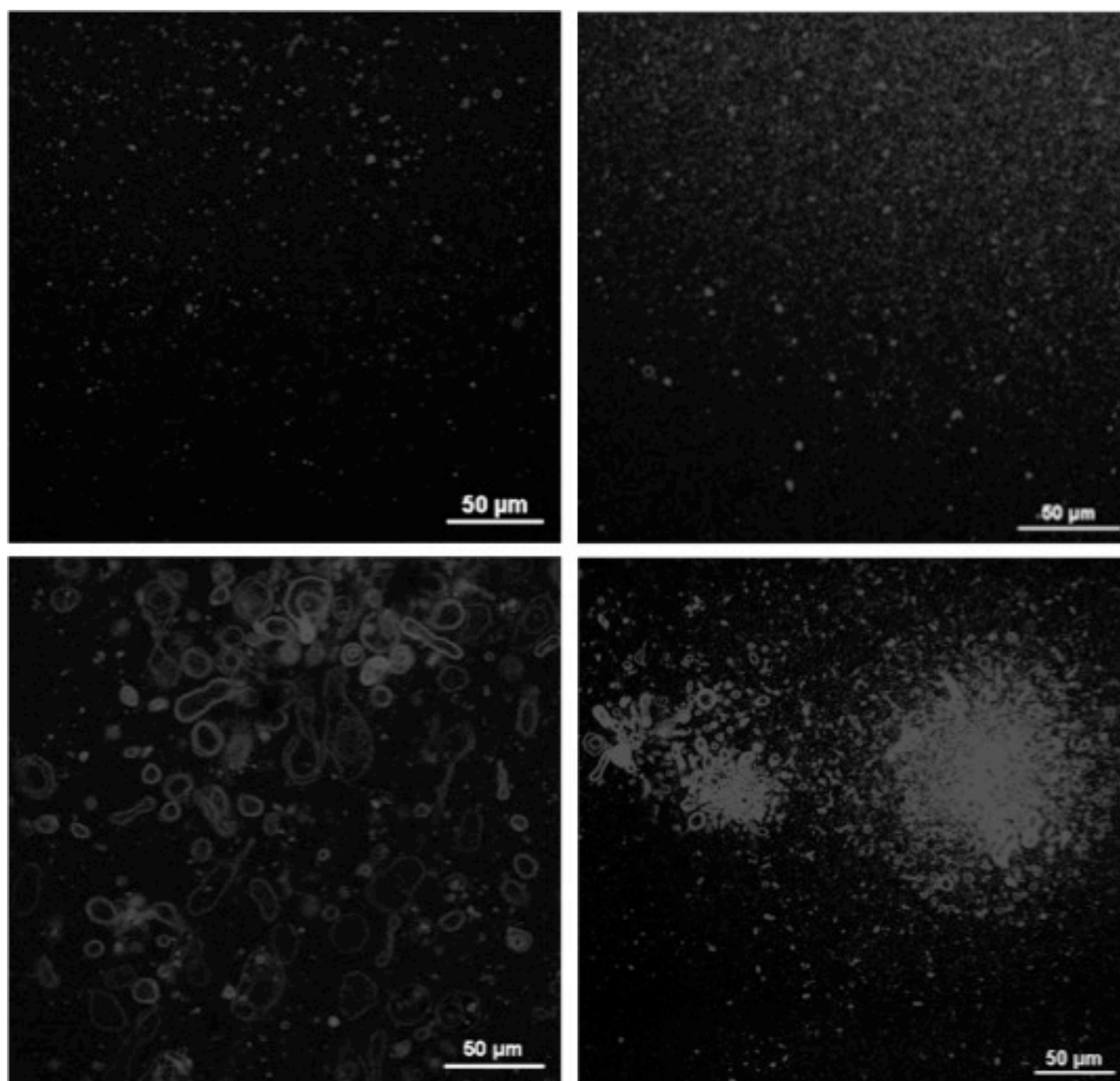


**Figure 3.5.** Sealed slides containing alkyne lysolipid (2.5mM), aliphatic azide (2.5mM), CAP (1wt%) and rhodamine-DHPE (2uM) were photopatterned with 400nm light over an area of 2mmx2mm at an intensity of 20mW/cm<sup>2</sup> for 10 minutes (left) or 50mW/cm<sup>2</sup> for 4 minutes (right). Representative images from each slide were taken to demonstrate formation of giant vesicles visible by fluorescence microscopy. An increase in vesicles of the largest dimensions is found in slides exposed at a lower intensity, while the density of the smaller vesicles appears to increase upon exposure to the higher intensity.

Alternatively, to determine the effect on size of this variation in intensity at which the photon dose is applied, vesicle populations were analyzed using Nanoparticle Tracking Analysis (NTA). Samples were prepared in vials fitted with glass inserts following the same lysolipid and aliphatic tail concentrations used previously with 1wt% CAP. Following

mixing, the entire vial was exposed to 20mW/cm<sup>2</sup> 400-500nm light for 10 minutes, or the same dose was applied by exposing samples to 50mW/cm<sup>2</sup> for 4 minutes. After undisturbed overnight development, samples were taken from the top of each vial and diluted before being injected into the NTA. Upon analysis of the results, it became apparent that the lower intensity produced vesicles which are large (over 200nm in diameter) as well as small vesicles (under 200nm in diameter) while the higher intensity primarily produced small vesicles (Figure 3.6).

To determine the potential cause of this variation in size, HPLC vials containing alkyne lysolipid, aliphatic azide, and CAP at the concentrations used above were exposed to 20mW/cm<sup>2</sup> 400-500nm light for 10 minutes and injected onto the LC-MS at various time points. Conversion halted two hours following the termination of exposure, despite not all alkyne lysolipid having been consumed (Figure S3.4). This incomplete conversion can be attributed to the squared concentration dependence on the copper catalyst<sup>153</sup> and could result in phospholipid vesicles budding from the surface of the lysolipid stabilized oil droplets at limited, irradiation dependent catalyst sites, leaving behind unreacted precursors.

Overall, this control over size could allow for more simple membrane dynamics studies as the size produced in shear-free environments generate relatively much larger vesicles, making visualization simpler. Additionally, giant vesicles formed around the exposure area tended to produce much more irregular structures while the smaller vesicles found at the periphery were more spherical. Due to their large size and alterable shape, vesicles formed in this manner make attractive candidates for the production of artificial cells.

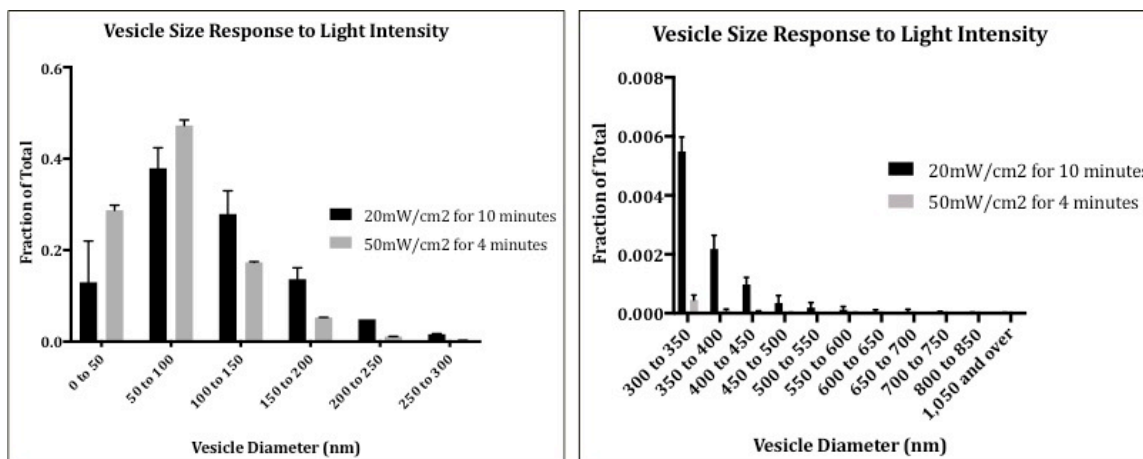


**Figure 3.6.** Vesicle initiation using a rapid, high dose (50 mW/cm<sup>2</sup> for 4 minutes) versus a slower dosing (20 mW/cm<sup>2</sup> for 10 minutes) when equal quantities of lipid precursors ([alkyne lysolipid]=[dodecyl azide]=2.5 mM) were used resulted in the formation of drastically different populations. Under the higher intensity exposure, vesicles have smaller cross-sectional areas with greater overall numbers while the slower dose results in larger vesicles that are fewer in number.

### Section 3.4. Conclusion

Through the incorporation of a copper-ligand photoinitiator complex into the CuAAC-based formation of phospholipids, it became possible to spatiotemporally control the initiation of vesicle formation using visible light. This process opens the door for two-wavelength formation and alteration processes incorporating this formation technique with previously documented vesicle alteration methods as well as protecting potentially encapsulated compounds. Beyond the development of a novel vesicle formation method, it was discovered that the maximum vesicle size was responsive to the intensity of light applied. Additionally, this method resulted in a much higher density of vesicles in the formation area. These advances expand the control over vesicle formation as well as their characteristics as is often desirable for the reliable study of membranes and the development of artificial cells.

### Section 3.5. Supplementary Figures

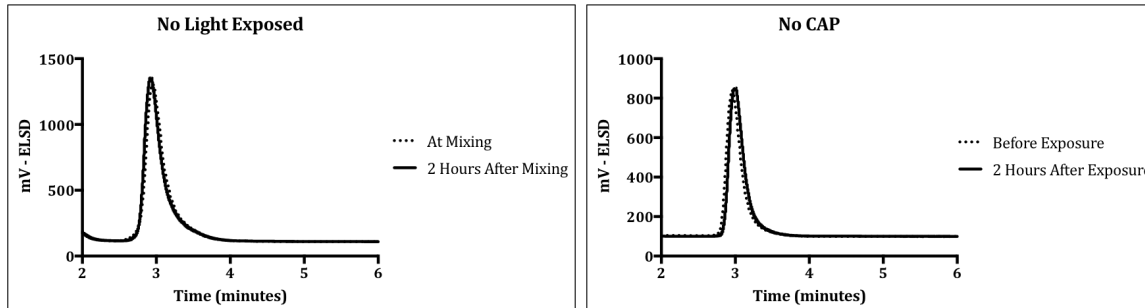


**Figure S3.1.** Mixtures containing alkyne functionalized lysolipid (2.5 mM), dodecyl azide (2.5 mM), and CAP (1 wt%), showed no formation of triazole phospholipid when left in the dark (left) and the same formulation for which CAP was removed and a 20mW/cm<sup>2</sup>, 400-500nm light exposure was applied for 60 minutes (right) also saw no formation of triazole phospholipid.

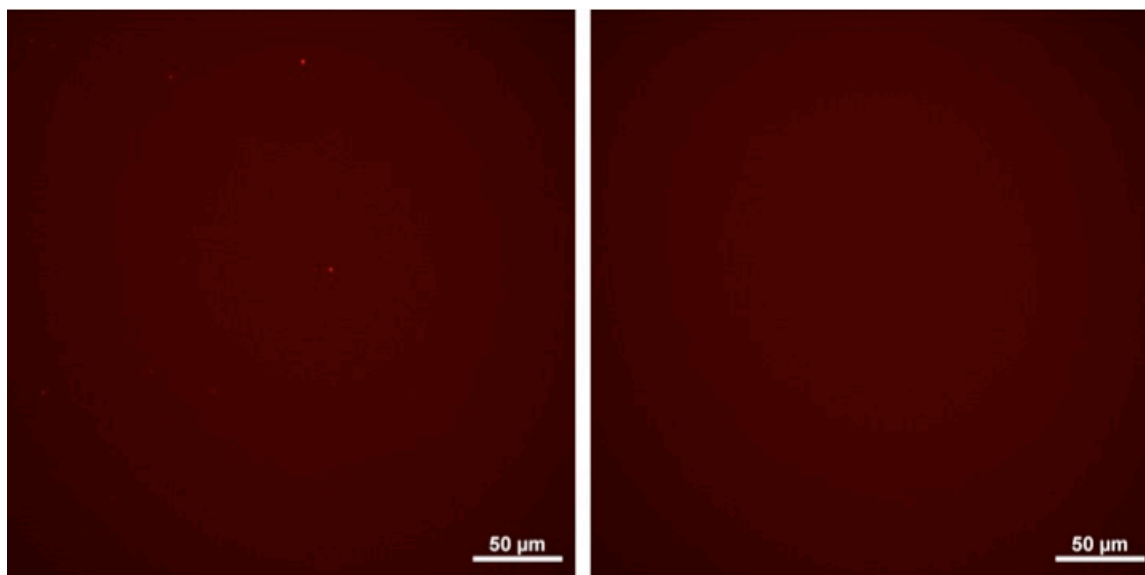


**Figure S3.2.** Samples containing alkyne functionalized lysolipid (2.5 mM), dodecyl azide (2.5 mM), CAP (1 wt%), and sulforhodamine (100uM) were either exposed to 20mW/cm<sup>2</sup> 400-500nm light for 30 minutes or were left in the dark. After 4 hours of development, both were diluted 1:10 on slides and imaged using fluorescent microscopy. Those exposed to light produced vesicles (left) while samples kept in the dark did not (right).

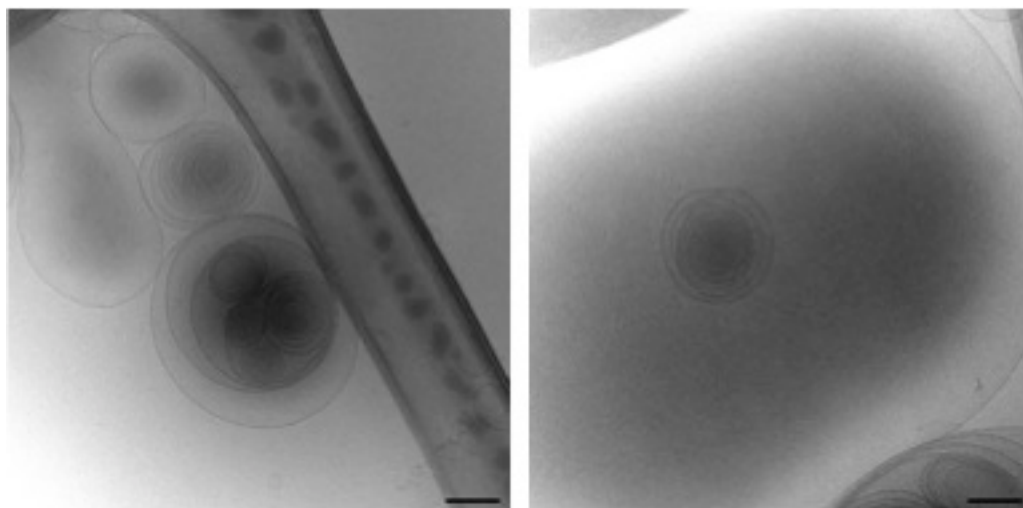


**Figure S3.3.** Cryo-TEM images of a standard formulation ([alkyne]=[azide]=2.5 mM and [CAP]= 1 wt%) exposed to 20mW/cm<sup>2</sup> 400-500nm light for 30 minutes. Scale bar denotes 200nm.

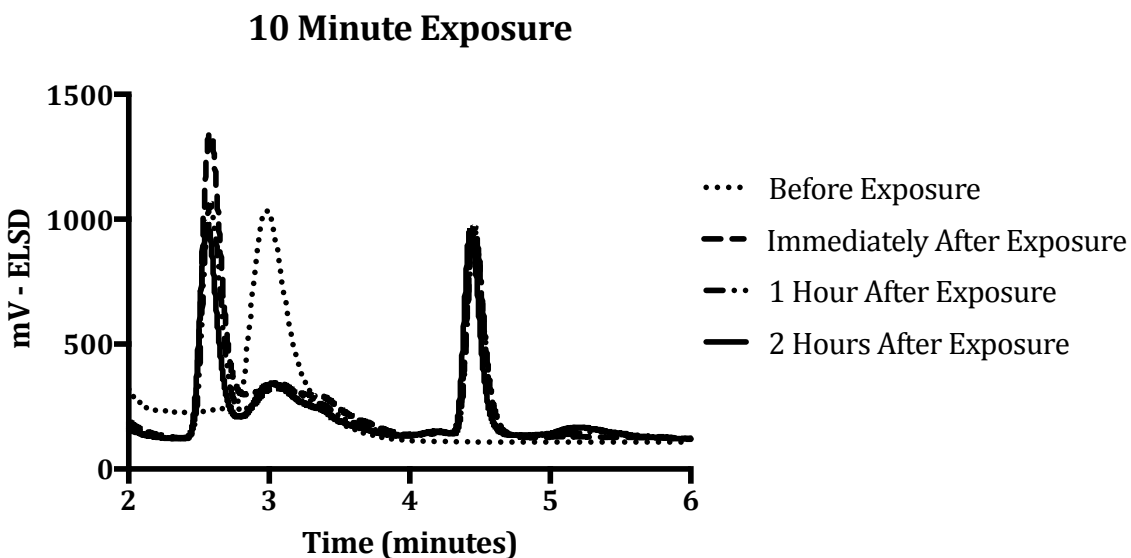


**Figure S3.4.** Vials containing alkyne functionalized lysolipid (2.5 mM), dodecyl azide (2.5 mM), and CAP (1 wt%) were exposed to 20mW/cm<sup>2</sup> 400-500nm light for 10 minutes. Formation of triazole phospholipid progressed over the first 2 hours following exposure, resulting in incomplete consumption of the alkyne lysolipid.

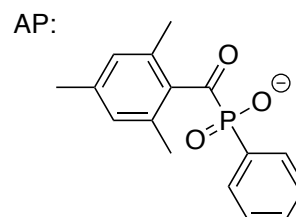
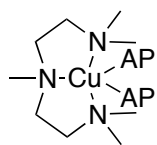
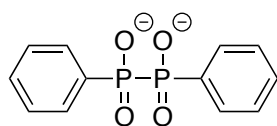




**Figure S3.5.** Hypophosphonate salts (left) produced from CAP photoinitiator (right) upon exposure to 400-500nm light<sup>154</sup>.

## Chapter 4

### Formation of Lipid Vesicles *In Situ* Utilizing the Thiol-Michael Reaction

#### Section 4.1. Introduction

In the fields of drug<sup>32,33,35,37,39</sup> and cosmetics delivery<sup>155-157</sup>, cellular membrane modeling<sup>60,61,63,158,159</sup>, artificial cell design<sup>76-78,80,87,104,160,161</sup>, microreactor development<sup>57-59,162</sup> as well as others, phospholipid-based vesicles have found great potential since their discovery in the early 1960s<sup>1</sup>. Composed primarily of phospholipid molecules, these lipid vesicles, or liposomes, mimic cell membranes. Lipids are assembled with charged head-groups extended into solution and hydrophobic tail domains sequestered into the middle of the bilayer. The bilayers enwrap an internal aqueous compartment, effectively separating it from the surrounding media, minimizing contact of the hydrophobic chains with the aqueous environment. This lipid-water interface enables encapsulation of hydrophobic molecules within the bilayer and hydrophilic compounds inside the interior compartment, thereby imparting their utility on this wide range of fields.

However, while their structure is ideal for encapsulation, to enable the use of liposomes for many of these applications, it becomes necessary to introduce novel behavior, responsiveness or other characteristics into the phospholipid membrane<sup>36</sup>. For example, synthetic phospholipid molecules bearing functionalities<sup>36</sup> such as photo-cleavable structures<sup>52</sup>, double or triple bonds for polymerization<sup>55,56</sup>, isomerizable structures<sup>53</sup> and porphyrin rings<sup>50,51</sup> have been studied to induce permeability of the membrane for stimuli-responsive drug delivery. However, in order to generate and utilize

these lipids, intensive and complicated syntheses are often necessary, resulting in a more laborious and time-consuming design-build-test process.

Recently, a new method for the *in situ* formation of phospholipid molecules was developed for covalently attaching a hydrophobic tail to a functionalized lysolipid backbone utilizing the copper-catalyzed azide-alkyne cycloaddition (CuAAC) reaction<sup>118,143,163</sup>. This lipid formation method could be employed to enable simplified incorporation of synthetic moieties into the lipid structure to generate designer lipids. However, many systems are not amenable to the copper catalyst necessary for the CuAAC reaction due to ligand-dependent toxicity effects in living systems<sup>146,164,165</sup>. Alternatively, the functionality of interest may not be orthogonal to the redox reaction necessary to generate the Cu(I) catalyst or if a terminal alkyne functionality is to be incorporated in the tail this formation chemistry could not be used. In contrast, the thiol-Michael click reaction has enhanced biocompatibility in that it avoids the use of Cu, is readily catalyzed by relatively weak bases and nucleophiles, is amenable to the aqueous conditions required for *in situ* liposome formation, proceeds rapidly to completion under ambient conditions without significant side reactions, and is compatible with the usage of a wide range of natural and synthetic thiols as well as alkene functionalities. In this reaction, thiol groups and electron deficient alkenes such as acrylates, maleimides, vinyl sulfones and others undergo coupling in the presence of basic or nucleophilic catalysts *via* a thiolate anion intermediate to produce a thioether product<sup>125</sup>. To increase the range of designer lipid systems compatible with the *in situ* formation method, we have incorporated acrylate and thiol functionalities into the tail and lysolipid structures, respectively, to enable thiol-Michael formation of phospholipids. The power of this formation chemistry lies in the fact

that this system is not limited to the acrylate tail used here. By utilizing the thiol-Michael addition reaction, lipids are functionalized using any number of acrylate and methacrylate monomers available for commercial purchase, and new vinyl sulfone or acrylate monomers can be easily synthesized from compounds of interest bearing free hydroxyl groups. Additionally, vast quantities of bioconjugate chemistry have revolved around the use of maleimide-functionalized molecules and cysteine-functionalized peptides, making each of those systems immediately available for use as the ene or thiol, respectively, in this synthetic membrane formation method. Beyond the array of molecules available for use in the thiol-Michael reaction, the use of photo-bases<sup>166,167</sup> for photo-initiated thiol-Michael reactions enables spatiotemporal control in liposome formation using this method.

## **Section 4.2. Methods**

**General.** <sup>1</sup>H nuclear magnetic resonance (NMR) spectra for product verification were gathered on a Bruker Ascend 400 spectrometer. Reactions were monitored on an Agilent 1100 Series HPLC fitted with an Agilent Zorbax 5um 4.6x50mm C8 column coupled with Agilent G1946D Mass Spectrometer and Sedex Evaporative Light Scattering Detector.

LAP was synthesized following a previously published method<sup>144</sup> and other compounds were purchased from standard sources and were used as received.

### **Synthesis of Thiol Lysolipid (SHPC):**

To a dry 10mL round-bottomed flask equipped with magnetic stir bar was added 70mg 1-palmitoyl-2-hydroxy-*sn*-glycero-3-phosphocholine and 3-3.5mL chloroform. Following stirring for 30 minutes under argon the solution was cooled to 0°C and 60mg 3,3'-dithiodipropionic acid, 80mg EDAC and 5mg DMAP was added while stirring. The solution

was allowed to react overnight under argon. Following reaction, the  $\text{CHCl}_3$  was removed and products were dissolved in  $\text{H}_2\text{O}$  for 30 minutes. This solution was transferred to 1,000MW cutoff dialysis tubing and dialyzed overnight. Following dialysis, the solution was transferred to a vial equipped with stir bar and 200mg TCEP-HCl was added. 1M NaOH was added dropwise to neutralize the solution followed by spinning overnight. This solution was then transferred to fresh 1,000MW cutoff dialysis tubing for overnight dialysis. The product was lyophilized to produce a white powder. Yield = 71%  $^1\text{H}$  NMR (400mHz,  $\text{CDCl}_3$ )  $\delta$ : 5.24 (m, 1H), 4.36 (dd,  $J=12.1, 3.0$  Hz, 1H), 4.27 (m, 2H), 4.15 (dd,  $J=12.1, 7.4$  Hz, 1H), 3.95 (m, 2H), 3.75 (m, 2H), 3.32 (s, 9H), 2.75 (m, 2H), 2.67 (m, 2H), 2.28 (m, 2H), 1.80 (t,  $J=8.2$  Hz, 1H), 1.57 (m, 2H), 1.25 (m, 24H), 0.87 (t, 3H).

#### **Synthesis of Dodecyl Acrylate:**

To a round bottom flask with stir bar was added 1.86g 1-dodecanol in 10mL THF and allowed to dissolve. 10mL of a THF mixture with 1.02g TEA was added to the round bottom and cooled to  $0^\circ\text{C}$ . 1.09g acryloyl chloride was added dropwise and the solution was allowed to equilibrate to room temperature. Stirring continued for at least 3 hours. Dodecyl acrylate product was extracted with methylene chloride and washed with water.  $^1\text{H}$  NMR (400mHz,  $\text{CDCl}_3$ )  $\delta$ : 6.35 (dd,  $J=17.3, 1.6$  Hz, 1H), 6.07 (dd,  $J=17.3, 10.4$  Hz, 1H), 5.75 (dd,  $J=10.4, 1.6$  Hz, 1H), 4.10 (t,  $J=6.8$  Hz, 2H), 1.63 (m, 2H), 1.23 (m, 18H), 0.84 (m, 3H).

#### **Synthesis of Alkyne-Acrylate Tail:**

To a round bottom flask with stir bar was added 0.57mL 10-undecyn-1-ol, 1.25mL TEA and 33mg BHT in 15mL methylene chloride under nitrogen. The mixture was cooled to  $0^\circ\text{C}$  and 0.36mL acryloyl chloride was added dropwise. 36mg DMAP was added and the mixture

was allowed to equilibrate to room temperature and left to react overnight. The product was washed with sodium bicarbonate, water and brine, dried and filtered before methylene chloride was removed leaving the product as an oil. Yield = 69%  $^1\text{H}$  NMR (400MHz,  $\text{CDCl}_3$ )  $\delta$ : 6.40 (dd,  $J=17.3, 1.5$  Hz, 1H), 6.12 (dd,  $J=17.3, 10.4$  Hz, 1H), 5.81 (dd,  $J=10.4, 1.5$  Hz, 1H), 4.14 (t,  $J=6.7$  Hz, 2H), 2.18 (td,  $J=7.1, 2.6$  Hz, 2H), 1.94 (t,  $J=2.7$  Hz, 1H), 1.66 (m, 2H), 1.57-1.44 (m, 2H), 1.42-1.2 (m, 10H)

**Preparation of Lipid Solutions.** Prior to use, SHPC was reduced overnight in an equimolar mixture of TCEP-HCl and NaOH in a 2:1 SHPC:TCEP solution. For monitoring of the phospholipid coupling reaction *via* LCMS, a 100uL solution was prepared of aliphatic acrylate in water (5mM), reduced SHPC mixture (5mM SHPC), and 2-methylimidazole (2.5mM) in HPLC vials fitted with 350uL Supelco glass inserts. The solution was then left at room temperature to react.

Fluorescence microscopy samples were prepared similarly ([reduced SHPC]=[acrylate tail] = 5mM, [2-methylimidazole]= 2.5mM) with the addition of 2 $\mu\text{M}$  rhodamine-DHPE. Samples were mixed, sealed under coverslips, and allowed to develop for 48 hours prior to imaging. Polymerizable lipids were prepared similarly to those described above ([reduced SHPC]=[alkyne AT]=5mM, [2-methylimidazole]=2.5mM, and [LAP]=5mM, as well as [rhodamine-DHPE]=2 $\mu\text{M}$  and [fluorescein]=500  $\mu\text{M}$  if sample was to be imaged under fluorescence microscopy).

**Microscope Imaging.** Fluorescence imaging was performed using a Nikon A1R laser scanning confocal microscope equipped with Nikon Elements software version 4.20. In all

cases, a 561nm laser was employed to excite the rhodamine-DHPE. For acquisition of TEM images, 4  $\mu$ l of sample solution was transferred onto a lacey holey-carbon grid, blotted for 1-2 seconds, and then plunge-frozen using an FEI-Vitrobot Mark IV at room temperature. The resulting vitrified sample was imaged on an FEI Tecnai F20 FEG-TEM, operating at 200kV and 25,000x magnification, using a Gatan US4000 CCD camera. The electron dose per image was limited to 20 electrons/ $\text{\AA}^2$ , with a defocus of -2 $\mu$ m, using the low-dose mode of Serial EM acquisition software.

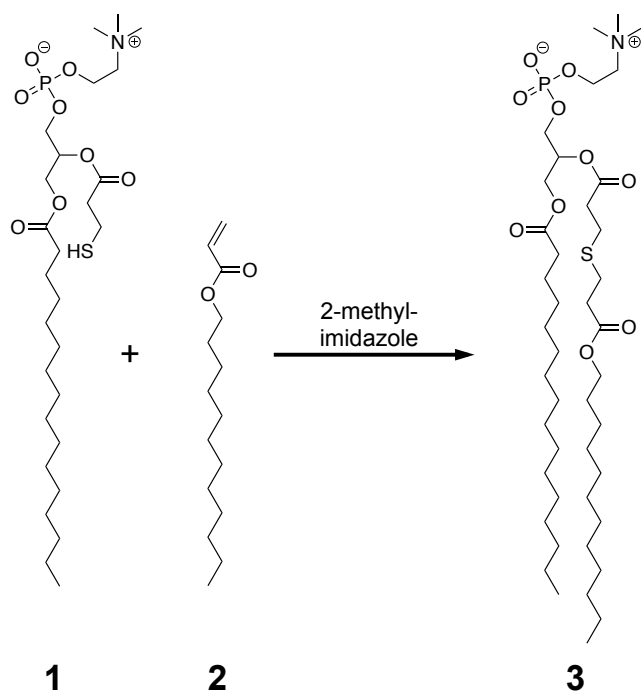
**LC-MS of Product Formation.** Phospholipid formation was conducted in HPLC vials fitted with 350 $\mu$ L glass inserts as described above with 5 $\mu$ L samples taken over the course of the reaction. Samples were injected onto an analytical Agilent LC-MS with Sedex Evaporative Light Scattering Detector controlled by ChemStation software and fitted with Agilent Zorbax 5 $\mu$ m 4.6x50mm C8 column column. A binary solvent system of 0.1% formic acid in 5:4:1 isopropanol:water:methanol and methanol was used at a flow rate of 0.9mL/minute. Peak areas of SHPC precursors were normalized to the peak area measured at 0 hours while products were normalized to the peak area at 48 hours to calculate the degree of conversion.

### **Section 4.3. Results and Discussion**

#### **Expanding the reaction toolbox for the generation of synthetic phospholipids**

The highly efficient thiol-Michael addition reaction was employed to form a functionalized phospholipid (see 3 in Scheme 4.1) *via* functionalization of the lysolipid with a primary thiol [1] and the subsequent nucleophile-catalyzed reaction of the thiol with an

aliphatic acrylate tail [2] as shown in Scheme 4.1. This approach enables the design and implementation of an incredible range of new, functionalized phospholipids based on aliphatic tails, other functionalized molecules chosen from the great variety of acrylate monomers already commercially available, molecules that are readily formed by reactions of acids or other terminal functional groups, or the array of maleimide-functionalized bioconjugate molecules available.



**Scheme 4.1.** A lysolipid bearing a free thiol functionality (1) readily and rapidly undergoes thiol-Michael addition with an acrylate functionalized tail (2) in the presence of a water-soluble, nucleophile catalyst, 2-methylimidazole, to produce a thioether-containing phospholipid product (3). The precursors in this process assemble into micelles and stabilized oil droplets and transition to bilayer structures and liposomes *in situ* upon addition of the second aliphatic tail and the subsequent Michael addition reaction.

SHPC and the aliphatic acrylate tail (AT) were mixed at a concentration of 5mM in the presence of 2.5mM of a water-soluble nucleophile catalyst, 2-methylimidazole. A weak base catalyst, triethylamine (TEA), was also explored as a potential catalyst. However, at



the dilute conditions necessary, the reaction rates were exceedingly slow whereas increased concentrations of TEA leads to hydrolytic degradation of the esters present in the lipid structures. Stronger nucleophiles were probed as well, but suffered from limitations in aqueous solubility. Samples drawn at various time points were injected into an analytical LC-MS equipped with an Evaporative Light Scattering Detector (ELSD) to monitor the progression of the reaction. Approximately 90% of SHPC [1] was coupled to AT [2] over the course of 48 hours, resulting in production of the synthetic phospholipid product [3] (Figure 4.1A,B). This relatively slow reaction time is likely due to the dilute reaction conditions, the weak nucleophile catalyst, and the stoichiometric reactant mixture. It should be noted that the progression of the reaction under these disadvantageous reaction conditions to near-completion is another illustration of the capabilities of the thiol-Michael addition reaction.

Certain alkene substituents, for example maleimides, and certain conditions, such as highly polar solvents, have been demonstrated to cause “catalyst-free,” solvent-mediated thiol-Michael addition<sup>168,169</sup>. Here, to assess whether a catalyst is necessary for this reaction, SHPC [1] (5mM) and AT [2] (5mM) were mixed in the absence of any catalyst. Over the course of 48 hours, approximately 50% of SHPC was consumed resulting in formation of phospholipid [3]. However, this insufficient degree of conversion demonstrates the need for a catalyst to reach satisfactory conversion under the desired conditions (Figure 4.1C,D).

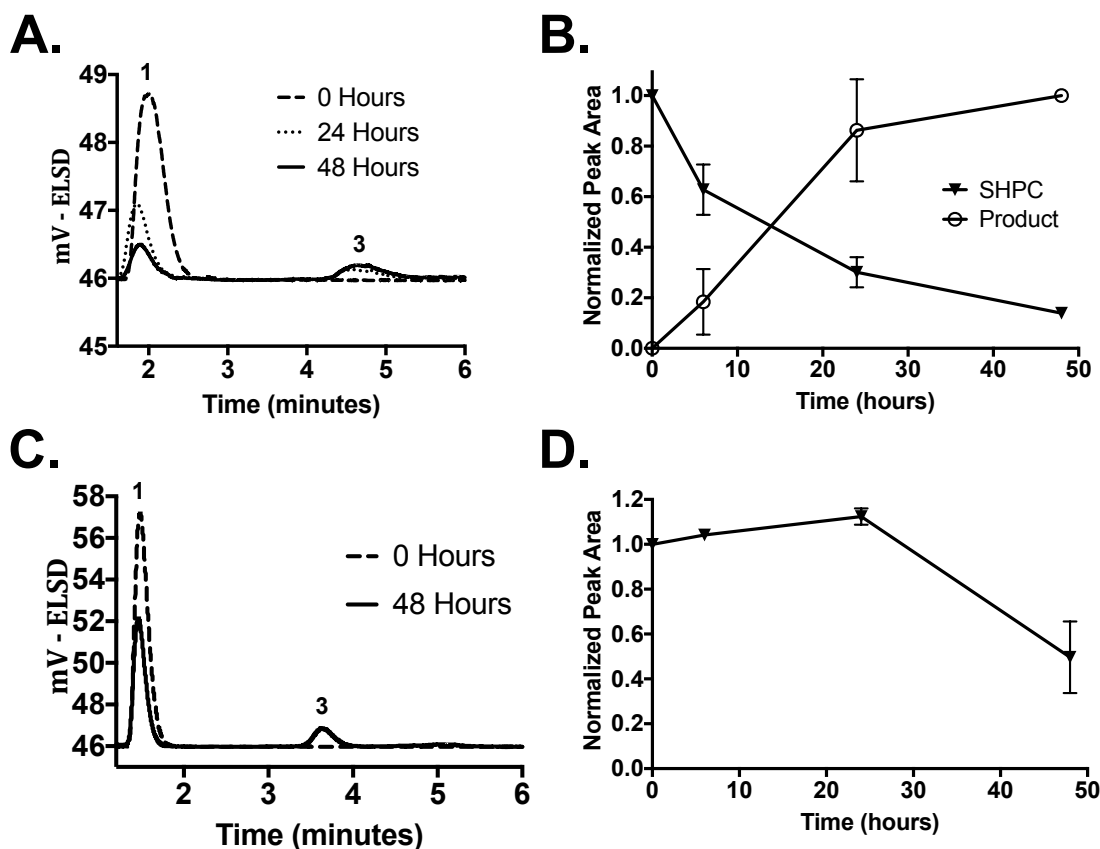


**Figure 4.1.** LC-MS coupled with an Evaporative Light Scattering Detector (ELSD) monitoring the progression of the thiol-Michael addition reaction. Reaction solutions of 5mM thiol lysolipid (SHPC) [1], 5mM aliphatic acrylate tail [2], and 2.5mM 2-methylimidazole catalyst were mixed and sampled at various time points to determine conversion (A). SHPC peak area, normalized to 0 hours, and product peak area, normalized to 48 hours, demonstrate almost 90% conversion over the course of 48 hours (B). When catalyst is absent, the reaction occurs to approximately 50% conversion over the course of 48 hours (C,D).

Fluorescence microscopy and cryo-TEM enable imaging of the lipid assemblies. In this way, it is possible to determine the ability of the phospholipid products to self-assemble into lipid vesicles, or liposomes. For fluorescence microscopy, the AT and reduced SHPC (5mM) were mixed in the presence of 2-methylimidazole catalyst (2.5mM) and a membrane bound, fluorescent dye, rhodamine-DHPE (2uM). Following mixing, a drop was placed on a sealed slide and allowed to develop at room temperature.

Fluorescence microscopy verified the presence of liposomal structures following 48 hours of development, as evidenced by a brightly fluorescent membrane surrounding a dark interior (Figure 4.2A). Cryo-TEM was conducted on the samples to verify the formation of lipid bilayers by thioether-containing phospholipids. Samples were prepared as in the fluorescence microscopy experiments, though excluding rhodamine-DHPE, and subsequently frozen following 48 hours of development. Cryo-TEM images show the presence of lipid bilayer structures in single rings rather than stacked lamellae, indicating that thiol-Michael addition mediated liposome formation using 2.5mM 2-methylimidazole catalyst results in predominantly unilamellar liposomes (Figure 4.2B). This configuration makes this *in situ* formation method particularly useful for applications requiring unilamellar structures for imaging purposes<sup>129</sup> as it results in vesicular structures over a micron in diameter directly from the reaction mixture and without any requirement of further processing.

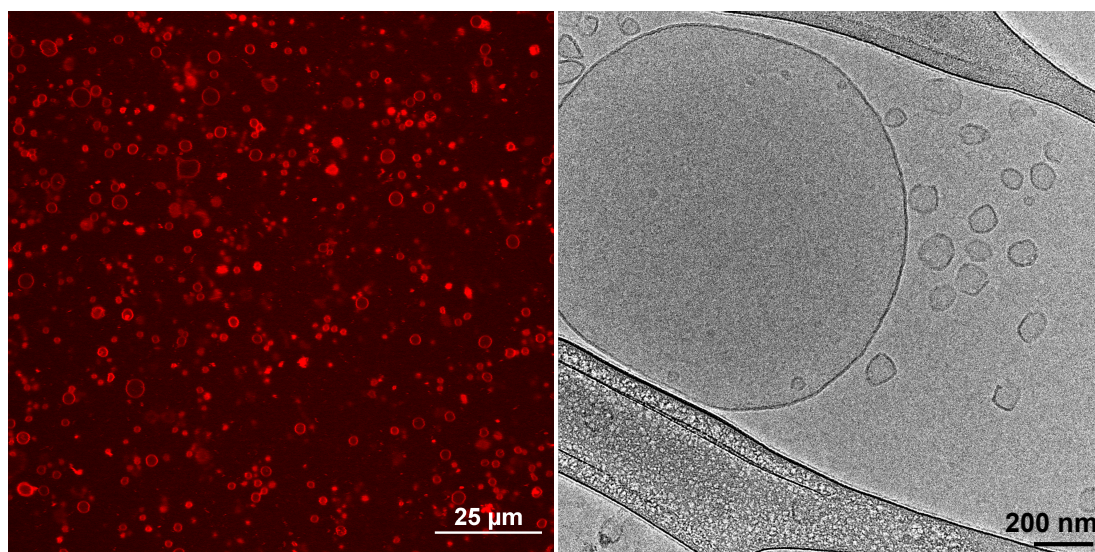
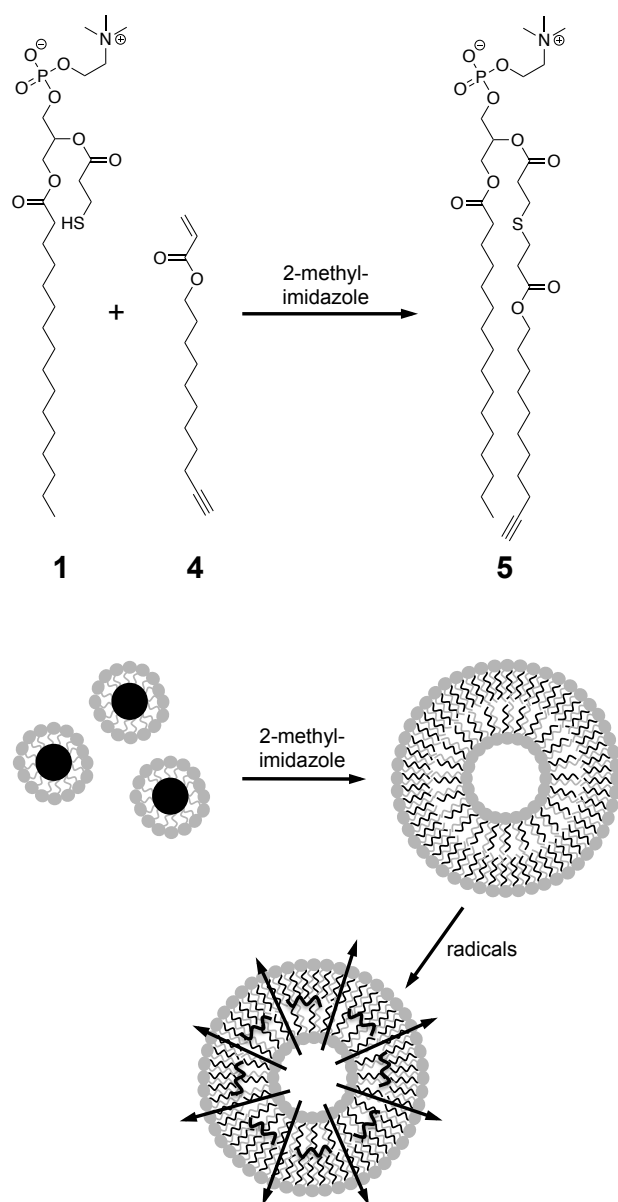


**Figure 4.2.** Microscopy images of liposomes assembled from thioether-containing phospholipid products [3]. 5mM reduced SHPC and aliphatic AT were reacted in the presence of 2.5mM 2-methylimidazole. For fluorescence microscopy imaging, 2μM rhodamine-DHPE was included in the reaction mixture. After 48 hours of reaction,

fluorescence microscopy demonstrated liposome formation (left) with most liposomes assembled in a unilamellar fashion as demonstrated using cryo-TEM (right).

### **Demonstration of the *facile* incorporation of functional moieties into the phospholipid structure**

To demonstrate the utility of the thiol-Michael induced formation of phospholipids capable of self-assembling into liposomal structures and to highlight the capacity of this approach to incorporate a variety of acrylic (or other) moieties, a second molecule capable of modifying the characteristics of the liposome system was reacted and incorporated into the phospholipid. A new aliphatic tail was designed and synthesized with an acrylate functionality for the thiol-Michael coupling as well as a terminal alkyne capable of a number of subsequent reactions. In particular, alkynes are orthogonal to the thiol-Michael addition reaction, providing a downstream functionality for a variety of reactions such as copper-catalyzed azide-alkyne cycloaddition (CUAAC)<sup>139,153</sup>, radical-mediated polymerization or radical-mediated thiol-yne addition<sup>123,170</sup>. This reactive capability could be used to modify the vesicle structure or characteristics, such as temporary enhancement of the permeability of the liposome systems upon polymerization as has been demonstrated in the literature<sup>55,56</sup> (scheme 4.2).



**Scheme 4.2.** A schematic illustrating the formation of a designer lipid bearing a terminal alkyne using the thiol-Michael formation method. A new terminal alkyne functionalized AT [4] couples to SHPC [1] in the presence of 2-methylimidazole resulting in liposomes with terminal alkynes buried in their hydrophobic core. These liposomes themselves enable subsequent modification of the membrane characteristics or behavior and as a whole demonstrate the ability to incorporate a wide array of new functionalities using this formation chemistry. As one example of characteristics enabled with this formulation, homopolymerization could be used to temporarily enhance permeability upon the generation of radicals.

Samples were injected into the LC-MS-ELSD to determine the reaction progress with samples prepared from stoichiometric reactants ([reduced SHPC]=[tail]=5mM and [2-methylimidazole]=2.5mM) including the acrylate-alkyne tail in place of the aliphatic acrylate tail. Additionally, a photoinitiator, lithium phenyl-2,4,6-trimethylbenzoylphosphinate (LAP), was included at a concentration of 5mM to enable subsequent photopolymerization and reaction of the alkyne tail following vesicle formation. Forty-eight hours after mixing, the reaction reached approximately 90% conversion (Figure 4.3A). The vesicle-containing solution was subsequently irradiated using 400-500nm light at 10mW/cm<sup>2</sup> for 10 minutes to react the alkyne. Injection of the sample on analytical LC-MS-ELSD after irradiation shows complete disappearance of the phospholipid product [5] upon radical generation, due to homopolymerization<sup>170</sup>. Lack of appearance of a new peak in the ELSD chromatogram suggests that the increased hydrophobic character of the polymer results in extensive interaction with the HPLC column causing increased retention, or the size of the polymer product results in removal from the flow by filtration upstream of column separation. Additionally, the disappearance of the phospholipid peak, without equivalent loss of SHPC, promotes the idea that phospholipid product [5] is undergoing homopolymerization and not thiol-yne reactions. To verify the persistence of liposome assembly in the presence of the terminal alkyne functionality, fluorescence microscopy was employed. Mixtures were prepared ([SHPC]=[alkyne AT]=[LAP]=5mM, [2-methylimidazole]=2.5mM, [rhodamine-DHPE]=2 μM, [fluorescein]=500 μM) and placed in a sealed glass slide. Fluorescence microscopy verified the assembly of giant liposomes following 48 hours of development (figure 4.3B).

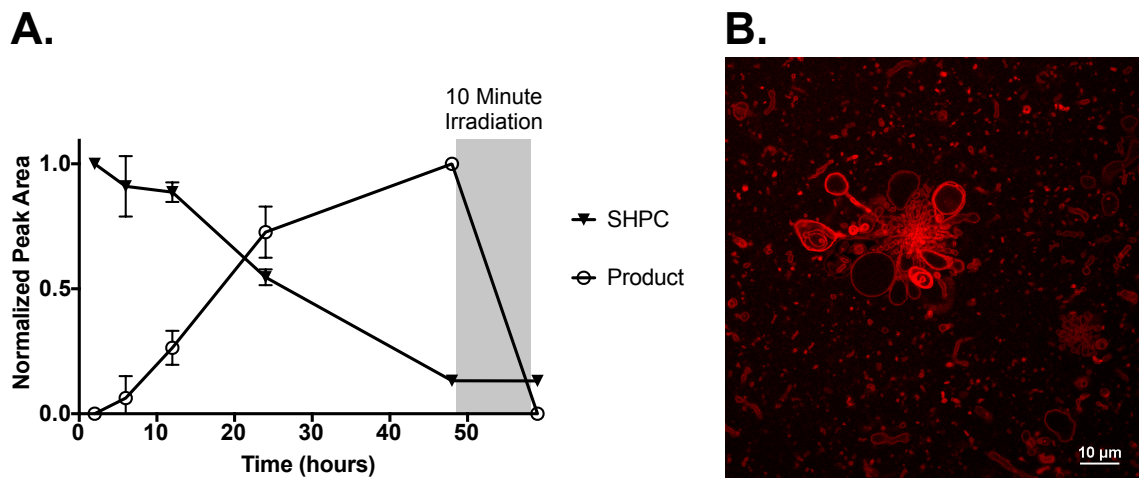


**Figure 4.3.** Designer lipid with terminal alkyne functionality synthesized using thiol-Michael addition. LC-MS with ELSD tracks the formation reaction with SHPC peak values normalized to the peak area at 0 hours while product peak values were normalized to the peak area at 48 hours. SHPC [1] and an alkyne-terminated acrylate tail [4] were reacted in the presence of 2.5mM 2-methylimidazole and 5mM LAP photoinitiator resulting in nearly 90% conversion to phospholipid [5] over the course of 48 hours. Subsequently, alkyne-functionalized phospholipids were irradiated with 10mW/cm<sup>2</sup> 400-500nm light for 10 minutes, resulting in complete consumption of the phospholipid as the alkyne polymerizes (A). Fluorescence microscopy verified the assembly of functionalized lipids into giant liposomes (B).

These results illustrate the ability to form liposomes *in situ* while incorporating new functionalities into the lipid structure by utilizing the thiol-Michael coupling reaction to functionalize the phospholipid. This formation reaction becomes part of a two-step formation and modification system where lipids can be functionalized with any of a wide range of compounds bearing electron deficient double bonds in the presence of nucleophilic catalysts followed by a second stimulus to use the incorporated moiety to enact changes in the bilayer characteristics or behavior. An added benefit of the system is the linkage connecting the lysolipid with its primary thiol is part of a class highly sensitive to hydrolytic degradation, offering future opportunities in pH-sensitive lipid degradation or triggered release of attached molecules.

#### **Section 4.4. Conclusion**

Synthetic liposomal systems have a vast array of potential applications, many of which require enhanced characteristics, tunable responses or modified behavior of the vesicles. The use of thiol-Michael click reactions for forming phospholipids to enable the *facile* incorporation of novel functionalities into the phospholipid structure is demonstrated here through the coupling of acrylate-functional tails with a thiol-functional lysolipid. This approach is compatible with the use of a wide array of acrylate, vinyl sulfone, maleimide and other functionalized compounds available commercially or readily synthesized.

The covalent coupling of thiol-functionalized lysolipids and acrylate functionalized tails using the thiol-Michael reaction enabled generation of synthetic phospholipids, and by extension liposomes, *in situ*. Assembled lipids formed giant, unilamellar vesicles making them highly useful for applications such as membrane dynamics studies and artificial cell membranes. By further modification of the acrylate tail, the ability to readily incorporate new characteristics or behaviors into the final lipid structure was demonstrated. This two-step process added a terminal alkyne tail to SHPC *via* thiol-Michael addition to produce phospholipids capable of assembling into liposomes. After the coupling reaction was complete, polymerization initiated by visible-light induced radical generation resulted in triggered homopolymerization of the lipid tails. This approach is suitable for incorporating functionalities needed to achieve a range of synthetic behaviors or characteristics based upon moieties coupled into the phospholipid structure.



## Chapter 5

### Production of Dynamic Lipid Bilayers Using the Reversible Thiol-Thioester Exchange Reaction

#### Section 5.1. Introduction

Synthetic liposomes, lipid structures<sup>1</sup> self-assembled with hydrophilic head groups extending into solution and hydrophobic chains sequestered into a bilayer core to minimize contact with water, effectively separate an aqueous compartment from the surrounding environment. With this assembly, liposomes mimic cell membrane structures and have garnered significant interest for their ability to encapsulate hydrophobic molecules within the bilayer core and hydrophilic components inside the internal compartment. These features have found applications in a wide range of fields from drug<sup>28,31-33,35-37,39</sup> and cosmetics<sup>155-157,171</sup> delivery to microreactors<sup>57-59,111,162,172</sup>. More recently, the pursuit of a bottom-up artificial cell<sup>75,78-80,82,87,104,107,160</sup> has garnered significant interest, frequently utilizing synthetic liposomes in place of the cell membrane. Their simplified structure, devoid of controlled sub-domains and countless proteins, makes liposomes ideal models for artificial cell membranes and for study of behaviors present in native cell membranes<sup>60-62</sup>.

Previous work has examined the ability to generate synthetic phospholipids, and by extension liposomes, *in situ* using a few reactions<sup>118,143,163,173</sup>. For example, utilizing coupling reactions, such as the copper-catalyzed azide-alkyne cycloaddition reaction, an aliphatic tail is added to a phospholipid-based structure bearing a charged head-group and a single aliphatic tail (lysolipid). Coupling drives the conversion of micelles and stabilized oil droplets to liposomes, enabling *in situ* assembly. However, little work has been done to

develop reversible chemistries, resulting in systems that serve as poor mimics for a native cell membrane's enzymatic ability to exchange one tail for another<sup>174</sup>. What work has been done to integrate reversibility into the membrane utilized native chemical ligation and reversible native chemical ligation, however this system requires addition of more lysolipid precursors<sup>175</sup>, limiting the number of exchanges possible before the bilayer becomes unstable due to disfavored packing.

Thiol-thioester exchange is a reversible reaction wherein a thiolate anion attacks the carbonyl carbon of a thioester resulting in a tetrahedral intermediate. Intermediates can break back down to the original compounds or to a new thiol-thioester pair<sup>176</sup>. Exchange in this fashion continues as long as thiolate anions are present, resulting in a dynamic system capable of constant remodeling. Applying this behavior to an *in situ* formation method would enable exchange of the lysolipid and tail pairs to produce a liposome mimic of cell membrane remodeling. Additionally, with this behavior present in liposome systems it would be possible to incorporate new functionalities into a pre-formed bilayer by subsequent introduction of compounds bearing thioester groups. Herein we report the use of this exchange reaction to develop a synthetic lipid bilayer capable of continued remodeling.

## **Section 5.2. Methods**

**General.** <sup>1</sup>H and <sup>13</sup>C nuclear magnetic resonance (NMR) spectra for product verification were gathered on a Bruker Ascend 400 spectrometer. Reactions were monitored on an Agilent 1100 Series HPLC fitted with an Agilent Zorbax 5um 4.6x50mm C8 column coupled with Agilent G1946D Mass Spectrometer and Sedex Evaporative Light Scattering Detector.

### **Synthesis of Thiol Lysolipid (SHPC):**

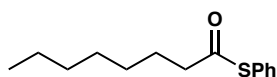
To a dry 10mL round-bottomed flask equipped with magnetic stir bar was added 70mg 1-palmitoyl-2-hydroxy-*sn*-glycero-3-phosphocholine and 3-3.5mL chloroform. Following stirring for 30 minutes under argon the solution was cooled to 0°C and 60mg 3,3'-dithiodipropionic acid, 80mg EDAC and 5mg DMAP were added while stirring. The solution was allowed to react overnight under argon. Following reaction, the CHCl<sub>3</sub> was removed and products were dissolved in H<sub>2</sub>O for 30 minutes. This solution was transferred to 1,000MW cutoff dialysis tubing and dialyzed overnight. Following dialysis, the solution was transferred to a 10mL round-bottom flask and 200mg TCEP-HCl was added. 1M NaOH was added dropwise to neutralize the solution followed by spinning overnight. This solution was then transferred to fresh 1,000MW cutoff dialysis tubing for overnight dialysis. The product was then lyophilized to produce a white powder. Yield = 71% <sup>1</sup>H NMR (400mHz, CDCl<sub>3</sub>) δ: 5.24 (m, 1H), 4.36 (dd, J=12.1, 3.0 Hz, 1H), 4.27 (m, 2H), 4.15 (dd, J=12.1, 7.4 Hz, 1H), 3.95 (m, 2H), 3.75 (m, 2H), 3.32 (s, 9H), 2.75 (m, 2H), 2.67 (m, 2H), 2.28 (m, 2H), 1.80 (t, J=8.2 Hz, 1H), 1.57 (m, 2H), 1.25 (m, 24H), 0.87 (t, 3H).

### **Synthesis of S-phenyl thioester:**

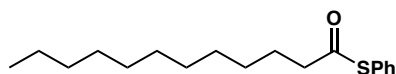
#### **S-phenyl thiooctanoate.**

To a 100 mL round-bottomed flask equipped with a magnetic stir bar was added 0.57 mLs (0.61 grams, 5.54 mmol, 1.1 equiv) of thiophenol, 0.98 mLs (0.71 grams, 7 mmol, 1.4 equiv) of triethylamine (Et<sub>3</sub>N), and was diluted with 25 mLs (0.2 M) of anhydrous CH<sub>2</sub>Cl<sub>2</sub>. This solution was cooled to 0°C and the octanoyl chloride 0.85 mLs (0.81 grams, 5 mmol, 1equiv.) was added drop-wise over a period of 15 min. The mixture was allowed to react for another 16 hours at room temperature. After this period, the contents of the reaction

mixture were diluted with 100 mLs of CH<sub>2</sub>Cl<sub>2</sub> and then water (30 mLs). This biphasic mixture was transferred to a separatory funnel, the organic layer was removed and the aqueous layer was further extracted with CH<sub>2</sub>Cl<sub>2</sub> (~50 mLs, 2X), the combined organics were washed with 1N HCl solution (~50 mLs, 1X), water (~50 mLs, 1X), (brine (~25 mLs, 1X), dried over Na<sub>2</sub>SO<sub>4</sub>, filtered, and concentrated to give 1.08 grams (92%) of the title compound (**S-phenyl thiooctanoate**) as a colorless liquid which was used directly with no further purifications.



**S-phenyl thiooctanoate:** colorless liquid; 92% yield; NMR (400 MHz, CDCl<sub>3</sub>)  $\delta$  = 7.41(m, 5H), 2.67 – 2.64 (m, 2H), 1.75-1.68 (m, 2H), 1.35-1.27(m, 8H), 0.91-0.87 (m, 3H); <sup>13</sup>C NMR (101 MHz, DMSO-d<sub>6</sub>)  $\delta$  = 197.8, 134.6, 129.4, 129.3, 128.1, 43.9, 31.8, 29.1, 29.1, 25.7, 22.7, 14.2.



**S-phenyl thiododecanoate:** colorless liquid; 91% yield; NMR (400 MHz, CDCl<sub>3</sub>)  $\delta$  = 7.41(m, 5H), 2.67 – 2.63 (m, 2H), 1.75-1.67 (m, 2H), 1.40-1.23(m, 16H), 0.90-0.86 (m, 3H); <sup>13</sup>C NMR (101 MHz, DMSO-d<sub>6</sub>)  $\delta$  = 197.8, 134.6, 129.4, 129.3, 128.1, 43.9, 32.1, 29.7, 29.7, 29.6, 29.5, 29.4, 29.1, 25.8, 22.8, 14.3.

All other compounds were purchased from standard sources and were used as received.

**Preparation of Lipid Solutions.** Prior to use, SHPC was reduced overnight in an equimolar mixture of TCEP-HCl and NaOH in a 2:1 SHPC:TCEP solution. For monitoring of the phospholipid coupling reaction *via* LCMS, a 100uL solution was prepared of aliphatic

phenyl thioester in water (5mM), reduced SHPC mixture (5mM SHPC), and TEA (10mM) in HPLC vials fitted with 350uL Supelco glass inserts. The solution was then left at room temperature to react.

Fluorescence microscopy samples were prepared similarly ([reduced SHPC]=[thioester tail] = 5mM, [TEA]= 10mM) with the addition of 2uM rhodamine-DHPE. Samples were mixed and sealed under coverslips for development of liposomal structures. C7 thioester samples were developed at room temperature for 48 hours and C11 samples were developed at 30°C for 24 hours prior to imaging. Photobleaching samples were prepared the same as the fluorescence microscopy samples, with the addition of 1mM HPTS in the reaction mixture.

Exchange reactions began the same as above ([reduced SHPC]=[thioester tail] = 5mM, [TEA]= 10mM, as well as [rhodamine-DHPE]=2uM if sample was to be used for fluorescence microscopy). C11 thioester samples were reacted for 24 hours and C7 thioester samples were reacted for 48 hours. Reaction was followed by addition of equimolar C7 thioester tail in C11 samples or up to 10 equivalents of C11 thioester tail into C7 samples. Microscopy samples for C11 thioester product exchange with C7 thioester tails were developed at 30°C.

**Microscope Imaging.** Fluorescent imaging was performed using a Nikon A1R laser scanning confocal microscope equipped with Nikon Elements software version 4.20-4.6. In all cases, a 561nm laser was employed to excite the rhodamine-DHPE while a 488nm laser was additionally used for photobleaching assays. For acquisition of TEM images, 4 µl of sample solution was transferred onto a lacey holey-carbon grid, blotted for 1-2 seconds,

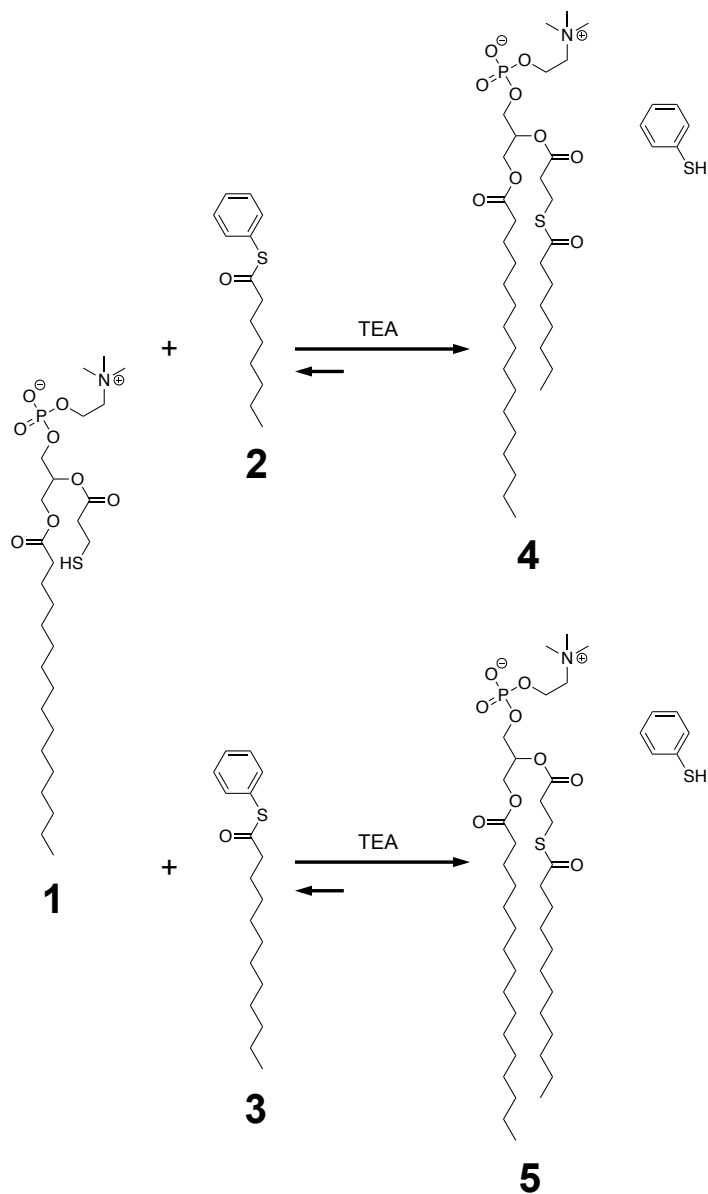
and then plunge-frozen using an FEI-Vitrobot Mark IV at room temperature. The resulting vitrified sample was imaged on an FEI Tecnai F20 FEG-TEM, operating at 200kV and 25,000x magnification, using a Gatan US4000 CCD camera. The electron dose per image was limited to 20 electrons/Å<sup>2</sup>, with a defocus of -2μm, using the low-dose mode of Serial EM acquisition software.

**LC-MS of Product Formation.** Phospholipid formation was conducted in HPLC vials fitted with 350uL glass inserts as described above with 5uL samples taken over the course of the reaction. Samples were injected onto an analytical 1100 Series Agilent LC-MS with Agilent G1946D Mass Spectrometer and Sedex Evaporative Light Scattering Detector controlled by ChemStation software and fitted with Agilent Zorbax 5um 4.6x50mm C8 column. A binary solvent system of 0.1% formic acid in 5:4:1 isopropanol:water:methanol and chloroform was used at a flow rate of 0.9mL/minute. To quantify conversion, SHPC peak area was normalized to the area measured at 0 hours while products were normalized to areas measured at 24 hours (C11 system) or 48 hours (C7 system). For phospholipid **5** to phospholipid **4** exchange, peak areas were normalized to 0 hours for phospholipid **5** and 96 hours for phospholipid **4**.

**Photobleaching Experiments.** Vesicle formation was conducted in sealed slides in the presence of 1mM HPTS and 2uM rhodamine-DHPE as described above. Following self assembly of bilayers, select liposomes were imaged for 5 seconds, exposed to high intensity 488nm light for 15 seconds to bleach encapsulated HPTS, then imaged for one minute to monitor for restoration of fluorescence. Mean internal fluorescence of photobleached

liposomes was measured using Nikon Elements software and values normalized to initial fluorescence intensity were averaged across 6 liposomes for phospholipid 4 and 3 liposomes for phospholipid 5.

### Section 5.3. Results and Discussion



**Scheme 5.1.** A schematic illustrating the formation of synthetic phospholipids using the thiol-thioester exchange reaction. Thiol-functionalized lysolipids [1] undergo reversible exchange with either C7 [2] or C11 [3] phenyl thioesters in the presence of a basic catalyst,

triethylamine (TEA), to generate phospholipid products [4 and 5]. These lipid products are then capable of assembling into bilayers to form liposomes.

Dynamic behavior enabled by the thiol-thioester exchange was introduced to liposome membranes through design and synthesis of lysolipids bearing primary thiol functionalities (SHPC) [1] and one of two aliphatic tails (C7 [2] and C11 [3]) terminated in phenyl thioesters as depicted in Scheme 5.1. Phenyl thioester functionalities were selected to drive the generation of synthetic phospholipid and free phenyl thiol due to the greater stability of the phenyl thiol as compared to the lipid thiol, driving tetrahedral intermediates to break down into full phospholipids and phenyl thiols. Reaction progress was monitored on an analytical LC-MS equipped with an Evaporative Light Scattering Detector (ELSD) to track consumption of lysolipid and production of phospholipid product. SHPC (5mM) was mixed with either C7 or C11 thioester tails (5mM) in the presence of the base catalyst triethylamine (TEA) (10mM) to generate the reactive thiolate anions. TEA, a weak base, was used sparingly to catalyze the exchange without significantly increasing hydrolytic cleavage of the ester linkages. In the presence of C7 phenyl thioesters, SHPC was consumed over the course of 48 hours leading to approximately 90% conversion to a C7 thioester-containing phospholipid product (phospholipid **4**) (Figure 5.1A,B). Exhibiting faster exchange, SHPC mixed with C11 phenyl thioester tails was consumed over 12 hours reaching nearly complete conversion to a C11 thioester-containing phospholipid product (phospholipid **5**) (Figure 5.1C,D). In either reaction if the TEA catalyst was excluded, no formation of phospholipid product was observed over the same time frames (SI Figure S5.1), verifying the dependence on the catalyst presence.



Relatively slow reaction times in both cases are attributed to the necessity of a weak base catalyst as needed to prevent hydrolysis, the dilute reactants, and a stoichiometric ratio of thiol to thioester precursors. However, the ability of the reaction to progress independent of these conditions conveys the strength the thiol-thioester exchange reaction offers the *in situ* formation system. Interestingly, C11 thioesters underwent more rapid exchange than the C7 thioesters, which may be due to a more favorable packing of the precursors to exclude water and thereby increase the lifetime of thiolate anion intermediates or to increase accessibility of thiolate anions to phenyl thioesters. Additional work would be necessary to determine the role tail hydrophobicity plays on the rate of the thiol-thioester exchange.

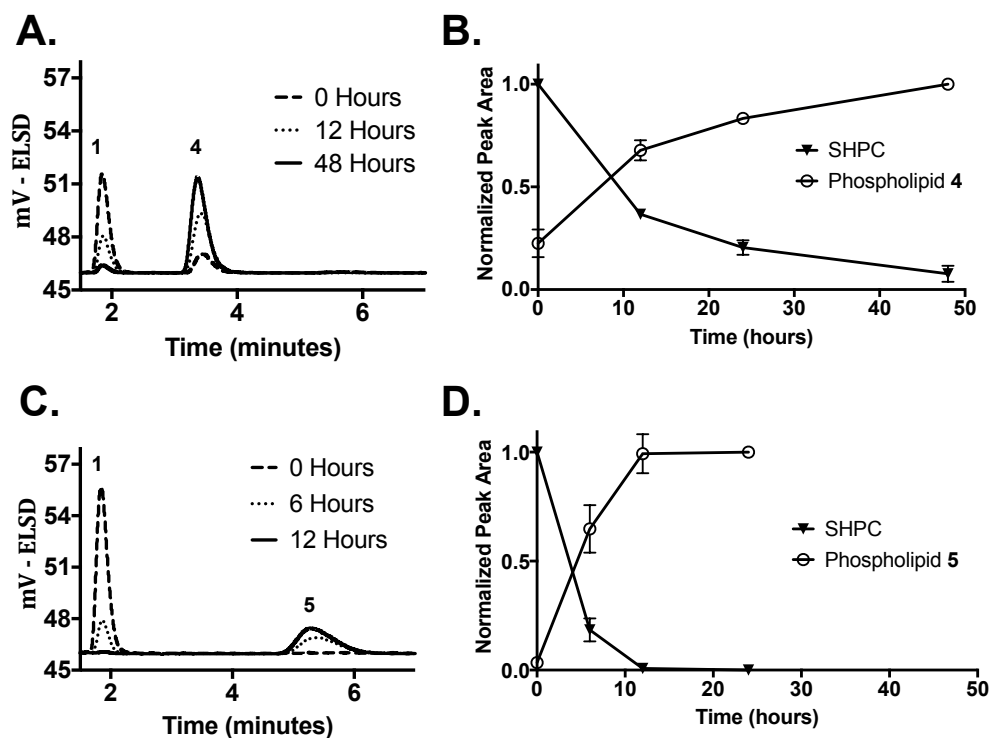


**Figure 5.1.** LC-MS-ELSD chromatography monitoring reactions containing 5mM reduced thiol lysolipid (SHPC) [1], 10mM TEA and 5mM thioester tail [2 or 3] (A, C). C7 thioester tails and SHPC, normalized to 0 hours, undergo approximately 90% conversion to phospholipid 4, normalized to 48 hours, over the course of 48 hours (B) and C11 thioester tails with SHPC, normalized to 0 hours, undergo nearly complete exchange over 12 hours to produce phospholipid 5, normalized to 24 hours (D).

Fluorescence microscopy and cryo-TEM were used to assess assembly of the phospholipid products into liposomes. Samples were prepared as in the LC-MS-ELSD experiments ( $[\text{reduced SHPC}] = [\text{thioester tail}] = 5\text{mM}$ ,  $[\text{TEA}] = 10\text{mM}$ ) with the addition of  $2\mu\text{M}$  rhodamine-DHPE for fluorescence microscopy samples. Liposomes greater than a micron in diameter were observed under fluorescence microscopy following development of the C7 phenyl thioester-based reaction at room temperature for 48 hours (Figure 5.2A). Cryo-TEM images display single rings rather than stacked layers, signifying assembly into predominantly unilamellar structures (Figure 5.2B). Unilamellar assemblies are likely due to the slow reaction times and make this liposome formation method particularly useful for applications such as artificial cells and membrane dynamics studies in which unilamellar structures are desired for imaging<sup>129</sup>.

Separately, it should be noted that phospholipid **5** exhibited dependence upon temperature for the assembly of liposomal structures. When developed at room temperature, phospholipid **5** assembled primarily into wormlike micelles, visualized under cryo-TEM as 2-4nm-wide strands (Figure 5.2D). If developed at slightly elevated temperatures such as  $30^\circ\text{C}$ , phospholipid **5** assembled into liposomes (Figure 5.2C). This temperature dependent assembly suggests that temperature plays a much stronger role in the packing of phospholipid **5** than phospholipid **4** near ambient conditions leading to these significant morphological transitions.

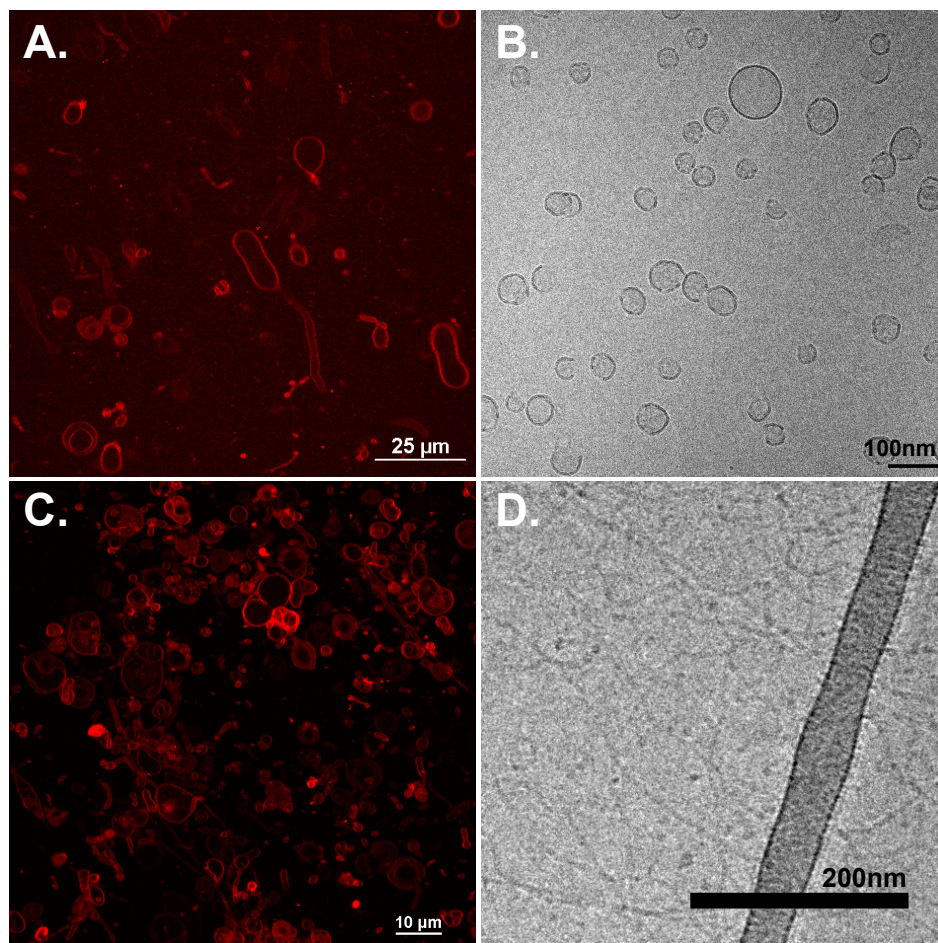


**Figure 5.2.** Fluorescence microscopy and cryo-TEM images of phospholipid assemblies. C7 thioester tails (5mM) undergo exchange with reduced SHPC (5mM) in the presence of 10mM TEA over 48 hours to produce predominantly unilamellar liposomes, as evidenced by fluorescence microscopy (A) and cryo-TEM (B). When reacted at 30°C for 24 hours, C11 thioester tails (5mM) undergo exchange with reduced SHPC (5mM) in the presence of 10mM TEA to produce liposomes, visualized using fluorescence microscopy (C) but at room temperature assemble into tubular micelles, visualized using cryo-TEM (D).

Under fluorescence microscopy, localization of rhodamine-DHPE to the membrane highlights the structures as closed membranes. However, to probe the integrity of the lipid bilayers as boundaries capable of encapsulating hydrophilic molecules, additional studies were necessary. Photo-bleaching of an encapsulated, charged dye followed by monitoring for recovery was used to examine the barrier to diffusion presented by the lipid membrane. Both vesicle populations displayed photobleaching of encapsulated HPTS immediately

following irradiation, with phospholipid 4 samples losing 74% of initial internal fluorescence intensity and phospholipid 5 samples losing 45% of initial internal fluorescence intensity. For phospholipid 4 samples, no increase in fluorescence within the membrane boundary was observed during the recovery period. Alternatively, restoration of fluorescence within phospholipid 5 liposomes occurred over the course of 20 seconds after which it was not possible to consistently distinguish liposomes (Figure 5.3), indicating that HPTS was able to diffuse from the external solution into the vesicle cavity. These results indicate that both phospholipids assemble into enclosed systems to enable the initial photobleaching, and indicate that phospholipid 4 vesicles produce a more impermeable membrane at room temperature. The greater degree of permeability in phospholipid 5 vesicles could be used for applications requiring a diffusion-limited system capable of taking up resources from the environment.

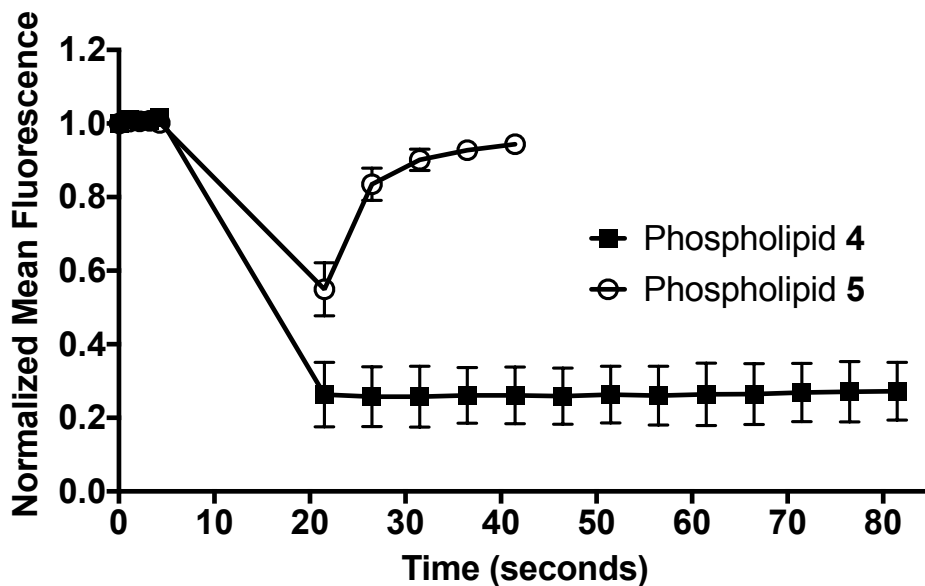


**Figure 5.3.** Photobleaching assays of phospholipid 4 and phospholipid 5 liposomes. Both systems enable bleaching of internal HPTS upon irradiation. Mean internal fluorescence normalized to initial fluorescence values shows restoration of fluorescence over 20 seconds for phospholipid 5 systems and no restoration of fluorescence for phospholipid 4 systems.

Due to the reversible nature of the thiol-thioester exchange reaction, it is possible to introduce new thioester-functionalized molecules following liposomal formation to incorporate new moieties into the lipid structures. This approach would enable downstream labelling or modification of the liposomes. To demonstrate this capability, following equilibration of the first thioester exchange reaction, an equimolar quantity of complementary aliphatic thioester tail was added. Samples were taken at various time points and injected onto the analytical LC-MS-ELSD to monitor exchange. Over the course of 96 hours, exchange of phospholipid **5** with C7 phenyl thioester tails was apparent, demonstrating over 30% conversion of phospholipid **5** to phospholipid **4**, and fluorescence microscopy verified the persistence of liposomal structures (Figure 5.4). However, when the opposite tail and phospholipid exchange was attempted, there was no exchange of C11 phenyl thioester tails into the phospholipid **4** system evident using either equimolar or excess quantities of C11 phenyl thioester. Together, these aliphatic tail exchange results promote the idea that phospholipid **4** has a more stable thioester than phospholipid **5** or that there are favorable lipid constructs that either prevent or facilitate exchange, respectively, in phospholipid **4** and **5**.

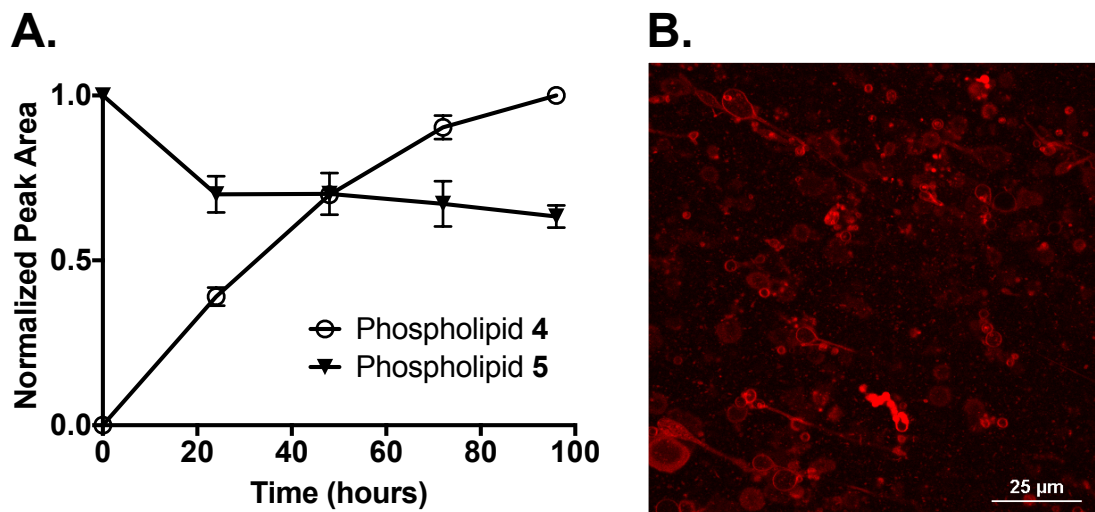


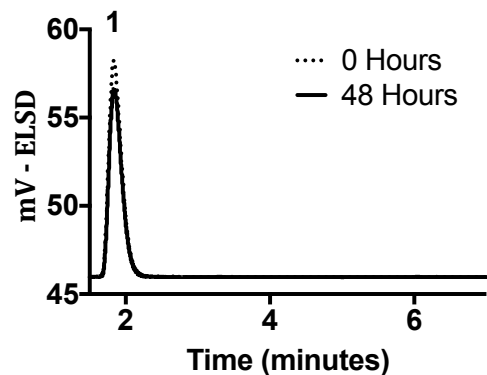
**Figure 5.4.** Phospholipid 5 undergoes exchange with C7 phenyl thioester tails. Following formation of phospholipid 5 over the course of 24 hours, equimolar C7 thioester tails [3] were added. Exchange of the two tails progressed over the course of 96 hours to convert over 30% of phospholipid 5, normalized to 0 hours, to phospholipid 4, normalized to 96 hours (A). Fluorescence microscopy verified persistence of liposomes following addition of C7 phenyl thioester tails after 48 hours of continued development at 30°C (B).

### Section 5.4. Conclusion

In this work a novel method for the *in situ* formation of synthetic phospholipids using a reversible reaction has been developed. Dynamic behavior in the bilayer was introduced using thiol-thioester exchange between SHPC and phenyl thioester tails. Two tails, C7 phenyl thioester and C11 phenyl thioester, exchange with SHPC to produce phospholipid products. These products assemble into liposomes capable of varying degrees of hydrophilic compound encapsulation. Beyond liposome assembly, phospholipid 5 demonstrates the ability to undergo further exchange with C7 phenyl thioesters. This continued exchange better mimics the remodeling present in native cell membranes, furthering the pursuit of a bottom-up artificial cell and enabling downstream modifications of liposomal structures following *in situ* formation.

## Section 5.5. Supplementary Figures

**A.**



**B.**

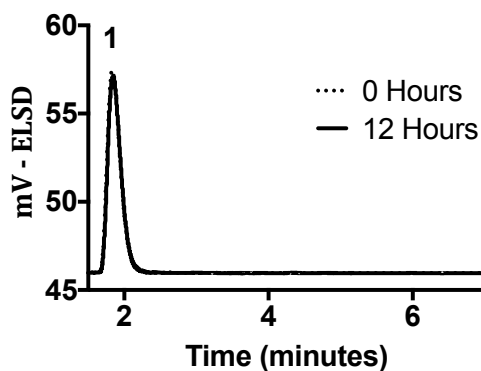


**Figure S5.1.** LC-MS-ELSD chromatography monitoring control reactions containing 5mM reduced thiol lysolipid (SHPC) [1] and 5mM thioester tail [2 or 3] but no catalyst. No formation of thioester-containing phospholipid product is apparent 48 hours after mixing SHPC [1] with C7 phenyl thioester tail [2] (A) or 12 hours after mixing SHPC [1] with C11 phenyl thioester tail [3] (B).

## Chapter 6

### Photoinduced Pinocytosis for Artificial and Proto-cell Systems

#### Section 6.1. Introduction

A pursuit to understand the conditions necessary to evolve living cells and utilize their complexity to produce a suite of biologically-inspired commercial compounds has driven the development of proto- and artificial cells. In top-down approaches for generating artificial cells, cellular components are eliminated over time to reach a minimal, living cell<sup>177</sup>. In contrast, protocells and bottom-up approaches for forming artificial cells both add components piece by piece to produce individual compartments capable of synthesizing products of interest (protocell)<sup>74</sup> or until a status of “living” is achieved (artificial cell)<sup>76,78,80,104</sup>. While there is no universally accepted definition of “living”, typical requirements include (1) self-replication and (2) the potential for evolution using a self-contained genetic code. For such living systems, significant progress has been made in the development of boundary/membrane materials<sup>129,178,179</sup>, cell-free expression systems<sup>75,81,86</sup>, and growth-dependent division behavior<sup>106,107,180-182</sup>. However, to limit the machinery needed in these simplified systems, it is generally necessary to feed in critical building molecules including those that provide energy, as well as proteins or genetic material.

Current methods to incorporate material into existing protocell and bottom-up artificial cell structures involve the use of selective poration<sup>51,183</sup> or surfactant addition,<sup>101,102</sup> either of which result in the equilibration of internal and external components. Other methods involve microinjection,<sup>99,100</sup> which requires precise control over the injection system, and



fusion of carrier vesicles,<sup>57,181,184,185</sup> both of which are labor intensive. In other strategies, membrane channels and translocation machinery have been expressed within the pre-formed membrane or have been introduced post formation. However, these systems suffer from bi-directional solute exchange resulting in the loss of encapsulated compounds, have limitations on size or charge density of compounds transported, require energy input, or entail the use of specific tags on the cargo of interest<sup>74,83,88-98</sup>.

Real cells are capable of taking in foreign material *via* endocytosis in the form of either phagocytosis (i.e., internalization of solid material<sup>186</sup>) or pinocytosis (i.e., internalization of liquids<sup>187,188</sup>). Achieving endocytic behavior in artificial cells offers an improved solution to the “feeding” problem, providing a time-dependent method for altering the state of the cell in any of a variety of ways. Towards this end, phagocytosis-inspired behavior has been reported for emulsion systems<sup>189</sup>, and a previous study reported the production of endocytic vesicles from lipid rafts in the presence of osmotic or surfactant stress<sup>190</sup>. However, no work to date has incorporated stimuli responsive endocytotic behavior using components already present in the lipid bilayer, particularly in a spatiotemporally controllable manner. Here, the introduction of photo-cleavable lipids into liposomes is used to enable photo-induced pinocytosis. Upon exposure to light, liposomes containing this photo-cleavable lipid engulf external solution without the apparent loss of internal constituents. This behavior has been achieved using two widely differing liposome formation methods, lipid film hydration and pull-down, indicating the versatility and robustness of this photo-induced pinocytosis behavior and underscoring its potential utility for future artificial cell systems.

## Section 6.2. Methods

**General.** Compounds were purchased from commercial sources and used as received. Synthesis of NBPC was conducted as published<sup>191</sup>. <sup>1</sup>H and <sup>13</sup>C nuclear magnetic resonance (NMR) spectra for product verification were gathered on a Bruker Ascend 400 spectrometer. Irradiation with 365nm light was conducted using an Acticure 4000 lamp fitted with a 365nm bandgap filter while 405nm irradiation was performed using the laser scanning confocal imaging laser. Microfluidic chips were produced using Optical Associates Inc. Model J500 mask aligner with ENM illumination controller exhibiting peak intensities at 367, 407, and 438nm at an intensity of 15mW/cm<sup>2</sup>, a Nikon Ci-L upright microscope equipped with a Mightex Polygon 400 multiwavelength dynamic spatial illuminator and a Mightex BLS series BioLED light source module and microfluidic devices were fused using a PlasmaEtch plasma cleaning system.

**Liposome Preparation.** *Lipid film hydration vesicles.* Lipid components were measured from prepared chloroform stocks resulting in a final molar ratio of 2:2:1:0.01 nitrobenzylphosphatidylcholine (NBPC):1,2-dioleoyl-*sn*-glycero-3-phosphocholine (DOPC):cholesterol:Lissamine rhodamine B 1,2-dihexadecanoyl-*sn*-glycero-3-phosphoethanolamine (rhodamine-DHPE). Chloroform was dried completely before addition of 500uM fluorescein solution or 100mM sucrose and 100uM AlexaFluor 647 solution. Hydration proceeded with or without sonication for the first hour followed by development at 40-45°C overnight with no clear impact of sonication. Prior to imaging, liposomes were lightly vortexed followed by 1:9 dilution in 100uM sulforhodamine and 350uM glucose for fluorescein vesicles and 100mM glucose and 5mM sodium chloride for AlexaFluor 647 vesicles.

*Pull-down vesicles.* Lipids were mixed using a similar 2:2:1:0.02 NBPC:DOPC:cholesterol:rhodamine-DHPE ratio in heavy mineral oil at a final concentration of 0.35mg lipids/mL heavy mineral oil. Lipids were dispersed by vortex and sonication and could be stored for a couple weeks at -18°C. 100uL 200mM glucose solution was pipetted into a 0.65mL eppendorf tube. In another tube, 10uL 1mM AlexaFluor647 and 200mM sucrose solution was pipetted into 200uL of the prepared lipid mixture. This was emulsified by dragging across a microcentrifuge tube rack before layering on top of the glucose solution followed by centrifugation at 10,000rcf for 10 minutes to generate a liposome pellet. The upper oil layer was aspirated off as well as a majority of the lower aqueous layer leaving 10-15uL. The liposomes were resuspended by light vortexing before use.

*Asymmetric vesicles.* Lipid mixtures were prepared as above for the pull-down vesicles, however mixtures contained either 4:1 DOPC: cholesterol or 4:1 NBPC:cholesterol, both with rhodamine-DHPE. 200uL 200mM glucose solution was layered at the bottom of Nunc Lab-Tec 8 well chambered cover glass followed by 200uL of the lipid mixture for the outer leaflet of lipids and 100uL heavy mineral oil. Following development for 2 hours, an emulsion of 200uL inner leaflet lipid mixture and 10uL 1mM AlexaFluor 647 and 200mM sucrose solution was layered on top and liposomes were allowed to precipitate overnight prior to imaging.

**Microscopy.** Fluorescence imaging was performed using a Nikon A1R laser scanning confocal microscope equipped with Nikon Elements software version 4.20 to 4.6. In all cases, a 561nm laser was employed to excite rhodamine-DHPE, a 488nm laser was used to

excite fluorescein, and a 638nm laser was used to excite AlexaFluor 647. For 405nm irradiation of lipid samples, the 405nm imaging laser was used.

**Assessment of Asymmetric Vesicle Formation Efficiency.** Two replicates of the formation pair were imaged using scanning laser confocal microscopy utilizing stitching software in Nikon Elements to image a large area. Images were analyzed using FIJI software to remove background fluorescence and count objects present. The count from sample formed with NBPC on the outside was divided by the count from sample formed with NBPC on the inside.

**Assessment of Internal Fluorescence Intensity.** Videos of lipid film hydration method liposomes with internal fluorescein were analyzed for internal fluorescence intensity during pinocytosis. Using Nikon Elements Software, circular ROIs were set in areas of the original encapsulated cavity at the beginning of irradiation and after pinocytosis and mean internal fluorescence intensity values were collected.

**Aspect Ratio Measurements.** Videos were collected using Nikon Elements software. In each video, non-spherical vesicle structures were identified which were in the imaging plane long enough to determine the presence of pinocytosis behavior. Selected vesicles were measured using Nikon Elements software to determine the length of each vesicle followed by a perpendicular characteristic width (not, for example, at the neck between two lobes but within those lobes) of the same vesicle.

**Microfluidics.** Microfluidic molds were produced using a thiol-ene polymerization process published previously<sup>192</sup>. Briefly, glass slides were prepared by etching with a solution of 3 parts sulfuric acid and 1 part hydrogen peroxide for 3 hours followed by overnight vapor deposition of methacryloxypropyltrimethoxysilane at room temperature

in a vacuum chamber. Using a clean glass slide as backing, onto custom printed FineLine Imaging nylon masks was deposited a monomer mixture for thiol-ene polymerization. Several mixtures were tested, with the most consistent results from a mixture of pentaerythritol tetra(3-mercaptopropionate) (PETMP) and triallyl-1,3,5-triazine-2,4,6-trione (TATATO) in a 1:1 stoichiometric thiol:ene ratio with 1wt% Irgacure 184 and 1wt% N-nitrosophenyl-hydroxylamine (Q1301) with 52um Precision Brand color coded shim as spacers at either end placed without obscuring printed features. Functionalized slides were placed atop assemblies without introducing bubbles and sides were clamped prior to irradiation using Optical Associated Inc. model J500 optical mask alignment system. Excess, unreacted monomer was washed away leaving polymerized channels and wells. The above assembly steps were repeated on the resulting features using masks of well features alone and 102um spacers for a multi-layer microfluidic chip. For PDMS devices, a 10:1 mixture of Sylgard 184 silicone elastomer was layered atop microfluidic chips, degassed for 30 minutes and cured in a 70°C oven for 4 hours. Independent devices were cut away and inlet and outlet ports were punched using a 0.5mm biopsy punch. Clean cover slips and PDMS surfaces were prepared in a PlasmaEtch plasma cleaning system for fusion.

**Osmotic Deformation and Pinocytosis Efficiency.** Microfluidic devices were prepared for liposome loading by incubation in a vacuum chamber with an inlet port sealed for a minimum of 10 minutes. Pull-down liposome solutions were deposited atop inlet ports immediately following release of vacuum to allow thorough loading of solution into wells. Upon completion of loading, a 0.012"IDx0.030"OD microbore PTFE tube primed with 300 or 400mM glucose and tracer dye solution was inserted into the loading port and the seal on the second port was removed. Fluid was exchanged at a flow rate of 5uL/hr for 30 to 50

minutes using a syringe pump monitoring for external fluid exchange and deformation of loaded liposomes. Deformed liposomes were irradiated with 405nm light using the imaging laser line of the microscope to induce shape change and pinocytosis while imaging the 638nm line. To analyze percentage of liposomes to undergo pinocytosis, liposomes were counted using FIJI software and the subset of the population that underwent pinocytosis were identified by hand.

### **Section 6.3. Results and Discussion**

Morphological changes in the lipid bilayer such as membrane budding<sup>68,69</sup> have been modeled using the introduction of amphiphilic compounds. Based on this same general concept, morphological changes in the bilayer structure were achieved here, without the introduction of new compounds, through photo-induced cleavage of lipids in the preformed membrane that alter the structure and character of the lipid bilayer. To this end, a photo-cleavable lipid was synthesized based upon a previously reported lipid synthesis method<sup>118</sup>. Specifically, an alkyne functionalized lysolipid was coupled to an azide-functionalized tail bearing a photosensitive *o*-nitrobenzyl moiety *via* copper-catalyzed azide-alkyne cycloaddition (CuAAC) to produce a synthetic phospholipid (NBPC)<sup>191</sup>. This product was mixed with natural lipids to achieve a 2:2:1 molar ratio of NBPC: 1,2-dioleoyl-*sn*-glycero-3-phosphocholine (DOPC):cholesterol (Figure 6.1). The photosensitive NBPC molecules absorb UV light, tailing into the 400nm range, resulting in the cleavage of the *o*-nitrobenzyl moiety to produce a lysolipid with a short second tail, carbon dioxide, and a free aliphatic tail. DOPC was included in the lipid mixture for increased fluidity of the membrane as it has a  $T_g$  of  $-17^\circ\text{C}$  while cholesterol was incorporated for enhanced

stability<sup>193</sup>. A small amount (0.4 mol%) of lissamine rhodamine B 1,2-dihexadecanoyl-*sn*-glycero-3-phosphoethanolamine, triethylammonium salt (rhodamine-DHPE) was incorporated into the lipid mixture to enable imaging of the lipid bilayer using fluorescence microscopy.

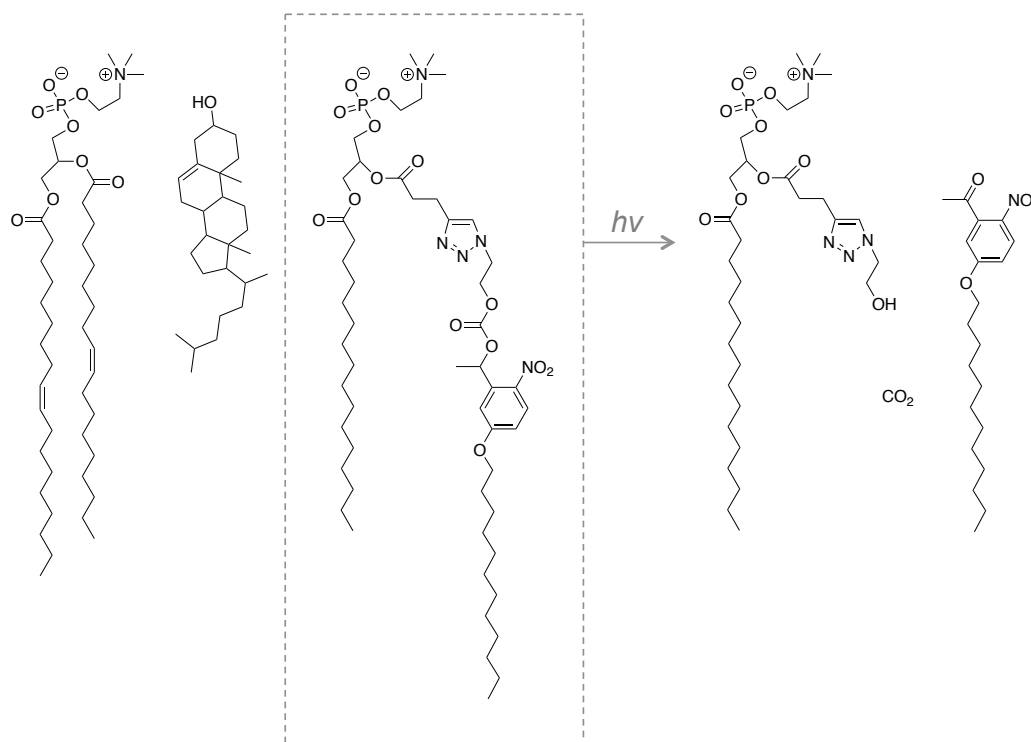


**Figure 6.1.** Liposome formulations consisted of a mixture of DOPC, NBPC, and cholesterol at a molar ratio of 2:2:1, respectively. NBPC undergoes photo-induced cleavage upon irradiation to produce lysolipids, carbon dioxide, and aliphatic tails. DOPC ensures fluidity of the membrane at room temperature and cholesterol increases stability.

It is expected that the bulky structure of NBPC leads to a selective partitioning of the NBPC to the outer leaflet due to the local positive curvature. This hypothesis was assessed using an asymmetric liposome formation strategy based on a previously reported methodology<sup>194</sup>. Different lipid mixtures (4:1) of either NBPC and cholesterol or DOPC and cholesterol were used for each leaflet. In both cases rhodamine-DHPE was included at 0.4-0.8 mol% as a means for imaging the vesicles. The presence of vesicles following overnight

development was verified using fluorescence microscopy to detect AlexaFluor 647 entrapped in the internal compartment and rhodamine-DHPE localized to the membrane. For samples in which the inner leaflet was formed with 4:1 NBPC:cholesterol and the outer leaflet consisted of 4:1 DOPC:cholesterol, few vesicles were found in the images. However, when the leaflet compositions were reversed with the NBPC-enriched layer on the outside, fluorescence microscopy images showed extensive vesicle formation. Specifically, 15 and 46 times more vesicles were reported in preparations with NBPC in the outer leaflet compared to NBPC in the inner leaflet, in two different repetitions of the asymmetric formation pairs (Figure 6.2). This behavior suggests a lower stability of liposomes that are assembled with NBPC in the inner leaflet or decreased efficiency of stabilized water in oil droplet assembly using NBPC-cholesterol mixtures. With these observations, it can be hypothesized that during assembly of water in oil emulsions using the mixed lipid system, DOPC will selectively partition to the water droplet and lipid films will selectively hydrate with increased DOPC at areas of negative curvature, which eventually form the internal compartment, resulting in greater concentrations of NBPC in the outer leaflet.



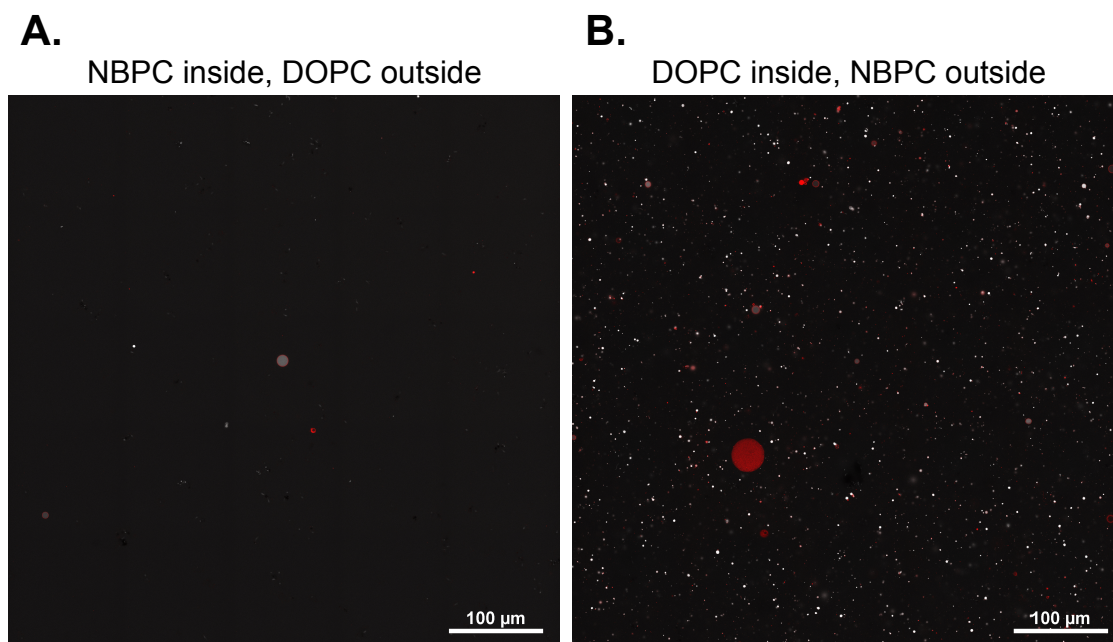


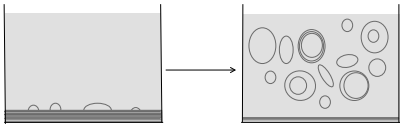
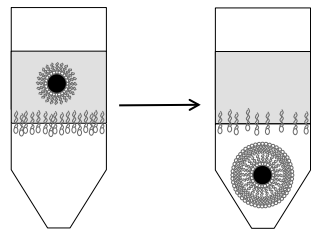
**Figure 6.2.** Liposomes formed using a precipitation method to produce asymmetric assembly of lipids between the inner and outer leaflet was used here to probe the leaflet selectivity of NBPC. Liposomes were formed with NBPC exclusively in the outer (B) or inner leaflet mixture (A), resulting in pronounced differences in the quantity of liposomes generated. Liposomes are indicated by a fluorescent interior marked by AlexaFluor 647 and membrane fluorescence assessed by rhodamine-DHPE.

With NBPC preferentially located in the outer leaflet, irradiation was expected to cause a more prominent outer leaflet-specific response. In particular, photo-cleavage would result in an un-charged aliphatic tail that may readily traverse the two bilayers more easily than the zwitterionic lysolipid, which is constrained by slow rates of trans-membrane flip-flop. This behavior would result in a rapid decrease in volume of the outer leaflet and constriction of the external surface area. The resultant tension in the membrane forces a shape change to minimize elastic energy, requiring that the liposomes adopt a new shape. Vesicle shape predictions modeled using the Area-Difference Elasticity Model<sup>195,196</sup> indicate a series of possible morphologies based upon the volume-to-surface-area ratio within the vesicle and the difference between the surface areas of the two leaflets in the bilayer. Past

research has verified these shape transformations by modulating these parameters through the addition of lipids<sup>67-69</sup> or the application of external forces<sup>64-66,197</sup>.

To visualize the shape transformations induced by NBPC cleavage, two different liposome formation methods were employed (Table 6.1). The lipid film hydration method<sup>108,109</sup> produces heterogeneous, multilamellar liposomes through the gentle hydration of a dried lipid film. In contrast, the pull-down technique<sup>111-113</sup> produces spherical, unilamellar liposomes by the application of centrifugal force to pull water-in-oil droplets through an oil/water interface.

**Table 6.1. Liposome Formation Methods**

Formation Method	Lipid Film Hydration	Pull-down
Schematic of Formation		
Vesicle Characteristics	Giant, Multilamellar, Irregular Morphologies	Giant, Unilamellar Spheres
Drawbacks for this System	Inconsistent Product Liposomes	Requires Deformation by Osmotic Pressure
Does it Pinocytose?	Yes	Yes

Formation of liposomes *via* lipid film hydration results predominantly in very large, multilamellar liposomes in a wide range of shapes and structures enabling assessment of the impact that aspect ratio and shape have upon the photo-induced pinocytosis behavior. These shapes include tubular liposomes (prolates), lobed structures (dumbbells, pears),

multiple lobes around a central axis (starfish), and strings of pearls. Upon irradiation and following the associated cleavage of the NBPC located preferentially in the outer layer, liposomes with lobed and prolate structures transformed to flattened discs (oblates and discocytes), eventually engulfing external fluid to form closed stomatocytes (Figure 6.3). No appreciable loss of encapsulated hydrophilic dye was observed during irradiation, indicating that the membrane remains intact and the internal volume of the original vesicle compartment does not appreciably mix with the surrounding material during shape changes leading up to the pinocytosis event. Specifically, fluorescence decreased in the original vesicle compartment an average of 15% across 6 representative vesicles, including those presented in figure 6.3. This moderate decrease is most likely due to gradual photobleaching as opposed to pores forming in the membrane. These shape transitions follow the Area-Difference Elasticity Model<sup>196</sup> assuming that the volume of the original vesicle compartment, i.e. excluding engulfed volume, is kept constant while the ratio of the outer to inner surface areas decreases, further validating the hypothesis that the shape change is driven by the change in outer leaflet surface area as compared with the inner leaflet surface area.

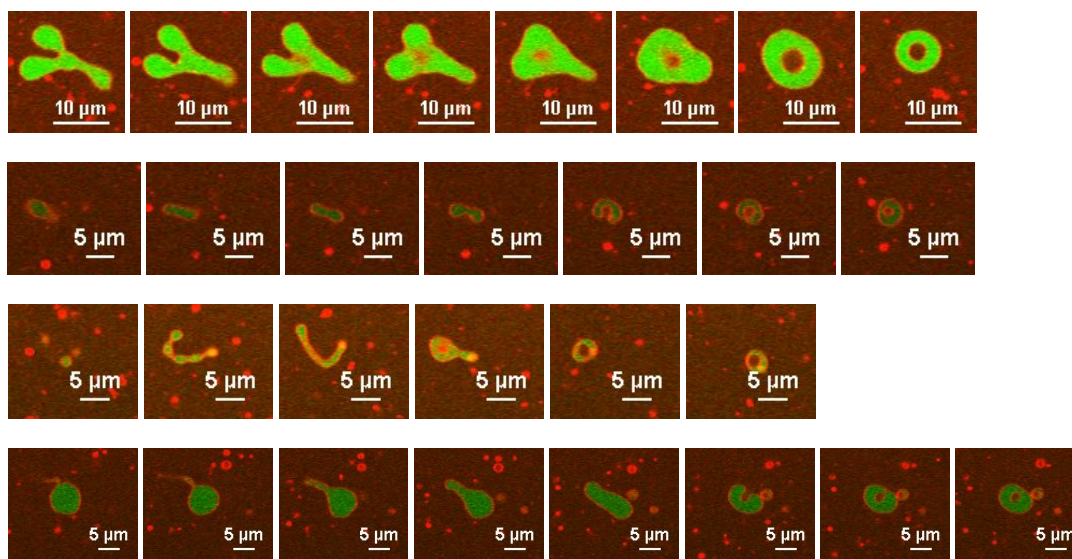


**Figure 6.3.** Fluorescence microscopy images during irradiation of elongated liposomes demonstrate photo-induced pinocytosis. Liposomes were formed *via* lipid film hydration composed of 2:2:1 NBPC:DOPC:cholesterol with rhodamine-DHPE. Internal compartments encapsulate 500uM fluorescein in an external solution of 100uM sulforhodamine B and 350mM glucose. Irradiation with 365nm 10mW/cm<sup>2</sup> light results in photo-cleavage of NBPC in the membrane and a shape change transition from lobed structures and tubules to oblate ellipsoids and closed stomatocytes. Each strip contains representative images of time points progressing left to right illustrating shape change steps of each vesicle. Strip length does not correlate to irradiation time.

Applied as an artificial or proto cell feeding system, this photo-induced behavior would potentially enable uptake of a wide range of compounds with fewer constraints on size or structure as compared to membrane protein-based systems. Additionally, because this uptake method did not disrupt membrane integrity, it would enable uptake of external substrates without compromising previously encapsulated molecules. This capacity would allow for the maintenance of gradients and chemical distinctions between the cell and its surroundings developed from formation methods or active behaviors such as protein pumps, which are necessary for processes such as calcium signaling<sup>198</sup> or pH gradients for ATP production<sup>60,199</sup>.

Interestingly, irradiation does not result in pinocytosis in all cases as some liposomes transition only to spheres. To better understand the system, aspect ratios (i.e., the ratio of the longest axis to the characteristic width) of the liposomes pre-irradiation were measured and compared with those of vesicles that underwent pinocytosis induced by 405nm irradiation. Using the fluorescent interior as a guide, structures were classified as liposomes and non-liposomes, based on the presence or absence of a fluorescent interior, respectively, and only non-spherical liposomes (31 total) were analyzed. Pinocytosis was consistently observed in two types of liposomes: those with an aspect ratio greater than or equal to two and those with lobed structures. In the case of tubular liposomes with aspect ratios between 1 and 2, only 17% underwent pinocytosis during the light-induced shape change. These findings suggest that there is a critical volume-to-surface area ratio to fate liposomes into a pinocytotic pathway. This finding is consistent with predictions of shape change based upon the area-difference elasticity model where closed stomatocytes only occur in systems bearing volume-to-surface-area ratios far from spherical. However, further studies would be necessary to determine the conditions that result in pinocytosis for the small subset of liposomes with aspect ratios between 1 and 2.

To study photo-induced pinocytosis behavior in unilamellar systems, a commonly utilized morphology in synthetic cell membranes, liposomes were formed using the so-called “pull-down” technique. This technique additionally enables the study of more consistent, spherical morphologies and the ability to induce the conditions required to determine efficiency of the pinocytosis activity across a vesicle population as would apply to photo-induced pinocytosis behavior for systems like those present in current proto- and artificial cell studies. For spherical liposomes an external stress, such as osmotic pressure,

is required to force liposome deformation to a state with a decreased volume-to-surface area ratio. To transition the liposomes from a solution that will cause minimal osmotic pressure to one with increased osmotic pressure which leads to more uniform, aspherical structures, pull-down liposomes were loaded into a microfluidic device. Following loading into the chambers within the microfluidic device, the liposomes' external 200mM glucose solution was replaced with a solution of 300 or 400mM glucose that was used both to remove the unencapsulated dye and to facilitate rapid deformation caused by the application of a large osmotic pressure. Following the deformation, the liposomes were still largely spherical with many now bearing thin tubule projections. Upon irradiation, an average of 44% of liposomes underwent pinocytosis, analyzed from 17 videos taken over 8 experiments (Figure 6.4). These results lead to two distinct and important conclusions. First, the morphological changes observed here that lead to pinocytosis do not appear to be dependent upon the lamellarity of the vesicle. Secondly, the liposomes need not be visibly elongated to result in pinocytosis.

The capability to induce deformation followed by irradiation would potentially enable multiple cycles of photo-induced pinocytosis in future proto- and artificial cell systems. Upon necessity of a feeding event, osmotic stimulus could be applied with the feeding solution followed by photo-induced pinocytosis. Following irradiation, liposomes adopt spherical morphologies, setting the system up for another round of deformation and irradiation at the next feeding cycle.

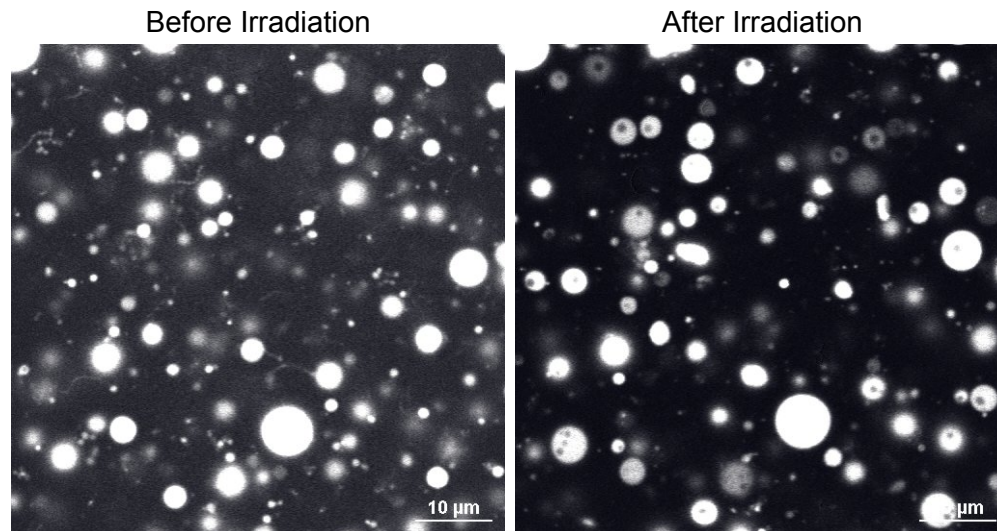


**Figure 6.4.** Microfluidic wells contain liposomes composed of 2:2:1:0.02 NBPC:DOPC:cholesterol:rhodamine-DHPE encapsulating 1mM AlexaFluor647 and 200mM sucrose. External solvent (200mM glucose) is exchanged with 300mM glucose to apply osmotic pressure to deform the liposomes. Following deformation, irradiation with 405nm light results in pinocytosis in an average of 44% of the imaged liposomes as observed here where the post-exposure vesicles are shown to contain internalized structures.

#### **Section 6.4. Conclusion**

These studies lay the groundwork for future applications in artificial cell feeding systems. We have demonstrated spatiotemporal control over pinocytosis-inspired behavior in synthetic liposomal systems using light. The spatiotemporal control of the pinocytosis behavior afforded by light enables uptake of external fluid only where and when the desired substrate is present without the loss of encapsulated compounds. Additionally, this behavior is tolerant of differing formation conditions, occurs over a wide range of shapes and is consistent with models for vesicle shape that have previously been developed, making it applicable to a wide range of protocell and bottom-up artificial cell types. Finally, the ability to induce necessary deformation of liposomes followed by photo-induced

pinocytosis in a large portion of the population sets the stage for multiple cycles of feeding in future systems.



## Chapter 7

### Conclusions and Future Directions

This dissertation focuses on the development of novel *in situ* formation chemistries for the production of functional, synthetic liposomes. First, spatiotemporal control was implemented into the Copper-catalyzed Azide-Alkyne Cycloaddition (CuAAC) reaction for the covalent attachment of a second aliphatic tail onto a lysolipid. Second, the toolbox of reaction chemistries available for *in situ* phospholipid formation was expanded to include both thiol-Michael addition and thiol-thioester exchange. Finally, these chemistries were utilized to enable added functionality of the membrane, incorporating remodeling behavior, homopolymerization, or photo-cleavage for engulfment of an external fluid. The following sections will be dedicated to summarizing the findings of this thesis work followed by reflections over potential future directions in this area.

#### Section 7.1. Development of Novel *In Situ* Liposome Formation Methods

Over the course of this thesis, three new methods for the covalent attachment of an aliphatic tail functionalized on one end to a complementarily functionalized lysolipid (a lipid structure bearing a zwitterionic headgroup and one aliphatic tail built off of a glycerol molecule) have been developed. The first of these methods built off of previous work to covalently attach an alkyne-functionalized lysolipid to an azide-functionalized tail *via* the CuAAC reaction<sup>118</sup>. From there, a photoinitiator composed of a copper-ligand pair and two radical generating acylphosphinate groups<sup>120</sup> was substituted for the sodium ascorbate-Cu(SO<sub>4</sub>)<sub>2</sub> catalyst system to produce the reduced copper catalyst upon generation of radicals<sup>119</sup>. By introducing a photoinitiation system, the conversion of lysolipids to

phospholipid molecules and by extension the transition of micelles and stabilized oil droplets to liposomes could be controlled in a spatiotemporal manner. Beyond spatiotemporal control over liposome formation, this technique afforded enhanced levels of liposome density in the area of irradiation as well as a degree of control over maximal liposome size based upon intensity of the applied photon dose. This system increases control over the formation of liposomes for a host of future applications such as membrane dynamics studies which require giant vesicles for imaging or studies which require the mixing of multiple components with stable lipid precursors and the initiation of membrane assembly at a later time and place.

Following characterization of the photo-CuAAC formation method, it became apparent that in order to realize the range of designer lipids which may be synthesized using the *in situ* formation method, another chemistry must be developed as not all moieties of interest are orthogonal to the CuAAC reaction and not all systems are amenable to the presence of copper or radicals. With that in mind, another “click” reaction, the thiol-Michael addition reaction, was developed for *in situ* formation of liposomes using a new thiol functionalized lysolipid and another aliphatic tail functionalized this time with an acrylate group. A water-soluble nucleophilic catalyst, 2-methyl imidazole, was selected for the reaction system and LC-MS-ELSD analysis demonstrated nearly complete conversion of the lipid precursors to the thioether-containing product over the course of 48 hours. Additionally, microscopy verified the assembly of thioether-containing products into lipid bilayers with a majority assembling into unilamellar liposomes. These structures make this system particularly useful for any systems requiring giant unilamellar vesicles (GUVs)<sup>129</sup>.

Finally, a third phospholipid coupling chemistry was designed with the intent of producing a dynamic liposome system capable of undergoing future exchange to mimic the ability of native cell membrane systems to exchange one fatty acid tail for another utilizing enzymes<sup>174</sup> and to enable downstream modification of liposomes. To accomplish this aim, the thiol lysolipid developed for the thiol-Michael formation system was combined with either of two new aliphatic tails (C7 and C11) functionalized with phenyl thioester moieties. Greater stability of the phenyl thiol leads to an equilibrium favoring the full phospholipid. LC-MS-ELSD was used to monitor the conversion of C11 thioester tails to products over the course of 12 hours while nearly complete conversion of C7 thioester tails was reached over 48 hours. These products were also probed for self-assembly capabilities, demonstrating a formation of mostly unilamellar liposomes from C7 thioester phospholipids while C11 thioester phospholipids displayed a temperature dependence for assembly, producing tubular micelles at room temperature and requiring elevated temperatures for liposome assembly. The faster reaction times and differences in assembly for the C11 product suggest a different packing profile of the C11 tail system as compared to that of the C7 system. Lysolipid and C11 tail packing may establish preferable accessibility of reactive groups resulting in faster reaction times; however, the assembly structure is less amenable to bilayer assembly upon phospholipid formation.

Both thiol-Michael addition and thiol-thioester exchange systems suffer from relatively slow reaction rates. This limitation may be attributed to dilute reaction conditions, weak catalysts and a stoichiometric ratio of tail and lysolipid precursors. However, the tolerance of each reaction to these conditions demonstrates the capability of each reaction for phospholipid coupling. Additionally, both thiol-Michael addition and

thiol-thioester exchange with the C7 phenyl thioester tail result in giant unilamellar structures, which may be attributed to the relatively slow reaction rates, making them desirable assembly processes for studies using fluorescence or brightfield microscopy techniques.

## **Section 7.2. Introduction of Synthetic Functionalities Using the *In Situ* Method**

Following development and characterization of the synthetic phospholipid formation reactions, the ability to incorporate new characteristics or behaviors into the lipid structure through the second aliphatic tail was probed. First, for use in the thiol-Michael reaction an aliphatic tail bearing the necessary acrylate functionality at one end and a new, terminal alkyne functionality at the other was synthesized, and the formation of synthetic phospholipids with this new tail was demonstrated. LC-MS-ELSD showed nearly complete conversion of the new lysolipid-tail system to the thioether-containing product over the course of 48 hours in the presence of 2-methylimidazole catalyst as well as a visible light photoinitiator, LAP. The presence of the photoinitiator had little effect on the conversion, and the product was able to self-assemble into liposomes. Following exposure, the homopolymerization of the alkyne functionalities was monitored on LC-MS-ELSD, showing complete consumption of the phospholipid upon irradiation.

Utilizing the dynamic nature of the thiol-thioester exchange reaction, the system was probed for the capability to exchange one tail for another. Following addition of a single equivalent of C7 thioester tail to the C11 thioester-containing phospholipid system, exchange was apparent over 72 hours. However, when up to 10 equivalents of C11 thioester tail was incorporated into the C7 thioester-containing phospholipid system, no

exchange was detected. This unidirectional exchange, in addition to the temperature dependence of the C11 thioester-containing phospholipid assembly, suggests that exchange with the C7 phenyl thioester tail results in a more stable thioester or that there are preferred structures for the phospholipid assemblies. In both cases, addition of an equivalent of the opposite tail did not disturb the assembly of the lipid bilayers.

Using the original CuAAC phospholipid formation method, lipids bearing an *o*-nitrobenzyl photo-cleavable moiety (NBPC) were synthesized. Liposomes with this lipid in conjunction with other, natural lipids (DOPC and cholesterol) were produced using two widely differing methods: lipid film hydration and the pull down technique. Both systems were capable of photo-induced pinocytosis when liposomes were far from the spherical volume to surface area ratio. Using microfluidic devices, pull-down vesicles could be rapidly deformed in the presence of osmotic pressure followed by irradiation with 405nm light to drive photo-induced pinocytosis in an average of 44% of imaged vesicles. This behavior was further characterized using aspect ratio measurements of the lipid film hydration method vesicles to determine the degree to which liposomes must be distorted to result in pinocytosis and not simply shape change to spheres. Finally, asymmetric assembly of liposomes displayed greater numbers of liposomes formed when NBPC was present only in the outer leaflet, suggesting that the photo-induced pinocytosis behavior is dependent upon the selective partitioning of NBPC to the outer leaflet. Overall, the tolerance of this behavior to a wide range of formation methods as well as the ability to control deformation and irradiation would enable this system to be applied as a future artificial cell feeding system.

### **Section 7.3. Outlook and Future Directions**

This thesis has furthered the field of designer lipid synthesis by simplifying the coupling of functionalities of interest into the lipid structure and tested that ability with a range of chemistries to instill synthetic behaviors and characteristics into the membrane that can be applied to fields such as drug delivery and artificial/proto-cell design. However, there is still much to explore in the functionalities used here and many more functionalities to probe in the future. Both thiol-Michael and thiol-thioester exchange chemistries could be expanded into the family of photo-initiated liposome formation reactions through the incorporation of photo-base systems. With careful selection of initiator systems, this would enable two-step formation with a long wavelength to generate the base catalyst followed by shorter wavelength irradiation for the generation of radicals for reactions such as homopolymerization, thiol-ene, thiol-yne or CuAAC. The polymerization of the lipid bilayer could be expanded to enable enhanced stability of the membrane by developing a crosslinking system utilizing multi-functional, hydrophobic small molecules or by producing new aliphatic tails bearing multiple reactive moieties. The thioester-containing phospholipid preference for certain tails could be probed further using new, shorter thioester tails and the ability to attach hydrophilic compounds to the membrane using thiol-thioester exchange could be explored. Finally, future work to enable site-specific enhanced permeability in the endocytosed vesicles following pinocytosis would improve the application of photo-induced pinocytosis behavior for the feeding of artificial and protocell systems.

## Chapter 8

### Bibliography

- (1) Bangham, A. D.; Horne, R. W. Negative Staining of Phospholipids and Their Structural Modification by Surface-Active Agents as Observed in the Electron Microscope. *J. Mol. Biol.* **1964**, *8* (5), 660–IN10.
- (2) Mueller, P.; Rudin, D. O.; Ti Tien, H.; Wescott, W. C. Reconstitution of Cell Membrane Structure in Vitro and Its Transformation into an Excitable System. *Nature* **1962**, *194* (4832), 979–980.
- (3) Bangham, A. D. Liposomes: The Babraham Connection. *Chem. Phys. Lipids* **1993**, *64* (1–3), 275–285.
- (4) Sweet, C.; Zull, J. E. Interaction of the Erythrocyte - Membrane Protein, Spectrin, with Model Membrane Systems. *Biochem. Biophys. Res. Commun.* **1970**, *41* (1), 135–141.
- (5) Troster, T.; Raveed, D.; Ke, B. Chlorophyll a-Containing Liposomes. *Biochim. Biophys. Acta BBA - Bioenerg.* **1970**, *223* (2), 463–465.
- (6) De Gier, J.; Mandersloot, J. G.; Van Deenen, L. L. M. The Role of Cholesterol in Lipid Membranes. *Biochim. Biophys. Acta BBA - Biomembr.* **1969**, *173* (1), 143–145.
- (7) Demel, R. A.; Kinsky, S. C.; Kinsky, C. B.; Van Deenen, L. L. M. Effects of Temperature and Cholesterol on the Glucose Permeability of Liposomes Prepared with Natural and Synthetic Lecithins. *Biochim. Biophys. Acta BBA - Biomembr.* **1968**, *150* (4), 655–665.
- (8) Daemen, F. J. M.; Bonting, S. L. Biochemical Aspects of the Visual Process IV. Aldehydes and Cation Permeability of Artificial Phospholipid Micelles. *Biochim. Biophys. Acta BBA - Biomembr.* **1969**, *183* (1), 90–97.
- (9) De Gier, J.; Mandersloot, J. G.; Van Deenen, L. L. M. Lipid Composition and Permeability of Liposomes. *Biochim. Biophys. Acta BBA - Biomembr.* **1968**, *150* (4), 666–675.
- (10) Heap, R. B.; Symons, A. M.; Watkins, J. C. Steroids and Their Interactions with Phospholipids: Solubility, Distribution Coefficient and Effect on Potassium Permeability of Liposomes. *Biochim. Biophys. Acta BBA - Lipids Lipid Metab.* **1970**, *218* (3), 482–495.
- (11) Selwyn Michael J.; Dawson Alan P.; Stockdale Martin; Gains Nigel. Chloride-Hydroxide Exchange across Mitochondrial, Erythrocyte and Artificial Lipid Membranes Mediated by Trialkyl- and Triphenyltin Compounds. *Eur. J. Biochem.* **2005**, *14* (1), 120–126.
- (12) Hsia, J.-C.; Schneider, H.; Smith, I. C. P. A Spin Label Study of the Effects of Cholesterol in Liposomes. *Chem. Phys. Lipids* **1970**, *4* (2), 238–242.
- (13) Hinkle, P. A Model System for Mitochondrial Ion Transport and Respiratory Control. *Biochem. Biophys. Res. Commun.* **1970**, *41* (6), 1375–1381.
- (14) Sessa, G.; Freer, J. H.; Colacicco, G.; Weissmann, G. Interaction of a Lytic Polypeptide, Melittin, with Lipid Membrane Systems. *J. Biol. Chem.* **1969**, *244* (13), 3575–3582.
- (15) Haxby, J. A.; Götze, O.; Müller-Eberhard, H. J.; Kinsky, S. C. Release of Trapped Marker from Liposomes by the Action of Purified Complement Components. *Proc. Natl. Acad. Sci.* **1969**, *64* (1), 290–295.

- (16) Sweet, C.; Zull, J. E. The Binding of Serum Albumin to Phospholipid Liposomes. *Biochim. Biophys. Acta BBA - Biomembr.* **1970**, *219* (2), 253–262.
- (17) Haxby, J. A.; Kinsky, C. B.; Kinsky, S. C. Immune Response of a Liposomal Model Membrane. *Proc. Natl. Acad. Sci.* **1968**, *61* (1), 300–307.
- (18) Alving, C. R.; Kinsky, S. C.; Haxby, J. A.; Kinsky, C. B. Antibody Binding and Complement Fixation by a Liposomal Model Membrane. *Biochemistry (Mosc.)* **1969**, *8* (4), 1582–1587.
- (19) Henrikson, K. P.; Henrikson, R. C. Disruption of Lecithin Spherulites during Hydrolysis by Phospholipase A: A Study by Electron Microscopy. *Experientia* **1970**, *26* (8), 842–843.
- (20) Kinsky, S. C.; Inoue, K. Fate of Phospholipids in Liposomal Model Membranes Damaged by Antibody and Complement. *Biochemistry (Mosc.)* **1970**, *9* (24), 4767–4776.
- (21) Structure of macromolecular aggregates. II. Construction of model membranes from phospholipids and polypeptides  
<https://pubs.acs.org/doi/pdf/10.1021/bi00815a001> (accessed Mar 19, 2018).
- (22) Kinsky, S. C.; Haxby, J.; Kinsky, C. B.; Demel, R. A.; Van Deenen, L. L. M. Effect of Cholesterol Incorporation on the Sensitivity of Liposomes to the Polyene Antibiotic, Filipin. *Biochim. Biophys. Acta BBA - Lipids Lipid Metab.* **1968**, *152* (1), 174–185.
- (23) Sessa, G.; Weissmann, G. Effects of Four Components of the Polyene Antibiotic, Filipin, on Phospholipid Spherules (Liposomes) and Erythrocytes. *J. Biol. Chem.* **1968**, *243* (16), 4364–4371.
- (24) Papahadjopoulos, D. Phospholipid Model Membranes III. Antagonistic Effects of Ca<sup>2+</sup> and Local Anesthetics on the Permeability of Phosphatidylserine Vesicles. *Biochim. Biophys. Acta BBA - Biomembr.* **1970**, *211* (3), 467–477.
- (25) Bangham, A. D. *Liposome Letters*; Academic Press, 1983.
- (26) Gregoriadis, G.; Leathwood, P. D.; Ryman, B. E. Enzyme Entrapment in Liposomes. *FEBS Lett.* **1971**, *14* (2), 95–99.
- (27) Hassan, S.; Prakash, G.; Bal Ozturk, A.; Saghadzadeh, S.; Farhan Sohail, M.; Seo, J.; Remzi Dokmeci, M.; Zhang, Y. S.; Khademhosseini, A. Evolution and Clinical Translation of Drug Delivery Nanomaterials. *Nano Today* **2017**, *15*, 91–106.
- (28) Bibi, S.; Lattmann, E.; Mohammed, A. R.; Perrie, Y. Trigger Release Liposome Systems: Local and Remote Controlled Delivery? *J. Microencapsul.* **2012**, *29* (3), 262–276.
- (29) Alvarez-Lorenzo, C.; Bromberg, L.; Concheiro, A. Light-Sensitive Intelligent Drug Delivery Systems†. *Photochem. Photobiol.* **2009**, *85* (4), 848–860.
- (30) Gerasimov, O. V.; Boomer, J. A.; Qualls, M. M.; Thompson, D. H. Cytosolic Drug Delivery Using pH- and Light-Sensitive Liposomes. *Adv. Drug Deliv. Rev.* **1999**, *38* (3), 317–338.
- (31) Cheng, Z.; Zaki, A. A.; Hui, J. Z.; Muzykantov, V. R.; Tsourkas, A. Multifunctional Nanoparticles: Cost Versus Benefit of Adding Targeting and Imaging Capabilities. *Science* **2012**, *338* (6109), 903–910.
- (32) Puri, A.; Loomis, K.; Smith, B.; Lee, J.-H.; Yavlovich, A.; Heldman, E.; Blumenthal, R. Lipid-Based Nanoparticles as Pharmaceutical Drug Carriers: From Concepts to Clinic. *Crit. Rev. Ther. Drug Carrier Syst.* **2009**, *26* (6), 523–580.



- (33) Yavlovich, A.; Smith, B.; Gupta, K.; Blumenthal, R.; Puri, A. Light-Sensitive Lipid-Based Nanoparticles for Drug Delivery: Design Principles and Future Considerations for Biological Applications. *Mol. Membr. Biol.* **2010**, *27* (7), 364–381.
- (34) Shum, P.; Kim, J.-M.; Thompson, D. H. Phototriggering of Liposomal Drug Delivery Systems. *Adv. Drug Deliv. Rev.* **2001**, *53* (3), 273–284.
- (35) Allen, T. M.; Cullis, P. R. Liposomal Drug Delivery Systems: From Concept to Clinical Applications. *Adv. Drug Deliv. Rev.* **2013**, *65* (1), 36–48.
- (36) Kohli, A. G.; Kierstead, P. H.; Venditto, V. J.; Walsh, C. L.; Szoka, F. C. Designer Lipids for Drug Delivery: From Heads to Tails. *J. Controlled Release* **2014**, *190*, 274–287.
- (37) Gregoriadis, P. G.; Florence, A. T. Liposomes in Drug Delivery. *Drugs* **2012**, *45* (1), 15–28.
- (38) Paleos, C. M.; Tsiourvas, D.; Sideratou, Z.; Pantos, A. Formation of Artificial Multicompartment Vesosome and Dendrosome as Prospected Drug and Gene Delivery Carriers. *J. Controlled Release* **2013**, *170* (1), 141–152.
- (39) Allen, T. M. Long-Circulating (sterically Stabilized) Liposomes for Targeted Drug Delivery. *Trends Pharmacol. Sci.* **1994**, *15* (7), 215–220.
- (40) Ragelle, H.; Danhier, F.; Pr at, V.; Langer, R.; Anderson, D. G. Nanoparticle-Based Drug Delivery Systems: A Commercial and Regulatory Outlook as the Field Matures. *Expert Opin. Drug Deliv.* **2017**, *14* (7), 851–864.
- (41) Torchilin, V. P. Multifunctional, Stimuli-Sensitive Nanoparticulate Systems for Drug Delivery. *Nat. Rev. Drug Discov.* **2014**, *13* (11), 813–827.
- (42) Pattni, B. S.; Chupin, V. V.; Torchilin, V. P. New Developments in Liposomal Drug Delivery. *Chem. Rev.* **2015**, *115* (19), 10938–10966.
- (43) Daraee, H.; Etemadi, A.; Kouhi, M.; Alimirzalu, S.; Akbarzadeh, A. Application of Liposomes in Medicine and Drug Delivery. *Artif. Cells Nanomedicine Biotechnol.* **2016**, *44* (1), 381–391.
- (44) Lipids & Cosmetics : Last innovations in Lipids for the Cosmetic Market - Sciencesconf.org <https://lipidscosmetics.sciencesconf.org/> (accessed Mar 16, 2018).
- (45) Zhang, Q.; Tang, J.; Fu, L.; Ran, R.; Liu, Y.; Yuan, M.; He, Q. A pH-Responsive  $\alpha$ -Helical Cell Penetrating Peptide-Mediated Liposomal Delivery System. *Biomaterials* **2013**, *34* (32), 7980–7993.
- (46) Huang, S.-L.; MacDonald, R. C. Acoustically Active Liposomes for Drug Encapsulation and Ultrasound-Triggered Release. *Biochim. Biophys. Acta BBA - Biomembr.* **2004**, *1665* (1), 134–141.
- (47) Ueno, Y.; Sonoda, S.; Suzuki, R.; Yokouchi, M.; Kawasoe, Y.; Tachibana, K.; Maruyama, K.; Sakamoto, T.; Komiya, S. Combination of Ultrasound and Bubble Liposome Enhance the Effect of Doxorubicin and Inhibit Murine Osteosarcoma Growth. *Cancer Biol. Ther.* **2011**, *12* (4), 270–277.
- (48) Spring, B. Q.; Bryan Sears, R.; Zheng, L. Z.; Mai, Z.; Watanabe, R.; Sherwood, M. E.; Schoenfeld, D. A.; Pogue, B. W.; Pereira, S. P.; Villa, E.; et al. A Photoactivable Multi-Inhibitor Nanoliposome for Tumour Control and Simultaneous Inhibition of Treatment Escape Pathways. *Nat. Nanotechnol.* **2016**.
- (49) Shi, J.; Su, Y.; Liu, W.; Chang, J.; Zhang, Z. A Nanoliposome-Based Photoactivable Drug Delivery System for Enhanced Cancer Therapy and Overcoming Treatment Resistance. *Int. J. Nanomedicine* **2017**, *12*, 8257–8275.

- (50) Carter, K. A.; Shao, S.; Hoopes, M. I.; Luo, D.; Ahsan, B.; Grigoryants, V. M.; Song, W.; Huang, H.; Zhang, G.; Pandey, R. K.; et al. Porphyrin–phospholipid Liposomes Permeabilized by near-Infrared Light. *Nat. Commun.* **2014**, *5*, 3546.
- (51) Huynh, E.; Lovell, J. F.; Fobel, R.; Zheng, G. Optically Controlled Pore Formation in Self-Sealing Giant Porphyrin Vesicles. *Small* **2014**, *10* (6), 1184–1193.
- (52) Bayer, A. M.; Alam, S.; Mattern-Schain, S. I.; Best, M. D. Triggered Liposomal Release through a Synthetic Phosphatidylcholine Analogue Bearing a Photocleavable Moiety Embedded within the Sn-2 Acyl Chain. *Chem. – Eur. J.* **2014**, *20* (12), 3350–3357.
- (53) Bisby, R. H.; Mead, C.; Morgan, C. G. Wavelength-Programmed Solute Release from Photosensitive Liposomes. *Biochem. Biophys. Res. Commun.* **2000**, *276* (1), 169–173.
- (54) Ohya, Y.; Okuyama, Y.; Fukunaga, A.; Ouchi, T. Photo-Sensitive Lipid Membrane Perturbation by a Single Chain Lipid Having Terminal Spiropyran Group. *Supramol. Sci.* **1998**, *5* (1–2), 21–29.
- (55) Mueller, A.; Bondurant, B.; O’Brien, D. F. Visible-Light-Stimulated Destabilization of PEG-Liposomes. *Macromolecules* **2000**, *33* (13), 4799–4804.
- (56) Yavlovich, A.; Singh, A.; Blumenthal, R.; Puri, A. A Novel Class of Photo-Triggerable Liposomes Containing DPPC:DC8,9PC as Vehicles for Delivery of Doxorubicin to Cells. *Biochim. Biophys. Acta BBA - Biomembr.* **2011**, *1808* (1), 117–126.
- (57) Kulin, S.; Kishore, R.; Helmerson, K.; Locascio, L. Optical Manipulation and Fusion of Liposomes as Microreactors. *Langmuir* **2003**, *19* (20), 8206–8210.
- (58) Elani, Y.; Law, R. V.; Ces, O. Vesicle-Based Artificial Cells as Chemical Microreactors with Spatially Segregated Reaction Pathways. *Nat. Commun.* **2014**, *5*.
- (59) Yu, J.; Guan, H.; Chi, D. An Amperometric Glucose Oxidase Biosensor Based on Liposome Microreactor-Chitosan Nanocomposite-Modified Electrode for Determination of Trace Mercury. *J. Solid State Electrochem.* **2017**, *21* (4), 1175–1183.
- (60) Altamura, E.; Milano, F.; Tangorra, R. R.; Trotta, M.; Omar, O. H.; Stano, P.; Mavelli, F. Highly Oriented Photosynthetic Reaction Centers Generate a Proton Gradient in Synthetic Protocells. *Proc. Natl. Acad. Sci.* **2017**, *114* (15), 3837–3842.
- (61) Ploier, B.; Menon, A. K. A Fluorescence-Based Assay of Phospholipid Scramblase Activity. *JoVE J. Vis. Exp.* **2016**, No. 115, e54635–e54635.
- (62) Matsuo, H.; Chevallier, J.; Mayran, N.; Blanc, I. L.; Ferguson, C.; Fauré, J.; Blanc, N. S.; Matile, S.; Dubochet, J.; Sadoul, R.; et al. Role of LBPA and Alix in Multivesicular Liposome Formation and Endosome Organization. *Science* **2004**, *303* (5657), 531–534.
- (63) Oglecka, K.; Sanborn, J.; Parikh, A. N.; Kraut, R. S. Osmotic Gradients Induce Bio-Reminiscent Morphological Transformations in Giant Unilamellar Vesicles. *Membr. Physiol. Membr. Biophys.* **2012**, *3*, 120.
- (64) Döbereiner, H. G.; Käs, J.; Noppl, D.; Sprenger, I.; Sackmann, E. Budding and Fission of Vesicles. *Biophys. J.* **1993**, *65* (4), 1396–1403.
- (65) Beney, L.; Perrier-Cornet, J. M.; Hayert, M.; Gervais, P. Shape Modification of Phospholipid Vesicles Induced by High Pressure: Influence of Bilayer Compressibility. *Biophys. J.* **1997**, *72* (3), 1258–1263.
- (66) Perrier-Cornet, J.-M.; Baddouj, K.; Gervais, P. Pressure-Induced Shape Change of Phospholipid Vesicles: Implication of Compression and Phase Transition. *J. Membr. Biol.* **2005**, *204* (3), 101–107.

- (67) Tsuda, S.; Sakakura, T.; Fujii, S.; Suzuki, H.; Yomo, T. Shape Transformations of Lipid Vesicles by Insertion of Bulky-Head Lipids. *PLoS ONE* **2015**, *10* (7).
- (68) Staneva, G.; Seigneuret, M.; Koumanov, K.; Trugnan, G.; Angelova, M. I. Detergents Induce Raft-like Domains Budding and Fission from Giant Unilamellar Heterogeneous Vesicles: A Direct Microscopy Observation. *Chem. Phys. Lipids* **2005**, *136* (1), 55–66.
- (69) Inaoka, Y.; Yamazaki, M. Vesicle Fission of Giant Unilamellar Vesicles of Liquid-Ordered-Phase Membranes Induced by Amphiphiles with a Single Long Hydrocarbon Chain. *Langmuir* **2007**, *23* (2), 720–728.
- (70) Griffith, E. C.; Rapf, R. J.; Shoemaker, R. K.; Carpenter, B. K.; Vaida, V. Photoinitiated Synthesis of Self-Assembled Vesicles. *J. Am. Chem. Soc.* **2014**, *136* (10), 3784–3787.
- (71) Svetina, S. Vesicle Budding and the Origin of Cellular Life. *ChemPhysChem* **2009**, *10* (16), 2769–2776.
- (72) Monnard, P.-A.; Luptak, A.; Deamer, D. W. Models of Primitive Cellular Life: Polymerases and Templates in Liposomes. *Philos. Trans. R. Soc. B Biol. Sci.* **2007**, *362* (1486), 1741–1750.
- (73) Mansy, S. S.; Schrum, J. P.; Krishnamurthy, M.; Tobé, S.; Treco, D. A.; Szostak, J. W. Template-Directed Synthesis of a Genetic Polymer in a Model Protocell. *Nature* **2008**, *454* (7200), 122–125.
- (74) Miller, D. M.; Gulbis, J. M. Engineering Protocells: Prospects for Self-Assembly and Nanoscale Production-Lines. *Life* **2015**, *5* (2), 1019–1053.
- (75) Jia, H.; Heymann, M.; Bernhard, F.; Schwille, P.; Kai, L. Cell-Free Protein Synthesis in Micro Compartments: Building a Minimal Cell from Biobricks. *New Biotechnol.* **2017**, *39*, 199–205.
- (76) Murtas, G. Artificial Assembly of a Minimal Cell. *Mol. Biosyst.* **2009**, *5* (11), 1292–1297.
- (77) Matosevic, S. Synthesizing Artificial Cells from Giant Unilamellar Vesicles: State-of-the Art in the Development of Microfluidic Technology. *BioEssays* **2012**, *34* (11), 992–1001.
- (78) Blain, J. C.; Szostak, J. W. Progress Toward Synthetic Cells. *Annu. Rev. Biochem.* **2014**, *83* (1), 615–640.
- (79) Fernandez-Trillo, F.; Grover, L. M.; Stephenson-Brown, A.; Harrison, P.; Mendes, P. M. Vesicles in Nature and the Laboratory: Elucidation of Their Biological Properties and Synthesis of Increasingly Complex Synthetic Vesicles. *Angew. Chem. Int. Ed.* **2017**, *56* (12), 3142–3160.
- (80) Buddingh', B. C.; van Hest, J. C. M. Artificial Cells: Synthetic Compartments with Life-like Functionality and Adaptivity. *Acc. Chem. Res.* **2017**, *50* (4), 769–777.
- (81) Shimizu, Y.; Inoue, A.; Tomari, Y.; Suzuki, T.; Yokogawa, T.; Nishikawa, K.; Ueda, T. Cell-Free Translation Reconstituted with Purified Components. *Nat. Biotechnol.* **2001**, *19* (8), 751–755.
- (82) Matsubayashi, H.; Kuruma, Y.; Ueda, T. In Vitro Synthesis of the E. Coli Sec Translocon from DNA. *Angew. Chem. Int. Ed.* **2014**, *53* (29), 7535–7538.
- (83) Kuruma, Y.; Nishiyama, K.; Shimizu, Y.; Müller, M.; Ueda, T. Development of a Minimal Cell-Free Translation System for the Synthesis of Presecretory and Integral Membrane Proteins. *Biotechnol. Prog.* **2005**, *21* (4), 1243–1251.

- (84) Nomura, S. M.; Kondoh, S.; Asayama, W.; Asada, A.; Nishikawa, S.; Akiyoshi, K. Direct Preparation of Giant Proteo-Liposomes by in Vitro Membrane Protein Synthesis. *J. Biotechnol.* **2008**, *133* (2), 190–195.
- (85) Yu, W.; Sato, K.; Wakabayashi, M.; Nakaishi, T.; Ko-Mitamura, E. P.; Shima, Y.; Urabe, I.; Yomo, T. Synthesis of Functional Protein in Liposome. *J. Biosci. Bioeng.* **2001**, *92* (6), 590–593.
- (86) van Nies, P.; Nourian, Z.; Kok, M.; van Wijk, R.; Moeskops, J.; Westerlaken, I.; Poolman, J. M.; Eelkema, R.; van Esch, J. H.; Kuruma, Y.; et al. Unbiased Tracking of the Progression of mRNA and Protein Synthesis in Bulk and in Liposome-Confined Reactions. *ChemBioChem* **2013**, *14* (15), 1963–1966.
- (87) Noireaux, V.; Libchaber, A. A Vesicle Bioreactor as a Step toward an Artificial Cell Assembly. *Proc. Natl. Acad. Sci. U. S. A.* **2004**, *101* (51), 17669–17674.
- (88) Hansen, J. S.; Elbing, K.; Thompson, J. R.; Malmstadt, N.; Lindkvist-Petersson, K. Glucose Transport Machinery Reconstituted in Cell Models. *Chem. Commun. Camb. Engl.* **2015**, *51* (12), 2316–2319.
- (89) Faudry, E.; Perdu, C.; Attrée, I. Pore Formation by T3SS Translocators: Liposome Leakage Assay. In *Bacterial Cell Surfaces; Methods in Molecular Biology*; Humana Press, Totowa, NJ, 2013; pp 173–185.
- (90) Zhang, T.; Muraih, J. K.; MacCormick, B.; Silverman, J.; Palmer, M. Daptomycin Forms Cation- and Size-Selective Pores in Model Membranes. *Biochim. Biophys. Acta BBA - Biomembr.* **2014**, *1838* (10), 2425–2430.
- (91) Hsieh, Y.; Zhang, H.; Wang, H.; Yang, H.; Jiang, C.; Sui, S.; Tai, P. C. Reconstitution of Functionally Efficient SecA-Dependent Protein-Conducting Channels: Transformation of Low-Affinity SecA-Liposome Channels to High-Affinity SecA-SecYEG-SecDF·YajC Channels. *Biochem. Biophys. Res. Commun.* **2013**, *431* (3), 388–392.
- (92) Zollmann, T.; Moiset, G.; Tumulka, F.; Tampé, R.; Poolman, B.; Abele, R. Single Liposome Analysis of Peptide Translocation by the ABC Transporter TAPL. *Proc. Natl. Acad. Sci.* **2015**, *112* (7), 2046–2051.
- (93) Koçer, A.; Walko, M.; Feringa, B. L. Synthesis and Utilization of Reversible and Irreversible Light-Activated Nanovalves Derived from the Channel Protein MscL. *Nat. Protoc.* **2007**, *2* (6), 1426–1437.
- (94) Russo, M. J.; Bayley, H.; Toner, M. Reversible Permeabilization of Plasma Membranes with an Engineered Switchable Pore. *Nat. Biotechnol.* **1997**, *15* (3), 278–282.
- (95) Price, C. E.; Kocer, A.; Kol, S.; van der Berg, J. P.; Driessen, A. J. M. In Vitro Synthesis and Oligomerization of the Mechanosensitive Channel of Large Conductance, MscL, into a Functional Ion Channel. *FEBS Lett.* **2011**, *585* (1), 249–254.
- (96) Hanss, B.; Leal-Pinto, E.; Teixeira, A.; Christian, R. E.; Shabanowitz, J.; Hunt, D. F.; Klotman, P. E. Cytosolic Malate Dehydrogenase Confers Selectivity of the Nucleic Acid-Conducting Channel. *Proc. Natl. Acad. Sci.* **2002**, *99* (3), 1707–1712.
- (97) Schleiff, E.; Jelic, M.; Soll, J. A GTP-Driven Motor Moves Proteins across the Outer Envelope of Chloroplasts. *Proc. Natl. Acad. Sci.* **2003**, *100* (8), 4604–4609.
- (98) Chaize, B.; Colletier, J.-P.; Winterhalter, M.; Fournier, D. Encapsulation of Enzymes in Liposomes: High Encapsulation Efficiency and Control of Substrate Permeability. *Artif. Cells Blood Substit. Biotechnol.* **2004**, *32* (1), 67–75.

- (99) Wick, R.; Luisi, P. L. Enzyme-Containing Liposomes Can Endogenously Produce Membrane-Constituting Lipids. *Chem. Biol.* **1996**, *3* (4), 277–285.
- (100) Wick, R.; Angelova, M. I.; Walde, P.; Luisi, P. L. Microinjection into Giant Vesicles and Light Microscopy Investigation of Enzyme-Mediated Vesicle Transformations. *Chem. Biol.* **1996**, *3* (2), 105–111.
- (101) Treyer, M.; Walde, P.; Oberholzer, T. Permeability Enhancement of Lipid Vesicles to Nucleotides by Use of Sodium Cholate: Basic Studies and Application to an Enzyme-Catalyzed Reaction Occurring inside the Vesicles. *Langmuir* **2002**, *18* (4), 1043–1050.
- (102) Yoshimoto, M.; Wang, S.; Fukunaga, K.; Walde, P.; Kuboi, R.; Nakao, K. Preparation and Characterization of Reactive and Stable Glucose Oxidase-Containing Liposomes Modulated with Detergent. *Biotechnol. Bioeng.* **2003**, *81* (6), 695–704.
- (103) Paleos, C. M.; Pantos, A. Molecular Recognition and Organizational and Polyvalent Effects in Vesicles Induce the Formation of Artificial Multicompartment Cells as Model Systems of Eukaryotes. *Acc. Chem. Res.* **2014**, *47* (5), 1475–1482.
- (104) Zong, W.; Ma, S.; Zhang, X.; Wang, X.; Li, Q.; Han, X. A Fissionable Artificial Eukaryote-like Cell Model. *J. Am. Chem. Soc.* **2017**, *139* (29), 9955–9960.
- (105) Dervaux, J.; Noireaux, V.; Libchaber, A. Growth and Instability of a Phospholipid Vesicle in a Bath of Fatty Acids. *ArXiv161204136 Cond-Mat Physicsphysics Q-Bio* **2016**.
- (106) Caspi, Y.; Dekker, C. Divided We Stand: Splitting Synthetic Cells for Their Proliferation. *Syst. Synth. Biol.* **2014**, *8* (3), 249–269.
- (107) Zhu, T. F.; Szostak, J. W. Coupled Growth and Division of Model protocell Membranes. *J. Am. Chem. Soc.* **2009**, *131* (15), 5705–5713.
- (108) Reeves, J. P.; Dowben, R. M. Formation and Properties of Thin-Walled Phospholipid Vesicles. *J. Cell. Physiol.* **1969**, *73* (1), 49–60.
- (109) Akashi, K.; Miyata, H.; Itoh, H.; Kinoshita Jr, K. Preparation of Giant Liposomes in Physiological Conditions and Their Characterization under an Optical Microscope. *Biophys. J.* **1996**, *71* (6), 3242–3250.
- (110) Angelova, M.; Dimitrov, D. S. A Mechanism of Liposome Electroformation. In *Trends in Colloid and Interface Science II*; Degiorgio, V., Ed.; Progress in Colloid & Polymer Science; Steinkopff, 1988; pp 59–67.
- (111) Pautot, S.; Frisken, B. J.; Weitz, D. A. Production of Unilamellar Vesicles Using an Inverted Emulsion. *Langmuir* **2003**, *19* (7), 2870–2879.
- (112) Yamada, A.; Yamanaka, T.; Hamada, T.; Hase, M.; Yoshikawa, K.; Baigl, D. Spontaneous Transfer of Phospholipid-Coated Oil-in-Oil and Water-in-Oil Microdroplets through an Oil/Water Interface. *Langmuir* **2006**, *22* (24), 9824–9828.
- (113) Yamada, A.; Le Berre, M.; Yoshikawa, K.; Baigl, D. Spontaneous Generation of Giant Liposomes from an Oil/Water Interface. *ChemBioChem* **2007**, *8* (18), 2215–2218.
- (114) Shum, H. C.; Lee, D.; Yoon, I.; Kodger, T.; Weitz, D. A. Double Emulsion Templated Monodisperse Phospholipid Vesicles. *Langmuir* **2008**, *24* (15), 7651–7653.
- (115) Deshpande, S.; Caspi, Y.; Meijering, A. E. C.; Dekker, C. Octanol-Assisted Liposome Assembly on Chip. *Nat. Commun.* **2016**, *7*, 10447.
- (116) Matosevic, S.; Paegel, B. M. Layer-by-Layer Cell Membrane Assembly. *Nat. Chem.* **2013**, *5* (11), 958–963.

- (117) Karamdad, K.; Law, R. V.; Seddon, J. M.; Brooks, N. J.; Ces, O. Preparation and Mechanical Characterisation of Giant Unilamellar Vesicles by a Microfluidic Method. *Lab. Chip* **2014**, *15* (2), 557–562.
- (118) Budin, I.; Devaraj, N. K. Membrane Assembly Driven by a Biomimetic Coupling Reaction. *J. Am. Chem. Soc.* **2012**, *134* (2), 751–753.
- (119) Adzima, B. J.; Tao, Y.; Kloxin, C. J.; DeForest, C. A.; Anseth, K. S.; Bowman, C. N. Spatial and Temporal Control of the Alkyne–azide Cycloaddition by Photoinitiated Cu(II) Reduction. *Nat. Chem.* **2011**, *3* (3), 256–259.
- (120) Gong, T.; Adzima, B. J.; Bowman, C. N. A Novel Copper Containing Photoinitiator, copper(II) Acylphosphinate, and Its Application in Both the Photomediated CuAAC Reaction and in Atom Transfer Radical Polymerization. *Chem. Commun.* **2013**, *49* (72), 7950–7952.
- (121) C. Jewett, J.; R. Bertozzi, C. Cu-Free Click Cycloaddition Reactions in Chemical Biology. *Chem. Soc. Rev.* **2010**, *39* (4), 1272–1279.
- (122) Kolb, H. C.; Finn, M. G.; Sharpless, K. B. Click Chemistry: Diverse Chemical Function from a Few Good Reactions. *Angew. Chem. Int. Ed Engl.* **2001**, *40* (11), 2004–2021.
- (123) Hoyle, C. E.; Lowe, A. B.; Bowman, C. N. Thiol-Click Chemistry: A Multifaceted Toolbox for Small Molecule and Polymer Synthesis. *Chem. Soc. Rev.* **2010**, *39* (4), 1355–1387.
- (124) Cramer, N. B.; Bowman, C. N. Kinetics of Thiol–ene and Thiol–acrylate Photopolymerizations with Real-Time Fourier Transform Infrared. *J. Polym. Sci. Part Polym. Chem.* **2001**, *39* (19), 3311–3319.
- (125) Nair, D. P.; Podgórski, M.; Chatani, S.; Gong, T.; Xi, W.; Fenoli, C. R.; Bowman, C. N. The Thiol-Michael Addition Click Reaction: A Powerful and Widely Used Tool in Materials Chemistry. *Chem. Mater.* **2014**, *26* (1), 724–744.
- (126) Bozzuto, G.; Molinari, A. Liposomes as Nanomedical Devices. *Int. J. Nanomedicine* **2015**, *10*, 975–999.
- (127) Hougeir, F. G.; Kircik, L. A Review of Delivery Systems in Cosmetics. *Dermatol. Ther.* **2012**, *25* (3), 234–237.
- (128) Bangham, A. D.; Hill, M. W.; Miller, N. G. A. Preparation and Use of Liposomes as Models of Biological Membranes. In *Methods in Membrane Biology*; Korn, E. D., Ed.; Springer US, 1974; pp 1–68.
- (129) Walde, P.; Cosentino, K.; Engel, H.; Stano, P. Giant Vesicles: Preparations and Applications. *ChemBioChem* **2010**, *11* (7), 848–865.
- (130) Tsumoto, K.; Matsuo, H.; Tomita, M.; Yoshimura, T. Efficient Formation of Giant Liposomes through the Gentle Hydration of Phosphatidylcholine Films Doped with Sugar. *Colloids Surf. B Biointerfaces* **2009**, *68* (1), 98–105.
- (131) Rodriguez, N.; Pincet, F.; Cribier, S. Giant Vesicles Formed by Gentle Hydration and Electroformation: A Comparison by Fluorescence Microscopy. *Colloids Surf. B Biointerfaces* **2005**, *42* (2), 125–130.
- (132) Batzri, S.; Korn, E. D. Single Bilayer Liposomes Prepared without Sonication. *Biochim. Biophys. Acta BBA - Biomembr.* **1973**, *298* (4), 1015–1019.
- (133) Miquel Pons, M. F. Liposomes Obtained by the Ethanol Injection Method. *Int. J. Pharm.* **1993**, *95* (1-3), 51–56.

- (134) Lorenceau, E.; Utada, A. S.; Link, D. R.; Cristobal, G.; Joanicot, M.; Weitz, D. A. Generation of Polymerosomes from Double-Emulsions. *Langmuir* **2005**, *21* (20), 9183–9186.
- (135) Billerit, C.; Jeffries, G. D. M.; Orwar, O.; Jesorka, A. Formation of Giant Unilamellar Vesicles from Spin-Coated Lipid Films by Localized IR Heating. *Soft Matter* **2012**, *8* (42), 10823.
- (136) Billerit, C.; Wegrzyn, I.; Jeffries, G. D. M.; Dommersnes, P.; Orwar, O.; Jesorka, A. Heat-Induced Formation of Single Giant Unilamellar Vesicles. *Soft Matter* **2011**, *7* (20), 9751.
- (137) Shima, T.; Muraoka, T.; Hamada, T.; Morita, M.; Takagi, M.; Fukuoka, H.; Inoue, Y.; Sagawa, T.; Ishijima, A.; Omata, Y.; et al. Micrometer-Size Vesicle Formation Triggered by UV Light. *Langmuir* **2014**, *30* (25), 7289–7295.
- (138) Shen, K. C.; Kakumanu, S.; Beckett, C. D.; Laugharn Jr., J. A. Use of Adaptive Focused Acoustics™ Ultrasound in Controlling Liposome Formation. *Ultrason. Sonochem.*
- (139) Rostovtsev, V. V.; Green, L. G.; Fokin, V. V.; Sharpless, K. B. A Stepwise Huisgen Cycloaddition Process: Copper (I)-Catalyzed Regioselective “ligation” of Azides and Terminal Alkynes. *Angew. Chem.* **2002**, *114* (14), 2708–2711.
- (140) Ritter, S. C.; König, B. Signal Amplification and Transduction by Photo-Activated Catalysis. *Chem. Commun.* **2006**, No. 45, 4694–4696.
- (141) Tasdelen, M. A.; Yagci, Y. Light-Induced copper(I)-Catalyzed Click Chemistry. *Tetrahedron Lett.* **2010**, *51* (52), 6945–6947.
- (142) Alzahrani, A. A.; Erbse, A. H.; Bowman, C. N. Evaluation and Development of Novel Photoinitiator Complexes for Photoinitiating the Copper-Catalyzed Azide–alkyne Cycloaddition Reaction. *Polym. Chem.* **2014**, *5* (6), 1874–1882.
- (143) Hardy, M. D.; Konetski, D.; Bowman, C. N.; Devaraj, N. K. Ruthenium Photoredox-Triggered Phospholipid Membrane Formation. *Org. Biomol. Chem.* **2016**, *14* (24), 5555–5558.
- (144) Fairbanks, B. D.; Schwartz, M. P.; Bowman, C. N.; Anseth, K. S. Photoinitiated Polymerization of PEG-Diacrylate with Lithium Phenyl-2,4,6-Trimethylbenzoylphosphinate: Polymerization Rate and Cytocompatibility. *Biomaterials* **2009**, *30* (35), 6702–6707.
- (145) Pattison, D. I.; Davies, M. J. Actions of Ultraviolet Light on Cellular Structures. *EXS* **2006**, No. 96, 131–157.
- (146) Kennedy, D. C.; McKay, C. S.; Legault, M. C. B.; Danielson, D. C.; Blake, J. A.; Pegoraro, A. F.; Stolow, A.; Mester, Z.; Pezacki, J. P. Cellular Consequences of Copper Complexes Used To Catalyze Bioorthogonal Click Reactions. *J. Am. Chem. Soc.* **2011**, *133* (44), 17993–18001.
- (147) Soriano del Amo, D.; Wang, W.; Jiang, H.; Besanceney, C.; Yan, A. C.; Levy, M.; Liu, Y.; Marlow, F. L.; Wu, P. Biocompatible Copper(I) Catalysts for in Vivo Imaging of Glycans. *J. Am. Chem. Soc.* **2010**, *132* (47), 16893–16899.
- (148) Hong, V.; Steinmetz, N. F.; Manchester, M.; Finn, M. G. Labeling Live Cells by Copper-Catalyzed Alkyne–Azide Click Chemistry. *Bioconjug. Chem.* **2010**, *21* (10), 1912–1916.
- (149) Pashkovskaya, A.; Kotova, E.; Zorlu, Y.; Dumoulin, F.; Ahsen, V.; Agapov, I.; Antonenko, Y. Light-Triggered Liposomal Release: Membrane Permeabilization by Photodynamic Action. *Langmuir* **2010**, *26* (8), 5726–5733.

- (150) Chandra, B.; Subramaniam, R.; Mallik, S.; Srivastava, D. K. Formulation of Photocleavable Liposomes and the Mechanism of Their Content Release. *Org. Biomol. Chem.* **2006**, *4* (9), 1730.
- (151) Spratt, T.; Bondurant, B.; O'Brien, D. F. Rapid Release of Liposomal Contents upon Photoinitiated Destabilization with UV Exposure. *Biochim. Biophys. Acta BBA - Biomembr.* **2003**, *1611* (1-2), 35-43.
- (152) Li, Z.; Wan, Y.; Kutateladze, A. G. Dithiane-Based Photolabile Amphiphiles: Toward Photolabile Liposomes<sup>1,2</sup>. *Langmuir* **2003**, *19* (16), 6381-6391.
- (153) Worrell, B. T.; Malik, J. A.; Fokin, V. V. Direct Evidence of a Dinuclear Copper Intermediate in Cu(I)-Catalyzed Azide-Alkyne Cycloadditions. *Science* **2013**, *340* (6131), 457-460.
- (154) Fairbanks, B. D.; Singh, S. P.; Bowman, C. N.; Anseth, K. S. Photodegradable, Photoadaptable Hydrogels via Radical-Mediated Disulfide Fragmentation Reaction. *Macromolecules* **2011**, *44* (8), 2444-2450.
- (155) Lohani, A.; Verma, A. Vesicles: Potential Nano Carriers for the Delivery of Skin Cosmetics. *J. Cosmet. Laser Ther.* **2017**, *19* (8), 485-493.
- (156) Guo, F.; Lin, M.; Gu, Y.; Zhao, X.; Hu, G. Preparation of PEG-Modified Proanthocyanidin Liposome and Its Application in Cosmetics. *Eur. Food Res. Technol.* **2015**, *240* (5), 1013-1021.
- (157) Ashtiani, H. R. A.; Bishe, P.; Lashgari, N.-A.; Nilforoushzadeh, M. A.; Zare, S. Liposomes in Cosmetics. *J. Skin Stem Cell In Press* (In Press).
- (158) Lorent, J.; Le Duff, C. S.; Quetin-Leclercq, J.; Mingeot-Leclercq, M.-P. Induction of Highly Curved Structures in Relation to Membrane Permeabilization and Budding by the Triterpenoid Saponins,  $\alpha$ - and  $\delta$ -Hederin. *J. Biol. Chem.* **2013**, *288* (20), 14000-14017.
- (159) Sessa, G.; Weissmann, G. Phospholipid Spherules (liposomes) as a Model for Biological Membranes. *J. Lipid Res.* **1968**, *9* (3), 310-318.
- (160) Qiao, Y.; Li, M.; Booth, R.; Mann, S. Predatory Behaviour in Synthetic Protocell Communities. *Nat. Chem.* **2017**, *9* (2), 110.
- (161) Kurihara, K.; Tamura, M.; Shohda, K.; Toyota, T.; Suzuki, K.; Sugawara, T. Self-Reproduction of Supramolecular Giant Vesicles Combined with the Amplification of Encapsulated DNA. *Nat. Chem.* **2011**, *3* (10), 775-781.
- (162) Barenholz, Y. *Handbook of Nonmedical Applications of Liposomes: Volume III: From Design to Microreactors*; CRC Press, 2018.
- (163) Konetski, D.; Gong, T.; Bowman, C. N. Photoinduced Vesicle Formation via the Copper-Catalyzed Azide-Alkyne Cycloaddition Reaction. *Langmuir* **2016**, *32* (32), 8195-8201.
- (164) Soares, E. V.; Hebbelinck, K.; Soares, H. M. Toxic Effects Caused by Heavy Metals in the Yeast *Saccharomyces Cerevisiae*: A Comparative Study. *Can. J. Microbiol.* **2003**, *49* (5), 336-343.
- (165) Brewer, G. J. Risks of Copper and Iron Toxicity during Aging in Humans. *Chem. Res. Toxicol.* **2010**, *23* (2), 319-326.
- (166) Chatani, S.; Gong, T.; Earle, B. A.; Podgórski, M.; Bowman, C. N. Visible-Light Initiated Thiol-Michael Addition Photopolymerization Reactions. *ACS Macro Lett.* **2014**, *3* (4), 315-318.



- (167) Xi, W.; Krieger, M.; Kloxin, C. J.; Bowman, C. N. A New Photoclick Reaction Strategy: Photo-Induced Catalysis of the Thiol-Michael Addition via a Caged Primary Amine. *Chem. Commun.* **2013**, 49 (40), 4504–4506.
- (168) B. Lowe, A. Thiol-Ene “click” Reactions and Recent Applications in Polymer and Materials Synthesis. *Polym. Chem.* **2010**, 1 (1), 17–36.
- (169) Kakwere, H.; Perrier, S. Orthogonal “Relay” Reactions for Designing Functionalized Soft Nanoparticles. *J. Am. Chem. Soc.* **2009**, 131 (5), 1889–1895.
- (170) Fairbanks, B. D.; Scott, T. F.; Kloxin, C. J.; Anseth, K. S.; Bowman, C. N. Thiol–Yne Photopolymerizations: Novel Mechanism, Kinetics, and Step-Growth Formation of Highly Cross-Linked Networks. *Macromolecules* **2009**, 42 (1), 211–217.
- (171) Zhao, G.; Hu, C.; Xue, Y. In Vitro Evaluation of Chitosan-Coated Liposome Containing Both Coenzyme Q10 and Alpha-Lipoic Acid: Cytotoxicity, Antioxidant Activity, and Antimicrobial Activity. *J. Cosmet. Dermatol.* n/a – n/a.
- (172) York-Duran, M. J.; Godoy-Gallardo, M.; Labay, C.; Urquhart, A. J.; Andresen, T. L.; Hosta-Rigau, L. Recent Advances in Compartmentalized Synthetic Architectures as Drug Carriers, Cell Mimics and Artificial Organelles. *Colloids Surf. B Biointerfaces* **2017**, 152, 199–213.
- (173) Brea, R. J.; Cole, C. M.; Devaraj, N. K. In Situ Vesicle Formation by Native Chemical Ligation. *Angew. Chem. Int. Ed.* **2014**, 53 (51), 14102–14105.
- (174) Yamashita, A.; Sugiura, T.; Waku, K. Acyltransferases and Transacylases Involved in Fatty Acid Remodeling of Phospholipids and Metabolism of Bioactive Lipids in Mammalian Cells. *J. Biochem. (Tokyo)* **1997**, 122 (1), 1–16.
- (175) Brea, R. J.; Rudd, A. K.; Devaraj, N. K. Nonenzymatic Biomimetic Remodeling of Phospholipids in Synthetic Liposomes. *Proc. Natl. Acad. Sci.* **2016**, 113 (31), 8589–8594.
- (176) Bracher, P. J.; Snyder, P. W.; Bohall, B. R.; Whitesides, G. M. The Relative Rates of Thiol–Thioester Exchange and Hydrolysis for Alkyl and Aryl Thioalkanoates in Water. *Orig. Life Evol. Biospheres* **2011**, 41 (5), 399–412.
- (177) Hutchison, C. A.; Chuang, R.-Y.; Noskov, V. N.; Assad-Garcia, N.; Deerinck, T. J.; Ellisman, M. H.; Gill, J.; Kannan, K.; Karas, B. J.; Ma, L.; et al. Design and Synthesis of a Minimal Bacterial Genome. *Science* **2016**, 351 (6280), aad6253.
- (178) Kita-Tokarczyk, K.; Grumelard, J.; Haefele, T.; Meier, W. Block Copolymer Vesicles—using Concepts from Polymer Chemistry to Mimic Biomembranes. *Polymer* **2005**, 46 (11), 3540–3563.
- (179) Feng, A.; Yuan, J. Smart Nanocontainers: Progress on Novel Stimuli-Responsive Polymer Vesicles. *Macromol. Rapid Commun.* **2014**, 35 (8), 767–779.
- (180) Zwicker, D.; Seyboldt, R.; Weber, C. A.; Hyman, A. A.; Jülicher, F. Growth and Division of Active Droplets Provides a Model for Protocells. *Nat. Phys.* **2017**, 13 (4), 408–413.
- (181) Kurihara, K.; Okura, Y.; Matsuo, M.; Toyota, T.; Suzuki, K.; Sugawara, T. A Recursive Vesicle-Based Model Protocell with a Primitive Model Cell Cycle. *Nat. Commun.* **2015**, 6, 8352.
- (182) Taylor, J. W.; Eghtesadi, S. A.; Points, L. J.; Liu, T.; Cronin, L. Autonomous Model Protocell Division Driven by Molecular Replication. *Nat. Commun.* **2017**, 8 (1), 237.
- (183) Chiu, D. T.; Wilson, C. F.; Ryttsén, F.; Strömberg, A.; Farre, C.; Karlsson, A.; Nordholm, S.; Gaggari, A.; Modi, B. P.; Moscho, A.; et al. Chemical Transformations in Individual Ultrasmall Biomimetic Containers. *Science* **1999**, 283 (5409), 1892–1895.

- (184) Caschera, F.; Sunami, T.; Matsuura, T.; Suzuki, H.; Hanczyc, M. M.; Yomo, T. Programmed Vesicle Fusion Triggers Gene Expression. *Langmuir* **2011**, *27* (21), 13082–13090.
- (185) Kahya, N.; Pécheur, E.-I.; de Boeij, W. P.; Wiersma, D. A.; Hoekstra, D. Reconstitution of Membrane Proteins into Giant Unilamellar Vesicles via Peptide-Induced Fusion. *Biophys. J.* **2001**, *81* (3), 1464–1474.
- (186) Griffin, F. M.; Griffin, J. A.; Leider, J. E.; Silverstein, S. C. Studies on the Mechanism of Phagocytosis. I. Requirements for Circumferential Attachment of Particle-Bound Ligands to Specific Receptors on the Macrophage Plasma Membrane. *J. Exp. Med.* **1975**, *142* (5), 1263–1282.
- (187) Brandt, P. W. A Study of the Mechanism of Pinocytosis. *Exp. Cell Res.* **1958**, *15* (2), 300–313.
- (188) Pratten, M. K.; Lloyd, J. B. Pinocytosis and Phagocytosis: The Effect of Size of a Particulate Substrate on Its Mode of Capture by Rat Peritoneal Macrophages Cultured in Vitro. *Biochim. Biophys. Acta BBA - Gen. Subj.* **1986**, *881* (3), 307–313.
- (189) Rodríguez-Arco, L.; Li, M.; Mann, S. Phagocytosis-Inspired Behaviour in Synthetic Protocell Communities of Compartmentalized Colloidal Objects. *Nat. Mater.* **2017**, *16* (8), 857–863.
- (190) Hamada, T.; Miura, Y.; Ishii, K.; Araki, S.; Yoshikawa, K.; Vestergaard, M. 'delanji; Takagi, M. Dynamic Processes in Endocytic Transformation of a Raft-Exhibiting Giant Liposome. *J. Phys. Chem. B* **2007**, *111* (37), 10853–10857.
- (191) Zhang, D.; Liu, Z.; Konetski, D.; Wang, C.; Worrell, B.; Bowman, C. Liposomes Formed from Photo-Cleavable Phospholipids-In-Situ Formation and Photo-Induced Enhancement in Permeability.
- (192) Ashley, J. F.; Cramer, N. B.; Davis, R. H.; Bowman, C. N. Soft-Lithography Fabrication of Microfluidic Features Using Thiol-Ene Formulations. *Lab. Chip* **2011**, *11* (16), 2772–2778.
- (193) Senior, J.; Gregoriadis, G. Stability of Small Unilamellar Liposomes in Serum and Clearance from the Circulation: The Effect of the Phospholipid and Cholesterol Components. *Life Sci.* **1982**, *30* (24), 2123–2136.
- (194) Pautot, S.; Frisken, B. J.; Weitz, D. A. Engineering Asymmetric Vesicles. *Proc. Natl. Acad. Sci.* **2003**, *100* (19), 10718–10721.
- (195) Miao, L.; Seifert, U.; Wortis, M.; Döbereiner, H.-G. Budding Transitions of Fluid-Bilayer Vesicles: The Effect of Area-Difference Elasticity. *Phys. Rev. E* **1994**, *49* (6), 5389–5407.
- (196) Coupling Chemical Reactions to Membrane Curvature: A Photochemical Morphology Switch. *EPL Europhys. Lett.* **1999**, *48* (4), 435.
- (197) Farge, E.; Devaux, P. F. Size-Dependent Response of Liposomes to Phospholipid Transmembrane Redistribution: From Shape Change to Induced Tension. *J. Phys. Chem.* **1993**, *97* (12), 2958–2961.
- (198) Clapham, D. E. Calcium Signaling. *Cell* **1995**, *80* (2), 259–268.
- (199) Sone, N.; Yoshida, M.; Hirata, H.; Kagawa, Y. Adenosine Triphosphate Synthesis by Electrochemical Proton Gradient in Vesicles Reconstituted from Purified Adenosine Triphosphatase and Phospholipids of Thermophilic Bacterium. *J. Biol. Chem.* **1977**, *252* (9), 2956–2960.